Brain thermal kinetics at brain-eyelid thermal tunnels overcoming COVID-19 thermometry limitations for automated asymptomatic infection detection in concert with thermophysical and biological principles

M Marc Abreu[1,2], Ricardo L. Smith[3], Trevor M. Banack[1], Alexander C. Arroyo[4], Robert F. Gochman[4], Anna L. Clebone[1], Feng Dai[5], Michael F. Bergeron[6], Ala S. Haddadin[1], Tyler J. Silverman[1], Adriano F. da Silva[7], David G. Silverman[1,8]†

1. Department of Anesthesiology, Yale University School of Medicine, 20 York Street, TMP3, New Haven, CT 06520-8051, USA

2. Department of Ophthalmology and Visual Science, Yale University School of Medicine, 333 Cedar Street, New Haven, CT 06520-8051, USA

3. Department of Morphology and Genetics, Paulista School of Medicine, Federal University of São Paulo, Rua Botucatu 740, São Paulo, SP 04023-900, Brazil

4. Department of Pediatric Emergency Medicine, North Shore - Long Island Jewish Medical Center, 430 Lakeville Road, New Hyde Park, NY 11040, USA

5. Yale Center for Analytical Sciences, Yale School of Public Health, Yale University, 60 College Street, New Haven, CT 06520-8034, USA

6. Department of Physical Therapy, Augusta University Medical Center, Medical College of Georgia, Augusta University, 987 St. Sebastian Way, Augusta, GA 30912, USA

7. Department of Radiology, Heart Institute, University of São Paulo Medical School, Av. Prof. Lineu Prestes, 2565, São Paulo, SP 05508, Brazil

8. John B. Pierce Foundation Laboratory, Yale University, 290 Congress Ave, New Haven, CT 06520, USA

† Correspondence and requests should be addressed to D.G.S. (david.silverman@yale.edu)

ABSTRACT

For centuries, temperature measurement deficiencies attributable to biological barriers and low thermo-conductivity (*k*) have precluded accurate surface-based fever assessment. At this stage of the pandemic, infection detection in children (who due to immature immune system may not effectively respond to vaccines) is critical because children can be readily infected and also become a large mutation reservoir. We reveal hitherto-unrecognized worldwide body temperature measurements (T°), in children and adults, over tissue typified by low-*k* similar to wood that may reach 6.8°C in thermal variability, hampering thereby COVID-19 control. Brain-eyelid thermal tunnels' (BTT) integration of low-*k* and high-*k* regions creating a thermal pathway for undisturbed heat transmission from hypothalamus to high-*k* skin eliminates current shortcomings and makes the brain indispensable for defeating COVID-19 given that brain thermoregulatory signals are not limited by mutations. Anatomo-histologic, emissive, physiologic, and thermometric bench-to-bedside studies characterized and overcome biophysical limitations of thermometry through high-*k* eyelid-enabled brain temperature measurements in children and adults. BTT eyelid features fat-free skin (~900 μm) and unique light emission through a blood/fat configuration in the underlying tunnel. Contrarily, forehead features variable and thick dermis (2000–2500 μm) and variable fat layers (1100–2800 μm) resulting in variable low-*k* as well as temperatures 1.97 °C lower than BTT temperature (BTT°). Highest emission present in only ~3.1% of forehead averaged 1.08±0.49 °C (mean±SD) less than BTT° (p=0.008). Environmental and biological impacts during fanning revealed thermal imaging limitations for COVID-19 screening. Comparison of paired measurements for 100 pediatric patients showed that in the children subgroup above 37°C, BTT° exceeded body core temperature (Core°) in 60/72 patients; the average difference in the 72 patients was 0.62±0.7°C ($p<0.001$ by unpaired t-test); and in the subgroup beyond 37.5°C, BTT° exceeded Core° in 30/32 patients. Delineating hypothalamic activity in children facilitates early infection detection, which is essential because children's immunogenicity prevents effective vaccination and causes accelerated viral evolution. Capturing hypothalamic thermal signals from BTT was further supported by brain thermal kinetics via BTT using wearables during anesthesia, sedation, sleep, brain injury, exercise, and asymptomatic infection, which revealed brain/core discordance and enabled automated noninvasive afebrile infection detection for interrupting asymptomatic human-to-human transmission. BTT-based spot-check thermometry can be harmlessly implemented for children worldwide without undue burden and costs; meanwhile, continuous brain-eyelid T° in concert with biological and physical principles affords a new dimension for combating pandemics. The "detection–vaccination" pair solution presented is required to mitigate COVID-19 from spreading indefinitely through mutations and vaccine evasion while opening a viable path for eradicating COVID-19.

Keywords: anatomy, brain-eyelid thermal tunnel, brain temperature, children, COVID-19, histology, infection detection, temperature monitoring, thermometry, wearables.

Background and Introduction

The COVID-19 pandemic remains a serious threat to the global health and economy, and humanity is heading into a world in which COVID-19 represents an ever-present and evolving danger. The World Health Organization (WHO) has predicted the emergence of even more harmful and deadly mutants capable of evading vaccines (**WHO, 2021**), and this has been substantiated by the recent identification of the most mutated strain of the virus (**Scheepers et al., 2021**), the Mu variant (**Roche, 2021**) and the R1 variant, already identified in 47 states in the U.S. (**Anglesey, 2021**), indicating the potential for COVID-19 causing an even bigger impact on the physical, emotional, and financial health of the world. COVID-19 can only be efficiently eliminated by effectively addressing the problems of transmissibility and mutations.

At this stage of the pandemic (i.e., after vaccine approval), the infection and transmission related to populations who cannot effectively respond to vaccines (i.e., children and the immunocompromised) is critical, because these groups can become a large source of dangerous mutations and thereby perpetuate the pandemic. Addressing children is particularly critical, because of their accelerated viral evolution and poor receptivity to vaccinations, attributable to their immature immune systems. This crucial need to protect children and mitigate the transmission and emergence of mutations in children is supported by the fact that, at time of writing (August 23, 2021), pediatric hospitalization numbers for COVID-19 are at their highest level since the U.S. Government began tracking them in 2020 (**Toy & Wernau, 2021**).

The global vulnerability pertaining to the transmission of severe acute respiratory syndrome coronavirus 2 (SARS-CoV-2) is evidenced and exemplified by passengers on a cruise ship, who are in imminent danger because a single child (or adult) carrying a vaccine-resistant SARS-CoV-2 lineage can cause disease and death at sea, even amongst fully-vaccinated passengers. SARS-CoV-2 is difficult to detect and has already killed passengers on cruise ships (**Dahl, 2020; Mallapaty, 2020**); furthermore, it has even bypassed nuclear ship security measures and infected over 1,000 U.S. and French military personnel on the U.S. nuclear-powered aircraft carrier the Theodore Roosevelt (**Baldor, 2020; Kasper et al., 2020**) and the French nuclear-powered aircraft carrier the Charles de Gaulle (**French Armed Forces, 2020; Simkins, 2020**).

This vulnerability recently became a reality when passengers on a cruise ship tested positive for COVID-19, despite all passengers and crew being fully-vaccinated 14 days prior to boarding and testing negative for COVID-19 within 72 hours prior thereto (**Hines, 2021**). Virus entry may arise from a reliance upon temperature measurements that are not in concert with morphological, physiological, and thermophysical principles for effective heat transfer (as evidenced by the military and civilian scenarios shown herein). SARS-CoV-2 has even circumvented the detection procedures of the most protected nuclear ships, and even killed a 41-year-old U.S. Navy officer (**LaGrone, 2021**); hence, it has become clear that nowhere in the world is immune to COVID-19 entry and deaths. This emphasizes the need for additional measures to combat COVID-19 and to detect infection; and as shown here, both military and civilians populations (of any age including children) can be protected by implementing effective infection detection in accordance with physical and biological and principles.

Further corroborating COVID-19's status as a seemly unstoppable pandemic, the U.S. Centers for Diseases Control and Prevention (CDC) reiterated an earlier March 2021 warning by stating (on May 19, 2021) that "*Because of the current situation in Japan, even fully-vaccinated travelers may be at risk for getting and spreading COVID-19 variants*" (**CDC, 2021a**). Furthermore, COVID-19 surges can occur even after the virus has been placed under control; in February 2021, India was reporting only 10,000 new cases daily; however, 2 months later it

suffered a massive, deadly surge of over 350,000 daily cases (**CNBC, 2021a**; **Ellis-Petersen, 2021)** associated with "double mutant" B.1.617 (**Ranjan et al., 2021)**. The surges are further evidenced by the COVID-19 surge in the U.S, which involved a 106% increase in new cases, a 22.8% increase in hospitalizations, and a 32.4% increase in deaths, as of July 15th, 2021 (**Washington Post, 2021**). Meanwhile, new cases are on the rise globally (**Fry and Rapp, 2021**); and on July 15th, 2021, the WHO's Emergency Committee warned that with the delta and three other variants of concern still circulating, there is a "*strong likelihood for the emergence and global spread of new and possibly more dangerous variants that may be even more challenging to control*" (**WHO, 2021**); this is evidenced by the newly identified Mu variant, which incorporates mutations that may allow it evade COVID-19 vaccines, thereby exposing the world population—vaccinated and non-vaccinated alike—to illness and death (**Roche, 2021**). COVID-19 continues to show its relentless ability to inflict suffering and to cause death, reflected by the long-feared rationing of medical care becoming a reality in the U.S., as Delta variant cases are pushing U.S. hospitals to the brink (**Knowles, 2021**).

The aforementioned cases show that fully-vaccinated people can become infected and spread COVID-19 (**CDC, 2021a; CDC, 2021b**), that SARS-CoV-2 infections remain in an upward trajectory, and that vaccines—although essential to safeguarding against disease and death—may face an immense challenge in trying to defeat SARS-CoV-2 unassisted. A modality that effectively addresses transmission and mutation (e.g., the temperature-based brain-enabled solution proposed here for both children and adults) is required to end the COVID-19 pandemic.

In this report, we present a unique and novel "detection–vaccination" pair solution to address the challenges faced by vaccination, by focusing on daily noninvasive automated early infection detection and mutation mitigation operating in concert with physical and biological principles. Thus, we open a viable path towards ending the pandemic, one that is centered upon our long experience regarding brain-enabled temperature-based infection detection with wearable devices, and which includes the collaborative efforts undertaken with Chinese colleagues in 2003 to detect coronaviruses using wearables (e.g., eyeglasses), as reported by the China Internet Information Center and detailed in this manuscript. Remarkably, the first coronavirus pandemic (SARS-CoV) was successfully eradicated by early infection detection and public health interventions, but without vaccines; this supports the eradication of SARS-CoV-2 via our proposed "detection–vaccination" pair solution. Further corroborating a viable path for coronavirus infection detection via wearable devices (that we had already demonstrated back in 2003), numerous universities, companies, and military organizations are working on the development of wearables to detect SARS-CoV-2 infections (e.g., **Eversden, 2020; Jeong et al., 2021; Smarr et al., 2020**). Our infection–detection methodology has been further developed over the years, via an integration of studies that—in aggregate—resulted in the new brain-temperature-based eyelid-facilitated early infection detection procedure for children and adults (which are disclosed in this manuscript), as well as the development of artificial intelligence for infection detection during sleep (to be presented in the second manuscript of this series), which predates the COVID-19 pandemic by more than 2 years (**Microsoft, 2017**).

Worldwide temperature-measurement screenings for COVID-19 (unaligned with physical and biological principles) are accordingly ineffectively mitigating (and, in fact, may be hastening) the uncontrolled spread of COVID-19 and facilitating the emergence of mutations. However, valid temperature measurements would be capable of mitigating mutations and even detecting early infection in children and adults if a noninvasive access to hypothalamic thermoregulatory activity measurements were to be achieved. Nevertheless, despite centuries of investigations, scientific and

medical procedures have only been able to access brain temperatures via trephination or invasive, aggressive procedures (**Foreman, et al., 2020; Kawamura & Sawyer, 1965; Kiyatkin, 2007; Kiyatkin, 2019; Maloney et al., 2001; Mosso, 1892, Rampone & Shirasu, 1964)**. The hypothalamus has remained "trapped" within the cranium, leading experts to conclude that the "hypothalamus itself is inaccessible for all practical purposes." (**Benzinger, 1969**). Remarkably, major and clinically significant investigations have relied upon inferred human brain temperatures; this has been true even of research seeking to delineate the "thermoregulatory frequency band" (~0.02–0.05 Hz), which was conducted without temperature measurements and instead based upon cardiovascular (i.e., not thermal) responses **(Hyndman et al, 1971**).

Here, we show that the hypothalamus is accessible to modern science, and that noninvasive hypothalamic activity measurements can be obtained by exploiting the thermal continuum between the hypothalamus and the highly thermally conductive eyelid skin overlying the right and left superomedial orbit ($SMOS_{BTT}$), as identified in the newly reported brain-eyelid thermal tunnels (BTTs) (**Abreu et al., 2020a**); this is supported by thermophysical and morphological evidence on the macro- and micro-scopic levels. Testing in the context of known brain/core discordances—arising during neuronal excitation and depression—has confirmed that a high resolution surface sensor placed at the $SMOS_{BTT}$ can capture the brain thermal signal (BTT°), as indicated by the differences between the BTT° and body core temperature (Core°) (**Abreu et al., 2020b**). The correspondence of the $SMOS_{BTT}$ surface temperature with brain temperature was demonstrated—without the need for corrective algorithms to account for thermal barriers—by comparison with an intra-brain tissue sensor during craniotomy (**Abreu et al. 2020a**), as well as by comparison to Core° during seizures and hypothermic cardiopulmonary bypass surgery (**Abreu et al., 2020b**).

The studies presented herein were undertaken to address the following major vulnerabilities in the global approach to the COVID-19 pandemic: the lack of temperature-measurement-based infection detection procedures underpinned by morphological, physiological and thermophysical principles for effective and undisturbed heat transfer; the challenges in protecting children and preventing children from getting infected; the unimpeded spread of COVID-19 that can be facilitated by children; and the emergence of viral mutations. The results provide a foundation for the noninvasive, automated, and continuous monitoring of brain temperature kinetics and hypothalamic activity to detect pre-febrile viral infection. This should have important consequences upon (1) intra-host viral evolution, (2) children's role as a key reservoir for mutations, and (3) COVID-19 resurgences involving deadly immune-resistant variants; these, taken together, represent a serious threat to the entire global population.

Unless these vulnerabilities are urgently and thoroughly addressed with strict criteria, COVID-19 will continue to mutate and endanger the world with unexpected surges. The fundamental criteria are as follows: First, unless surface temperature measurements are aligned with physical and biological principles for effective and undisturbed heat transfer, temperature-based detection will fail; second, metrics must be based upon thermoregulatory brain signals; and third, detection must not be susceptible to mutations. Timely detection can be achieved by continuous, automated, and daily BTT-based temperature kinetics monitoring. Because the infectivity of SARS-CoV-2 is maximal prior to symptom onset (**He et al, 2020**), detection should be achieved in the afebrile stages—particularly in target populations who cannot be as readily assisted by vaccines (e.g., children)—with unobtrusive detection preferably taking place during sleep. Additionally, to address a fundamental requirement of early brain-thermoregulatory-change detection procedures, we developed a high-resolution sensor (0.001 °C +/- 0.003 °C) based on

optical and nanofluidic technologies from the U.S. Naval Research Laboratory (**Lagakos & Bucaro, 2010**).

This report presents a proven method that rigorously meets the aforementioned criteria whilst overcoming the thermophysical and biological limitations of current thermometry, which includes deficient temperature measurements on the body surface ranging from the forehead (and its temporal region) and wrist. Furthermore, we document the worldwide presence of surface-temperature measurements not in concert with physical and biological principles for effective heat transfer, which may have precluded effective COVID-19 detection and thereby prevented mutation mitigation.

We undertook studies to delineate the anatomical (i.e., via cranio-orbital dissections), histological (i.e., via comparative histo-morphometric analyses), and radiological features of the BTT and other body surfaces considered for thermal emission measurements. Our method is based upon aggregated anatomical, histological, emissive, physiological, and thermometric studies, which were piloted by a series of macro- and micro-scopic assessments and thermal-emission analyses; with these, we determined whether emissions at the $SMOS_{BTT}$ were distinguishable from those at neighboring sites. Then, we further identified the macro- and micro-thermo-anatomical features responsible for the distinction(s). Prominent distinctions—especially topographical and temporal variations—can be used to explain the recognized failure of skin-surface thermometry [of the forehead (including superficial temporal artery area), wrist, finger, arm, axilla, chest, and other skin surfaces, except the eyelid at $SMOS_{BTT}$] to accurately detect fever. Such inability to identify febrile states are of "pandemic magnitude," because COVID-19 spreading encourages mutations, and countries use non-contact skin-surface thermometry unaligned with biophysical principles for optimal heat transfer in attempts to screen for COVID-19, as shown here (in section 4) for ethnicities and countries of every continent in which COVID-19 was identified.

The primary thermometry practices used for COVID-19 detection are based on temperature measurements taken on or over skin surfaces which are thermodynamically equivalent to a "wooden shield" that erratically and constantly changes in thickness within the same individual, across different populations, and over time in the same skin-surface location. Hence, results tend to be highly inaccurate, and it is impossible to produce a universal algorithm or correction factor – in attempts to estimate temperature, leading to a multitude of algorithms and factors that have been used in standard infrared thermometry estimating temperature of the body surface including temporal scanners estimating forehead temperature. Thus, mutations are promoted by temperatures being acquired from wood-like body surfaces and the inability to simply measure body temperatures (instead temperatures are being estimated); this creates an immense obstacle to detect infection and thereby prevent viral transmissions from infected hosts. As a result, mutation mitigation and COVID-19 surge-prevention measures fail at the fundamental level.

Body temperature assessments (obtained from measurements on or over a wood-like surface of the body) are at odds with thermal physics, as evidenced by research from the Forest Products Laboratory of the U.S. Government, who showed that oak has such a low thermal conductivity that it acts as a highly effective insulator, preventing heat transfer (**Lewis, 1968; MacLean, 1941; TenWolde et al., 1988**). Notably, tissue thermal conductivity studies conducted by the U.S. Army indicate that fat tissue has a thermal conductivity equivalent to that of oak [k = 0.00004 Kcal/(s·N·C)], as reported in the Textbook of Military Medicine, Table 2.1 (**Wenger, 2002**). Thus, measuring the temperature of fat-containing skin is effectively equivalent to measuring temperature over a wooden barrier (or "wooden shield") that obstructs thermal transfer (**Lewis, 1968; MacLean, 1941; TenWolde et al., 1988**). Studies herein reveal that fat is the

primary component of forehead surface anatomy; this, combined with the heretofore-unrecognized thick and low-*k* dermis [*k* = 0.00009 Kcal/(s·N·C)] (**Wenger, 2002**) creates a thick low-*k* thermal barrier that covers the entire surface of the human body, except at the $SMOS_{BTT}$. Hence, the world's foremost screening method against COVID-19 spreading relies upon a technique that measures temperature at a highly insulated surface equivalent to wood. As a results, SARS-CoV-2 infection detection inevitably also fails at the most fundamental level.

This fact (i.e., that skin has a *k* value equivalent to that of wood) has not been widely appreciated in practice, as documented by governmental, military, and other authorities around the world, who have relied on low-*k* measurements that may significantly compromise—if not entirely preclude—efforts to obtain clinically useful temperature measurements. In addition to thermophysical factors, our study also characterizes the confounding biological factors relating to the anatomy of the entire body's surface, which are virtually impossible to predict; these include significantly variable quantities of fat and dermis, which differ between different individuals and ethnicities as well as topographically and temporally within the same individual. In addition, the vascular physiology of these wood-like surfaces is characterized by a highly reactive vasculature beneath the low-*k* skin, which may lead to a remarkable 6.8 °C thermal variability of the skin surface, as we show here. Owing to this largely variable volumetric heat capacity, the temperatures measured on the body surface may primarily reflect unpredictable local vascular functions and variable thermophysical features of the skin structure, rather than the thermal status of the body. This is in sharp contrast to temperature measurements (in concert with physical and biological principles) taken through the high-*k* eyelid skin at the $SMOS_{BTT}$, which represent brain temperature and the true thermal status of the body.

Based on our expertise and experience in previous pandemics (described here), we aim to interrupt asymptomatic human-to-human transmission (including children-to-children) and mitigate mutations by continuous automated infection detection to reduce the Basic Reproduction Number (R_0) benchmark; and early infection detection led to the successful eradication of the first coronavirus pandemic (SARS-CoV) in 2003. To this end, we undertook a series of bedside investigations in addition to the bench studies. Pharmacological and physiological neuronal depressions of the brain (during sedation, anesthesia, and sleep) suggest a foundation for an early infection-detection procedure that can be administered during sleep. To this additional end, we examined the brain thermal kinetics patterns of the non-infected, identifying distinctions through comparison with the asymptomatic afebrile phases of negative-sense RNA virus (influenza) infection in subjects both asleep and awake. BTT-based brain-temperature measurements were confirmed by concomitant intracerebral temperature monitoring in brain injury patients and by our study of 100 pediatric fever patients. We use the second of these studies to detect hypothalamic thermoregulatory responses in children, which is of crucial significance because SARS-CoV-2 may spread and mutate via an atypical source: the bodies of children. Failure to address the infection of children may lead to virus reservoirs and derail the process of eradicating the COVID-19 pandemic.

SARS-CoV-2 can exploit the immature bodies of children—who may not effectively respond to vaccines—to perpetuate the pandemic and cause new surges. Concerning evidence regarding SARS-CoV-2 mutations originating from children has been published: the body of a baby was shown to contain an unprecedented RNA viral load (51,418 higher than the median) and to have produced a new variant with a novel spike protein (**LoTempio et al., 2021**); this documents that accelerated intra-host viral evolution, generated in infants' immature immune systems, leads to mutations. This means that, in the U.S alone, 23.6 million children aged 0–5 years old **(US**

childstats.gov, 2021), although not yet extensively documented, may potentially become a major source for high viral loads and mutations, because children cannot be effectively protected (by vaccines) and thus can be readily infected and easily transmit the virus by largely increased viral loads. Further considering that children up to 17 years old are associated with higher infectivity (**Li et al, 2021**) brings the total source of infection to 74 million solely in the U.S. Here, we address children's role as sources and reservoirs for mutations, whilst protecting the lives of this defenseless population (who because of their immunogenicity may not benefit from vaccines) using a methodology that can be immediately and harmlessly implemented, completely fre-of-charge, for children in every country around the world.

In March 2021, the CDC warned that "*Vaccinated people could potentially still get COVID-19 and spread it to others*" (**CDC, 2021b)**; this was reiterated on May 19, 2021 (**CDC, 2021a**); this highlights fully-vaccinated teachers' ability to transmit COVID-19 to children in school, as well as children's ability to infect fully-vaccinated teachers or family members. This may lead to unanticipated fatalities, because infections in children have been associated with the U.K. Alpha variant (**Day, 2021**), which has been reported as increasing the risk of fatality by 64% compared to previous lineages (**Challen et al., 2021**) as well as infections by the Delta variant, which also cause more severe infection (**Sheikh et al, 2021**). Our studies show the feasibility of performing automated early infection-detection monitoring via a headgear that can be worn during sleep; this facilitates the protection of children, which is critical because other indicators of infection (e.g., irritability, crying, and respiratory rate changes) in children are subjective. This, in turn, protects adults by preventing COVID-19 transmission from children (including babies).

Our proposed "detection–vaccination" pair solution, in which vaccines prevent infection *of the host* and our BTT-based eyelid-enabled infection-detection method prevents transmission *from the host,* can interrupt human-to-human transmission, including transmission from children. Without infection detection, children (and babies/toddlers), through their free interactions with adults and other children, may become key sources of the unimpeded, unchecked, and rapid spread of COVID-19, as recently documented by a fully-vaccinated mother who was infected by her child (**Brueck, 2021**).

A recent report provided guidance for non-contact infrared thermometry and infection detection (**Foster et al., 2021**). Here, we provide new guidelines that consider a new site, the eyelid at the $SMOS_{BTT}$, as a potential site for improved fever detection via thermal imaging in adults and children. However, confounding biological factors and strict criteria for the thermal imaging of the $SMOS_{BTT}$ prevent reliable fever screening. Furthermore, only one narrow light beam is emitted by each eyelid at the $SMOS_{BTT}$ and used during the procedure; therefore, unless subjects are completely motionless, fever detection may be precluded, as revealed by our video documentation.

In a pandemic, "none of us will be safe until everyone is safe" (**WHO, 2020**). This highlights the need for worldwide cooperation. Results of collaborative research involving Chinese colleagues and Dr. Abreu in China during the first coronavirus pandemic in 2003 led to the recognition (during the SARS pandemic) that BTT-based brain-temperature-monitoring wearables can detect coronavirus (SARS-CoV) infections; and in August 2003, our Chinese colleagues reported through the China Internet Information Center that BTT eyeglasses, patches, and temp-alert systems can be used *"…to detect diseases such as the flu-like SARS (severe acute respiratory syndrome) that spread early this year to about 30 countries…*" (**China Internet Information Center, 2003; China Daily, 2003**). However, the eradication of SARS-CoV around that time has prevented continued collaborative efforts in China toward early detection of SARS-CoV infections via wearables (i.e., BTT wireless monitoring eyeglasses) and intelligent temp-alert systems.

The emergence of SARS-CoV-2 approximately 17 years later has presented an opportunity to further develop the previous coronavirus detection research begun in China, as well as to gather further data and continue pioneering the brain-based eyelid-enabled temperature measuring technologies required to detect COVID-19 in adults and children. Extensive testing—to validate the safety and efficacy of BTT-based detection technologies for adults and children—was subsequently pursued; this resulted in the regulatory approval of the Abreu-BTT 700 System (and its hardware, software, and specialized sensors) by the U.S. Food and Drug Administration (FDA) in 2010 (**FDA, 2010**). Additional efforts involving academia and industry, under U.S. Government support (Qualifying Therapeutic Discovery grant), led to the development of the new wearables shown here, as well as a machine learning approach that applies brain thermodynamics to diagnose neurological disorders and detect infections during sleep, as described in detail elsewhere (**Microsoft, 2017**).

Here, we also freely offer to the global community our knowledge [including information on methods developed in two previous pandemics [SARS (**China Internet Information Center, 2003)** and H1N1 "Swine Flu" **(Abreu, 2009)**] and the associated brain-based eyelid-enabled infection detection methodologies, which have been developed over the past 15 years; with these contributions, any country in the world can immediately save lives and reduce human suffering (for children and adults alike) by swiftly detecting COVID-19 via methods aligned with physical and biological principles, through performing spot-check temperature measurements according to natural engineering (which is uniquely present in the BTT) instead of forcing human engineering on nature (e.g., by using artificial correction factors and algorithms, to estimate temperature, as currently employed by various infrared thermometers and infrared temporal scanners).

We present guidelines for the use and adaptation of current infrared thermometers to perform detection at the $SMOS_{BTT}$; these guidelines are based upon thermophysical and biological principles for optimal thermal signal capture, and enable the (heretofore unrecognized) eyelid as the body region that can provide a viable path to end the COVID-19 pandemic. We provide our brain-based eyelid-enabled thermal detection methodologies free-of-cost to every government, every company, and every individual around the world, such that they can be readily implemented by all countries, regardless of their economic status and geographic location, to immediately protect lives without undue burden and expense; this may potentially lead to the improvement (or even redesign) of thermometric practices for pandemic control.

Our study presents a proof-of-concept of the feasibility of the BTT-based noninvasive monitoring of brain-temperature kinetics via the eyelid at $SMOS_{BTT}$, to facilitate the detection of afebrile asymptomatic infection from a negative-sense RNA virus (influenza) whilst awake or asleep. This expands our investigation of the thermal signatures of afebrile infection of a positive-sense RNA virus (SARS-CoV-2), to be presented in the second manuscript of the series. Notably, BTT-based detection is not inherently limited by mutations, because the hypothalamus always mounts a cytokine-autonomic thermal defense against viruses or variants, which later on leads to the disinhibition of thermogenic neurons (**Lazarus et al., 2007; Nakamura et al., 2009; Ott, 1884**).

A review on brain-temperature research showed data that considerably expanded the existing knowledge on animal brain temperatures, but also emphasized the current lack of human brain temperature data (**Kiyatkin, 2019**). Whilst advancing knowledge regarding human brain temperature, we here present brain-based eyelid-enabled temperature measurement methodologies that harness engineering solutions *provided by nature*, instead of imposing human engineering *upon nature*. Hypothalamic thermal signals naturally reveal the virus, making the enemy "visible"

and rendering it vulnerable to detection and more effective advance treatment before organ invasion. Our studies present promising avenues for public health interventions (including effective isolation to protect family and community) and future countermeasures, as evidenced by the fact that (i) neither race nor age affects the unique emissions found in the eyelids at $SMOS_{BTT}$ and (ii) both vaccinated and non-vaccinated individuals (including children) can benefit from wearables-based brain-temperature kinetics monitoring and hypothalamic activity detection to timely identify afebrile asymptomatic and initial febrile stages on a daily, harmless, and fully automated basis, thereby preventing shedding during the most infective period (**He et al., 2020**). This will help to interrupt asymptomatic and symptomatic human-to-human transmission and reduce R_0 to < 1, thereby ensuring a viable method for preventing spread and mitigating mutations, which is integral to eradicating the COVID-19 pandemic.

Materials and Methods

Approvals and Consents. All the investigational protocols were reviewed and approved by the authorized ethics committees, in accordance with the relevant guidelines of the Institutional Review Board of the Yale University School of Medicine, the Medical College of Georgia of Augusta University, and the North Shore - Long Island Jewish Hospital of New York. Informed consent was obtained from all participants after a complete description of the study procedures, risks, and potential benefits prior to participation in the studies. All adult subjects and children who are depicted in images herein, are participants of our research group or a family member of a member of our research group, and gave written permission themselves or permission was given by the parents or legal guardians, for the use of their image(s) in the photos and the publication of their identifying image(s) in an online open-access research publication.

Tissue Preparation and Analysis. Anatomo-histologic studies were performed on 13 adult cadavers, which were fixed in 4% formaldehyde solution. Intravascular injection of stained Neoprene® was administered according to standard procedures, to make the venous and arterial systems more evident. Photomicrographs were obtained with a Carl Zeiss Axiovision microscope with digital imaging and Zeiss lenses 10X e 40X. Dissections were performed through the orbital bone walls to show the SOV, the orbital fat, and their anatomical relationships. Intracranial dissections were conducted to expose the intracranial portion of the SOV and the neighboring vessels communicating via the cavernous sinus components of the triunal system using axial and parasagittal cuts. Facial dissections included removal of the skin to expose arterial and venous networks. Histologic studies and measurements (in a micrometer scale) were performed upon skin fragments. Specimens supplied from the medial eyelid were embedded in paraffin, 7-µm sectioned, and stained with hematoxylin-eosin. All anatomic and histologic studies were performed in accordance with the relevant guidelines of the Paulista School of Medicine of the Federal University of Sao Paulo.

Thermal imaging studies. Using the criteria of Supplementary Table 1, infrared light was captured from the face, neck, and BTT region, in a controlled-temperature (20–22 °C) draft-free room. Sections 1–4 and 6: TyTron C500IR, Titronics R&D, Tiffin, Iowa, USA. Specifications for the analyses were as follows: image temperature range: 8 ºC [gradient indicated in view by bar on the right (highest at top)]; infrared spectral range: 7.5–13 microns; absolute resolution: 76,800 IR sensors; spatial resolution: 1.3 mrad; and thermal sensitivity: 0.08 °C. A computerized isotherm analysis of the gray-scale images was performed. The hottest area on the image was demarcated with a red isotherm. The warmest non-adjacent site was demarcated with a green isotherm. Temperature comparisons between these sites was performed using the two-tailed paired t-test.

The heterogeneity of the readings is displayed in Table 1. The distribution of the red and green isotherms were quantified according to the dimensions in each cell of the grid and superimposed on the gray-scale images. Sections 5 and 7: FLIR Termocam Medical, FLIR, USA. Software: VisionFY, ThermoFy, University of Sao Paulo School of Medicine, Brazil.

Clinical and Experimental Studies. Human studies involved multiple clinical and experimental protocols. When not specified in this Materials and Methods section, additional details regarding the methodology (e.g., the numbers of subjects, demographics, and analyses) have been provided in the relevant sections of the Results. Any invasive monitoring to which BTT° was compared was a component of ongoing clinical care. There were no reports of adverse effects of any type, and no subject was harmed during the investigational monitoring or procedures.

Engineered designs facilitated intermittent and continuous surface measurement of the brain temperature (BTT°) and the acquisition of thermal patterns without tissue disturbance in a fully noninvasive and unrestricted manner. To achieve biologically fit devices, the dimensions were carefully selected to match the BTT area configuration. Miniature specialized contact sensors (thermistors) for continuous temperature measurement were designed and fabricated to overlie the BTT on the skin between the edge of the upper eyelid and the eyebrow adjacent to the superior aspect of the medial canthal region. The high-resolution thermal sensors developed were mounted on a headgear and the frames of the eyeglass or as an isolated FDA-approved sensor, anchored to the neighboring skin by an adhesive surface (Abreu BTT C1 sensor, Brain Tunnelgenix Technologies Corp, Aventura, FL). This included an adhesive portion secured to the forehead, with the sensor embedded in a rubberized housing to be positioned over the $SMOS_{BTT}$ via a flexible arm, which was electrically coupled to a continuously monitoring brain-temperature system running on a FDA-approved computer system (Model Abreu BTT 700 System, Brain Tunnelgenix Technologies Corp, Aventura, FL) via wired or wireless transmission. Optimal sensor positioning was determined by thermal-to-auditory conversion (an auditory tone was generated with an increasing frequency proportional to the increase in temperature).

All BTT° and FH° sensors were equally calibrated using water bath testing, and an NIST-based thermometer was used as reference (Thermoregulator, Omega Instruments, Norwalk, CT, US). Comparisons of the temperature overlying the BTT (BTT°) and one or more temperature monitors at the other sites were performed during steady states and states of brain/core discordance. These included continuous FH° using the BTT C1 sensor on the forehead skin as well as a spot-check forehead scanner (Exergen Corporation, Boston MA).

Comparative temperature measurements in normal subjects*.* BTT°, Core° (SL°), and Surface° comparative measurements: Measurements were performed upon 18 normal volunteers who were requested to refrain from eating or drinking for 30 min before being studied; they were seated comfortably in a room after five minutes of stabilization. Sites were compared on five separate days, using equally calibrated thermistors, and without any offset or correction factor. SL° measurements used a bare thermistor placed on the sublingual pocket. The consistency of BTT° and SL°, under resting conditions, was assessed with a bias (and 95% limits of agreement corrected for repeated measures). See Text for other details. *During Sleep:* Comparison of BTT° with Rct° and FH° during at-home sleep was performed upon members of our research team. See text for details. *Assessment during exercise:* A 40-year-old healthy male jogged on a treadmill in an environmental chamber (40 °C) at the Medical College of Georgia whilst being monitored via BTT° and a Capsule° (CorTemp, HQ Inc.) ingested eight hours earlier. BTT° and Capsule° were recorded one minute before the start of the exercise and at 1 minute intervals for its duration.

Comparative temperature measurements during suspected fever in pediatric patients. (All performed at the at the Long Island Jewish Medical Center, New York, NY). Temperature measurements at $SMOS_{BTT}$ were performed upon 100 pediatric patients using the non-contact Abreu BTT Brain-Eyelid Thermometer 3.1 shown in Figure 8E (BTTCorp, Aventura, FL)—see text for details.

Comparisons during invasive monitoring in anesthetized surgical patients (All performed at the Yale-New Haven Hospital of Yale University School of Medicine, New Haven, CT). *Comparative intra- and post-operative monitoring.* BTT^{o} was monitored in 12 patients who received propofol infusion to induce Level 3 sedation during minor surgery. BTT° – SL° was determined prior to and at the 30^{th} min of propofol infusion (see text). In two additional patients (68 year-old male, 60 year-old female), BTT° was compared with the Core° measurements during general anesthesia. Monitoring included BTT°, nasopharynx (NP°) measurement during anesthesia, an esophageal probe in the esophagus (Esg°) during anesthesia and withdrawn to the oropharynx after emergence therefrom, and FH_{scan}° obtained intermittently by nurses in the post-anesthesia care unit. Esg° was measured using an esophageal stethoscope and temperature probe (#ES-400-18, Smith's Medical). When a patient was not deeply anesthetized, the esophageal probe was placed at the rear of the tongue in the oropharynx, because advancing the probe to the esophagus would cause discomfort. *Monitoring in Intensive Care Unit (ICU):* The BTT° of ICU patients at the Clinics Hospital of Sao Paulo University Medical School, Sao Paulo, Brazil were monitored in two patients (7 year-old male with traumatic brain injury, 55 year-old female with stroke) using a intraventricular thermal probe (hpbio.com) inserted for clinical management. See text for details.

Analysis: Thermal emission differences in the BTT site and sites outside the BTT were assessed with two-tailed paired t-test. Inter-device differences during at rest conditions at 59 time points (16 subjects) were assessed with Bland-Altman plots and paired t-test. Intradevice and interdevice differences during propofol infusion were assessed with one-tail paired t-test. Inter-device differences during sleep were assessed with two-tailed paired t-test. Interdevice differences in the pediatric emergency room patients were assessed with Bland-Altman plots; the differences were analyzed with unpaired t-test, and the relative number of measurements when BTT° exceeded SL° above a mean of 37.5° vs below a mean of 37.0° was compared using chi-square analysis. The bias and limits of the agreement were also determined. The level of statistical significance was determined by a P-value of $<.05$. See text for details.

Results

We sought to determine the macro- and micro-scopic relationships and distinctions of the BTT morphology as applied to thermal emissions at the peri-orbital region, the remainder of the face, the neck, and other thermometric sites, to determine its consistency with thermophysical and biological principles regarding the capture of undisturbed thermal signals for infection detection (***Sections 1 and 2***). Then, for normal subjects (over a period of up to 5 days), we quantified the measurement distinctions between the BTT site (based on scientific principles for optimal heat transfer) and an unaligned site (forehead), as well as a third site representing Core°, to further characterize inter-site distinctions (***Section 3***); this work complements our earlier comparative studies (**Abreu et al., 2020a; Abreu et al., 2020b**). Then, we pursued functional studies and considered their epidemiological implications for COVID-19 spread in light of global thermometric practices unaligned with physical and biological principles for optimal heat transmission; namely, the use of low-*k* surfaces exhibiting variable volumetric heat capacity

(***Section 4***). In ***Section 5***, the alignment with physical and biological principles was determined and used to identify the practical applications and impediments of thermal imaging, via radiological and video documentation. Topographically consistent thermal emissions, realized by physical and biological alignment across different races, produce consistent and precise results from the illuminated BTT region (***Sections 6 and 7***); this facilitates the use of the herein-described brain-based detection methodology around the world.

Once the thermophysical and biological principles for effective heat transfer were met, the basis of the method—which consists of the undisturbed acquisition of brain thermal signals and detection of hypothalamic activity through the eyelid at $SMOS_{BTT}$—was validated across multiple scenarios, including children, who may pose a risk for COVID-19 spreading, accelerated viral evolution, and emergence of mutation (***Section 8***). These studies establish the basis for monitoring brain temperature kinetics and detecting thermoregulatory brain responses, to identify viral infections at inception. Detection during sleep is key; hence, we conducted investigations during brain neuronal depressions (sedation, anesthesia, and sleep) in addition to brain injury, brain hyperthermia (continuous exercise in a 40 °C environmental chamber), and brain thermoregulation states (including asymptomatic RNA virus infection detection and fever studies in 100 pediatric patients), to detect hypothalamic responses.

Section 1. Macroscopic, histo-morphometric, and thermal-emission inter-site relationships of $SMOS_{BTT}$ at forehead; their implications for low-*k* thermometry

We initially focused on the forehead because of its proximity to the $SMOS_{BTT}$, the fact that its frontal vein is a tributary of the superior ophthalmic vein (SOV) (**Abreu et al., 2020a**), the presence of a large artery [superficial temporal artery (STA)] thereat, and the widespread global reliance upon forehead skin temperature measurements for COVID-19 screening (**Section 4**).

Thermal emission. Colored and gray-scale images (**Figures 1A, B**) of facial thermal emissions (with overlying grids for delineating emission topography) revealed that the largest light emission (marked in red in the gray-scale figures) was detected only at the BTT terminus in the eyelid region of the SMO, beneath the orbital rim. The second-highest emission (the green line in the gray-scale figures) was the corona surrounding the BTT site. This is in sharp contrast to the low and inconsistent thermal emissions obtained across the forehead and face (**Figures 1A, B**). Five subjects were compared using the grids; the highest skin temperature at sites outside the BTT was 1.07 ± 0.49 °C (mean ± SD) lower, on average, than at the BTT ($p = 0.008$; two-tailed paired t-test) and was present in only ~3.1% of the forehead; the remaining 96.9% of the forehead (including the STA region) exhibited temperatures of 1.3–3.6 °C below the BTT-site result (**Table #1**). This is not surprising, because the forehead surface is characterized by a comparatively low *k*, and measurements taken there do not align with thermophysical and biological principles.

Table #1. Emission comparison between BTT, forehead, and other facial sites: Data generated by overlaying a grid onto the gray-scale emission images obtained from the faces of five subjects (male: Subjects 1 and 3; female: Subjects 2, 4, and 5), to delineate site and temperature: (a) no site exhibited a temperature (temp.) exceeding $SMOS_{BTT}$; (b) the highest-temperature sites were those at the $SMOS_{BTT}$; (c) the difference between the $SMOS_{BTT}$ and the highest temperature outside it varied as 0.74–1.92 °C; (d) only a very small region of the forehead (3%) exhibited the forehead's maximum temperature, and the forehead retained an average temperature 1.07 °C below that at the $SMOS_{BTT}$ (only four sites exhibited the highest forehead emission in more than 50% of the cell area; meanwhile, 23 sites exhibited the highest forehead emission in less than 50% of the cell area);

and (e) forehead scanning resulted in lower temperatures than at the $SMOS_{BTT}$ (average: 1.75 °C). Figure 1A corresponds to Subject 1 and Figure 1B corresponds to Subject 3.

Table 1. Comparative emission at BTT, forehead, and other facial sites

	Subject 1 (69 y/o)	Subject 2 (54 y/o)	Subject 3 (28 y/o)	Subject 4 (35 y/o)	Subject 5 (48 y/o)
Site(s) of highest temp. on entire grid	b1,2-A1,2;B1,2	b1,2-B1	b1;2,B1	c1,B1-2,C1	b1, B1
Difference (°C) between highest temp. on grid (always at BTT) & highest on FH, face, or neck	0.75	1.04	1.92	0.74	0.88
% of FH with highest FH temp. (grenn isotherm)	<1%	4.5%	1.5%	2.5%	6.0%
Difference (°C) between highest temp. on grid (always at BTT) & highest temp. by FH scan	1.10	1.87	2.72	1.76	1.38
Sites of highest temp on FH (all of which are < BTT)					
>50% of cell		a8, A8, B8	C9		
<50% of cell	E5	d7, A7, C8 B4, C4, C5, F4	a9, F6, A8, A9, A10	a10, G5, C5	e7, e8, a8, a9, A9, B5, B9, F5

Despite a 41-year age difference (**Figure 1A**: 69 years old; **Figure 1B**: 28 years old) between the two male subjects, the right and left BTT sites of both subjects [shown in the color panels as red (Figure 1A) and gray (Figure 1B)] exhibited maximal thermal emissions. Hence, aging does not measurably impact light emissions from the eyelid at the BTT site. This is an interesting observation that we are further exploring in our ongoing research. In contrast to other tissues in the body (whose emissions vary over time), the blood/fat/skin morphological configuration and the resulting light emission from the eyelid at the brain tunnel are apparently resistant to aging. SARS-CoV-2 attacks all age groups; hence, this thermodynamic consistency of the BTT further supports BTT° as a consistent and reliable indicator, as required to combat COVID-19 via effective infection detection at inception across different age groups.

Macroscopy applied to thermal emission. The forehead skin and its underlying venous system is in direct continuum with the SOV at the external terminus of the BTT (**Abreu et al., 2020a**); however, as shown in **Figure 1C** (middle and right panels), its morphology and thermal emissions differ remarkably from the eyelid skin at the $SMOS_{BTT}$. Moreover, despite its prominent vasculature [featuring a large-caliber vessel (the STA) (**Figure 1C**, left panel)], the forehead exhibits low and variable thermal emission levels (denoted in orange and dark red), because it is covered by a low-*k* barrier equivalent to wood. This is in sharp contrast to the highest emission observed at the high-*k* BTT-site eyelid skin, shown in gray (**Figure 1C**, middle and right panels). Both the venous system (outside the $SMOS_{BTT}$) and arterial system suffer from thermal conductivity and biological impediments, owing to thermophysical barriers (low-*k* surfaces)

(**Figure 1D**) and biological challenges entailed by the highly active and variable forehead arterial vasculature and cutaneous blood vessels (**Silverman et al., 1987**). The hampered thermal transmission produced by the low-*k* barrier is thereby coupled with an inconsistent vasomotor tone; this confounds temperature measurements at the forehead (and other low-*k* body surface areas).

Furthermore, it is impossible to adjust to the vasomotor tone changes that characterize arteries (e.g., STA), because arteries feature large elastic lamina and thick, smooth muscle layers, which produces a continually varying blood volume; hence, variable temperatures reflect local vascular changes (e.g., those elicited by ambient temperature, drugs, or emotions) rather than the internal thermal status of the body. In sharp contrast, the SOV at the BTT features a low-velocity blood flow and thin wall and, as a vein, lacks the external elastic lamina; this, coupled with its thin, smooth muscle layer, results in virtually no volume variability (**Abreu et al., 2020a**). Thus, the BTT exhibits a consistent volumetric heat capacity that facilitates the true assessment of pre-febrile and early febrile states from thermoregulatory brain signals; this is essential for the effective and early detection of SARS-CoV-2 infections in vaccinated and non-vaccinated populations, including children.

Microscopy applied to thermal emission. Comparative histo-morphometry and the local superficial anatomy of the forehead produces thick and variable layers of dermis and palisades of subcutaneous (SC) fat, (shown in the left and middle photomicrographs of **Figure 1D**). Forehead skin has a low *k*, comparable to that of oak (**Wenger, 2002**); this insulation prevents the transmission of thermal energy. It can be clearly observed in **Figure 1D** that the "invisible" and highly variable thickness of the fat and dermis (and the subsequent highly variable thermal conductivity) reveals histomorphometrically that a reliance on forehead, wrist, and body surface thermometry is not in accordance with *physical* properties of effective heat transfer (i.e., because it measures temperature on such a low-*k* surface), *morphological* attributes (i.e., because it measures temperature on a highly variable tissue: fat), and *physiological* characteristics (i.e., because it measures an area with a continually varying vasomotor tone). Thus, forehead thermometry (and temperature measurements at other low-*k* surface sites) may prevent us from obtaining the useful assessments required to combat COVID-19, resulting in two types of inaccurate result: false-negative readings, where fever is actually present but undetected; and false-positive readings, where fever is falsely detected but the person is actually afebrile (**Section 3**). Both of these can spread infection and facilitate mutations.

In sharp contrast to the variable histology outside the $SMOS_{BTT}$, the eyelid skin overlying the BTT terminus is fat-free and features a consistently thin dermis (**Table #2**) without the typical capillary networks (shown in the right photomicrograph of **Figure 1D)**. This ensures stable and maximal thermal conductivity at the skin of the $SMOS_{BTT}$. The histomorphometry of the BTT surface is consistent across different subjects (of different races), who all feature a uniformly high-*k* skin (**Abreu et al., 2020a**). This was confirmed in the thermal emission studies described here, which show the equivalent light emissions from the BTT across different races (**Section 7**). Thus, BTT° provides accurate and consistent temperature measurements across diverse populations and races, as required to effectively detect the thermal status of the different populations exposed to such globally prolific diseases as COVID-19. Accordingly, the temperature-based brain-enabled methodology that employs the BTT facilitates measurements that can accurately detect pre-febrile and febrile states across different ethnicities infected with SARS-CoV-2.

Table #2. Comparative histomorphometry of skin at BTT site and other regions:
Thickness (in microns) of the epidermis, dermis, and fat layers. The two BTT skin specimens were the only ones exhibiting a similar dermis thickness and no SC fat (further corroborating our

earlier histological study of eyelid skin at the BTT site, **Abreu et al., 2020a**). In contrast, the forehead skin from different cadavers featured highly variable epidermis, dermis, and fat layer thicknesses. Thick dermis and fat layers were measured at the neck and axilla (**Section 2**); these follow the same pattern as the forehead, with variable thicknesses between cadavers (not shown).

Table 2. Comparative histomorphometry of skin at BTT site and other regions

Tissue	BTT (1)	BTT (2)	Forehead (1)	Forehead (2)	Neck	Axilla
Epidermis	~70	~70	~70	~100	~70	~100
Dermis	~900	~900	~2000	~2600	~2500	~2000--3000
Fat	0	0	~2800	~1100	~2200	~3000--8000

The radiative emissions from the $SMOS_{BTT}$ are consistently located in the eyelid, facilitate consistent BTT skin microscopy (**Table #2**), are aligned with previous histological findings (**Abreu et al., 2020a**), and are associated with a consistent vein anatomy (**Bergen, 1981; Cheung & McNab, 2003; Festal, 1887**). This results in remarkably consistent biological characteristics, comprising a combination of uniform macro- and micro-scopic features only occurring at the BTT site. Furthermore, it provides uniform brain ↔ surface thermophysical characteristics, which optimizes the intensity and consistency of BTT light-emission measurements. In sharp contrast, the presence of fat and thick dermis layers in the forehead (and areas outside the $SMOS_{BTT}$) (**Table #2**) have required the application of correction algorithms and factors in forehead thermometry. These further hinder effective temperature measurements, owing to the large variability of the fat and dermis thicknesses between different individuals, over time within the same individual, and between different surface regions across the body.

BTT site measurements provide unique thermal transmission characteristics, facilitating accurate temperature measurements that are not influenced by ambient temperature or vasomotor tone. This is because the tunnel is shielded inside the orbit and the vein lacks external elastic lamina, preventing any significant volume changes. In contrast, the STA (**Figure 1C**) and other facial vessels (**Section 2**) run parallel to the skin surface and are therefore vulnerable to changes in ambient temperature and air velocity. Moreover, their elastic walls makes their caliber prone to variation under different environmental temperatures and emotional states (data not shown, manuscript in preparation). Thus, forehead temperature measurements are unreliable and inconsistent, because they do not accord with physical and biological principles, as demonstrated at other body surface sites (e.g., the wrist and finger).

Notably, another distinction that facilitates unique, accurate, and precise brain thermometry at the BTT site (and the application of brain-based thermal patterns for infection detection) is the lack of an artery accompanying the vein (SOV) of the tunnel (**Abreu et al., 2020a**); this prevents countercurrent heat exchange. In contrast, the vascular system on the body's surface is focused on the presence of an artery–vein configuration (which results in the inherent drawbacks of the artery's presence) and the corresponding internal and external elastic lamina and variable vasomotor tone, which also significantly impacts temperature measurements. For

example, the wrists—another site employed for temperature measurement—consist of radial veins, which are paired veins that accompany the radial artery through the back of the hand and the lateral aspect of the forearm. Furthermore, the finger features a similar pair of palmar and dorsal digital veins and arteries. Thus, wrist and finger measurements, besides exhibiting the wood-like variable low-*k* surface, suffer from the impacts of countercurrent heat exchange and erratically varying vascular reactions.

Furthermore, cold environments induce vasoconstriction; this reduces volumetric heat capacity and leads to cold wrists and finger skin, causing measurement underestimations which may produce false-negative readings that prevent fever detection in adults and children alike. A blood vessel (e.g., radial and ulnar arteries) in the wrist beneath a watch may undergo vasoconstrictive effects from the portion of the vessel outside the region covered by the watch. The same interference occurs beneath finger-worn rings, because this region is vulnerable to blood-volume changes in the palmar and dorsal digital blood vessels. This occurs across the remainder of the body's surface, except at the eyelid skin of the $SMOS_{BTT}$.

Likewise, warm environments also interfere with measurements on the body's surface (except at the $SMOS_{BTT}$). This is exemplified at the wrists and fingers: warm environments induce vasodilation, which increases the volumetric heat capacity and produces warm wrist and finger skin; this leads to overestimations that may result in false-positive readings. Such false detections may cause normal afebrile individuals (including children) to be considered infected and potentially exposed to infected people in a hospital environment or at home.

The numerator of the heat dissipation (and therefore thermal transmission) equation is largely dependent on *k*, whereas the denominator varies with respect to thickness. Because the dermis and fat layers exhibit low *k* values, a lack of fat and a minimal dermal thickness increase the skin's thermal conductivity (**Table #2**). We showed previously (**Abreu et al., 2020a**) that the skin above the BTT terminus is fat-free and features the thinnest dermis, resulting in uniquely radiative high-*k* skin. This is further confirmed by the morphological (**Figure 1D**) and emission studies (**Figures 1A–C**) shown here. Thus, the $SMOS_{BTT}$—as a skin site characterized by high thermal conductivity—represents an optimal body surface region for internal temperature measurements.

The BTT features one unique and highly radiative surface, corresponding to the underlying anterior orbital portion of the tunnel in the right and left eyelids. A single beam of light is generated at each BTT site (**Figures 1A–C)**. The uniquely thermally transmissive and emissive thermodynamics of the brain tunnel and its architecture allow a BTT sensor to measure brain temperatures consistently and continuously. A sensor applied to the radiative surface of the BTT also provides maximally accurate body-temperature measurements—both individually and across populations—via a unique, natural, thermo-physically uniform brain ↔ surface pathway, as demonstrated here and in previous works (**Abreu et al., 2020a; Abreu et al., 2020b).**

Figure 1. Macroscopic, histo-morphometric, and thermal-emission relationships at $SMOS_{BTT}$ for low-*k* forehead surfaces. Bars denote grades of infrared light emission, from highest (gray) to lowest (brown-black). Temperature levels are provided in Table #1 and in the text. (**A, B**) Comparative thermal images of two normal resting subjects' faces [69 years old (Figure A) and 28 years old (Figure B)], depicted as color and gray-scale images with overlying grids to delineate the thermal map and sites of maximal light emission. The grid identifies the right and left BTT as the only sites of maximal light emission in both subjects, demonstrating the inability of forehead thermometry to provide useful COVID-19 measurements in both mature and

young populations. In sharp contrast, BTT° shows consistent emissions across age groups. All infrared images of the $SMOS_{BTT}$ were captured according to the criteria in Table 4.

Figure 1A

Macroscopic, histo-morphometric, and thermal-emission relationships

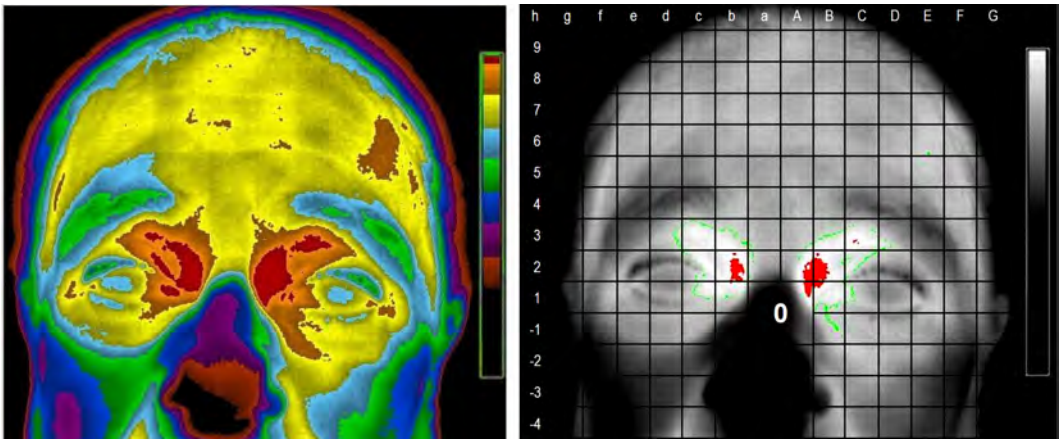

The BTT site shows the maximal thermal emission (red); the b1, 2-A1, 2 and B1, 2 cells in the grid (Table #1) reveal the precise, consistent position of the BTT terminus in the $SMOS_{BTT}$. In contrast, the forehead and STA region have considerably lower temperatures and variable thermal emissions (yellow). One small region far from the BTT (red) and its corona [which corresponds to a < 1.5 mm diameter zone (E6)] exhibited equivalent emissions to the corona, though with far lower emissions than at the BTT. Numerical values given in text and Table #1.

Figure 1B

Macroscopic, histo-morphometric, and thermal-emission relationships

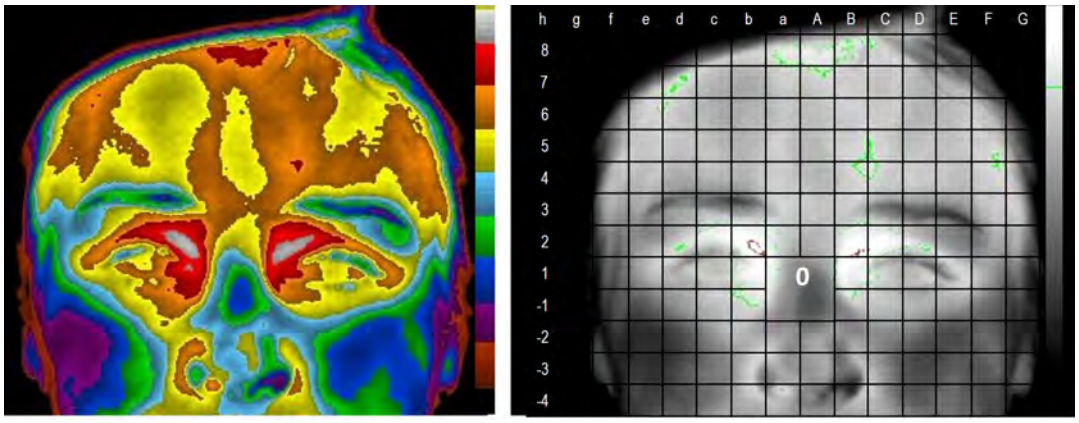

(**B**) The BTT site shows the highest thermal emissions in this young subject, denoted in gray (b1, 2 and B1 in thermal grid; Table #1). This corresponds to the grid cells of the older subjects (Figure 1A). The forehead exhibits low emissions (yellow-orange) and very few areas of green isotherm, concentrated in less than 3% of the total area (Table #1).

Figure 1C

Macroscopic, histo-morphometric, and thermal-emission relationships

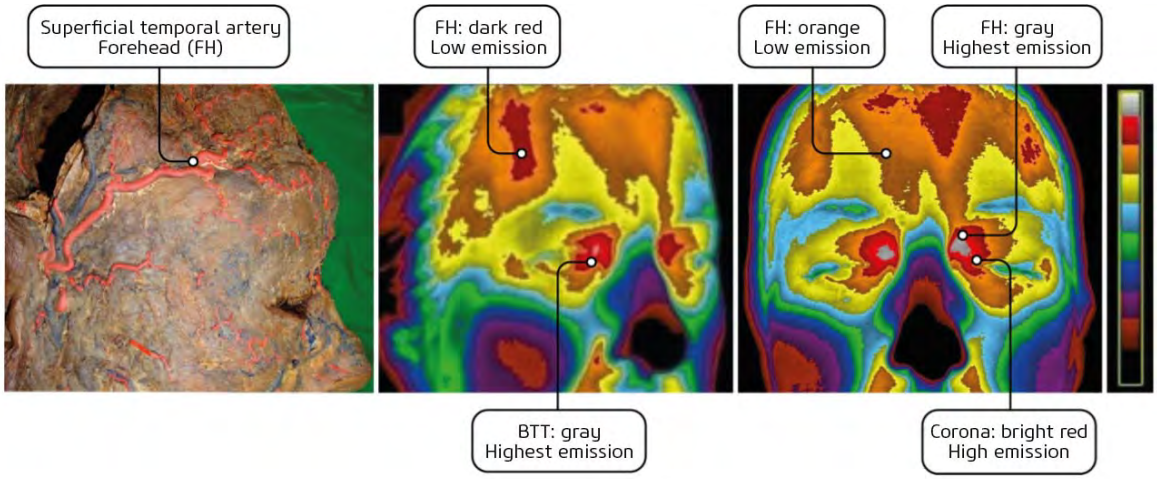

(**C**) Comparison of forehead vasculature and thermal emission. *Left*: Formalinized head showing STA infused with red neoprene. *Middle*: Thermal emission from the side of the face, showing the STA region, which exhibits low thermal emissions (orange and dark red) despite the large-caliber artery; in contrast, the highest emissions are observed at the BTT site (gray) and its corona (bright red). *Right*: Front-view of light emission, showing the BTT in the upper medial eyelid as the area of highest light intensity; the second-highest emission is located in the corona (bright red), whilst the forehead (orange and dark red) and all other facial areas exhibit lower thermal emissions, attributable to the low-k surface (Figure 1D, left and middle).

Figure 1D

Macroscopic, histo-morphometric, and thermal-emission relationships

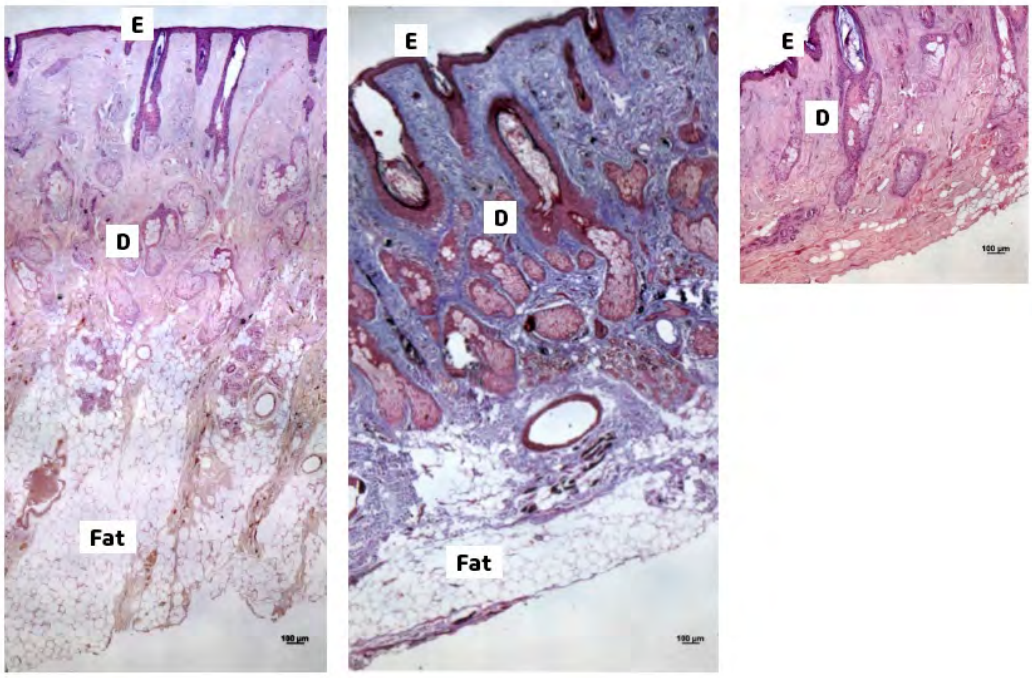

(D) Photomicrographs comparing skin specimens from the forehead and above the BTT. E = epidermis, D = Dermis, SC = subcutaneous. Dimensions given in Table #2. *Left*: The forehead skin has a variable, thick dermis, as well as layers of SC fat. The combined thickness of the SC fat and dermis is so broad that a *three-slide composite* was required to depict all layers together. *Middle:* Markedly different thicknesses and histological structures extracted from the same forehead region in a second cadaver specimen, revealing the flat thick fat layer that comprises one third of the left-hand specimen (Table #2). *Right*: In sharp contrast, the BTT skin specimen has the thinnest D and lacks SC fat, permitting inclusion of all layers in *a single slide.* As reported previously (**Abreu et al., 2020a**), all $SMOS_{BTT}$ specimens exhibited equivalent thicknesses and structures, despite being from cadavers of different races and ages. Scale bars denote 100 micrometers.

Section 2. Macroscopic, histo-morphometric, and thermal-emission relationships of $SMOS_{BTT}$ with periocular and facial surfaces

Next, we focused on vein regions adjacent to the $SMOS_{BTT}$ and anatomic surface regions relevant to thermometry. The BTT terminus in the medial eyelid is the point of convergence for three veins [frontal vein (FV), superior palpebral vein (SPV), and angular vein (AV) (**Abreu et al., 2020a**)]. Notably, all three veins exhibit consistently lower emissions compared to the BTT, which is characterized by a highly emissive central zone with a surrounding corona of lower

emission (**Figures 1A–C**). However, the SPV exhibits a specific, unique pattern of high-intensity thermal emission that declines in proportion to the distance from the medial eyelid at the BTT.

Superior palpebral vein region. To further characterize the region adjacent to the $SMOS_{BTT}$ and obtain a morphological basis for the uniquely radiative emissions along the SPV, we dissected an SPV region adjacent to where it joins the BTT site, and we performed a histo-morphometric analysis of the specimens obtained. Remarkably, the SPV skin region is devoid of fat and features a similar structure and dimension (~900 μm) to the eyelid skin of the $SMOS_{BTT}$; that is, the skin thickness and structure is equivalent to that of the BTT skin, and both anatomic regions (SPV and BTT) lack a fat layer (**Figure 2A**). This corroborates the fact that, without an underlying tunnel, thermal emissions on the body surface (except the eyelid region of the $SMOS_{BTT}$) do not correspond to the internal (brain or core) thermal status of the human body, even if measured through minimal or a complete absence (as with SPV) of fat. This applies to all body surface sites currently used for thermometric COVID-19 screening, including the wrist, finger, arm, chest, and forehead, as detailed in Section 4. The reduction of SPV emission with respect to distance from the BTT site further indicates the lack of an underlying thermal path—akin to the MCF ↔ SMOS transorbital thermal tunnel—from the middle cranial fossa (MCF) (**Abreu et al., 2020a**).

The difference between highly vascularized facial sites (e.g., the forehead) and the BTT site at the medial upper eyelid is largely attributable to the consistently thin and fat-free high-*k* skin of the $SMOS_{BTT}$ (**Figure 1D**). However, the essential feature required for the unique light emission capacities and minimal inter-subject variability we identified is the presence of an underlying tunnel consisting of a biological thermal waveguide (with the heat of the blood as the active region and the fat as the "thermally reflective" interface). This unique thermally transmissive brain-tunnel structure combines an external interface (i.e., a fat-free surface overlying a blood/fat tunnel configuration) with an internal terminus in thermal continuum with the hypothalamus. This allows a BTT sensor on the eyelid skin to acquire undisturbed brain thermal energy signals, thereby providing the most accurate body temperature measurements and thermoregulatory assessments (**Abreu et al., 2020a; Abreu et al., 2020b**).

Angular vein region. Likewise, despite its rich and large vascular network (**Figure 2B,** left panel), which includes large-caliber vessels (the angular vein and artery), the malar region exhibits low thermal emissions [shown in orange-yellow-blue in the middle panel, in contrast to the highest intensity (gray) at the $SMOS_{BTT}$]. This is attributable to the low-*k* histology (thick dermis and fat layers, shown in the right panel) and the lack of an underlying tunnel (**Abreu et al., 2020a**).

Neck. Despite containing major vessels such as the jugular vein and carotid artery [which communicate with the BTT via the triunal system (**Abreu et al., 2020a**)], the neck likewise produces low thermal emissions (**Figure 2C**, left panel) and is a low-*k* surface, owing to the thick dermis/fat histology (**Table #2**) and the lack of an underlying tunnel. Hence, the neck (like the malar and forehead regions), despite containing large-caliber vessels, fails to produce a thermal emission comparable to that of the eyelid at the $SMOS_{BTT}$.

The thermal-emission evidence for the inability of forehead measurements (and general skin-surface measurements, except at the $SMOS_{BTT}$) to accurately detect infection (owing to their violation of physical and biological principles for effective and undisturbed heat transfer) is displayed in the thermal emission data for a 53-year-old female, shown in **Figure 2C**. As clearly seen, the forehead is very cold (blue and green isotherms) and has a temperature 3.0 °C lower than at the $SMOS_{BTT}$ (shown in gray), which represents the region of highest thermal emission. The low thermal emission observed in **Figure 2C** reflects the temperature of a *local* cold tissue, as opposed to the true *internal* heat status of the body, as measurable at the BTT site.

If the forehead thermometry procedures in use around the word (as documented in **Section 4**) measure the temperature of populations with similar thermal characteristics to the subject of Figure 2C, who produces a forehead reading 3.0 °C colder than their body's true thermal status, then the measured forehead temperatures will deceptively indicate normothermia (or hypothermia) and fail to identify fevers in infected populations (e.g., those infected with SARS-CoV-2). This can occur at the individual level or during mass screenings at airports, hotels, cruise ships, military bases, ports of entry, schools, large entertainment venues, and more (as documented below). These false-negative readings may increase virus spread and replication, promote mutations, and increase morbidity and mortality through delays in care.

Axilla. Another skin site frequently used for temperature measurements, the axilla, illustrates the combination of low-*k* barriers with highly variable fat layers. In contrast to the skin at the $SMOS_{BTT}$, which exhibits the thinnest dermis (**Table #2**), the axilla and the remainder of the body surface [except the SPV region (**Figure 2A**)] is characterized by the presence of fat and a thick dermis layer. This is exemplified in the axilla specimen of two corpses (**Figure 2D**), where a large low-*k* barrier comprised of thick dermis and fat is clearly shown. Macroscopically, the dermis is visible as a thick white band between the epidermis and fat. Histologically speaking, due to its thickness, the dermis encompasses most of the slide. Axillary temperature measurements and thermometry on other body surfaces suffer similar impediments to the forehead, owing to the low-*k* barrier. This leads to false-positive and -negative readings for the forehead (as illustrated in **Section 3)**. Thermophysical barriers that create a thermal wall in the human body become barriers that preclude effective COVID-19 countermeasures, because measurements on any skin surface (asides from at the $SMOS_{BTT}$) encounter a combination of low-*k* tissues and highly variable thicknesses and structures between subjects; this prevents the clinically useful readings required during pandemics from being obtained.

Figure 2. Macroscopic, histo-morphometric, and thermal-emission relationships of $SMOS_{BTT}$ with periocular and facial surfaces. Bars represent grades of infrared light emission, from highest (gray) to lowest (brown-black). Temperatures are stated in the text. Comparison of macroscopy, microscopy, and thermal emissions for areas adjacent to the BTT and the low-*k* surface used for thermometry. All infrared images of the $SMOS_{BTT}$ were captured according to the criteria of Table 4.

Figure 2A

Periocular macroscopic, microscopic, and thermal-emission relationships

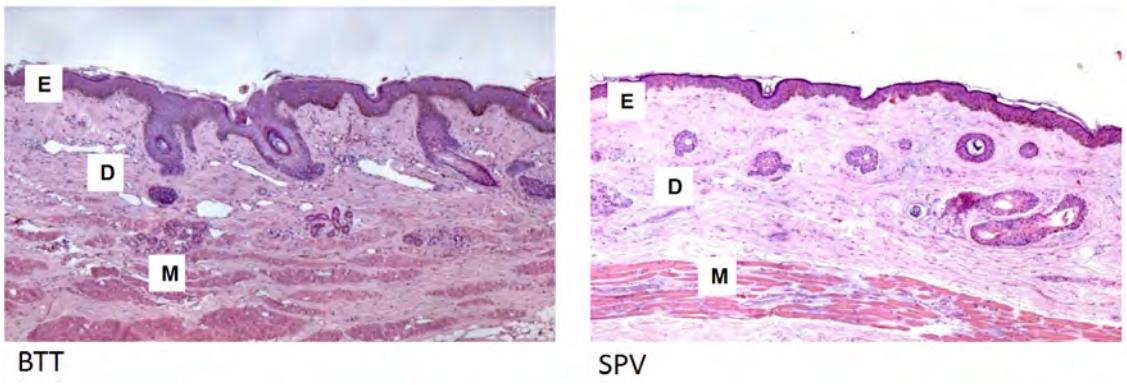

(**A**) Skin histology comparisons, showing the similar skin histomorphometries of the BTT (left) and SPV (right). Both skin specimens have thin D and lack SC fat layers (900 microns). The orbicularis (left) and tarsal (right) muscles are visible below the dermis; these reveal unique morphologies in the body, where the dermis rests directly on muscle (M).

Figure 2B

Macroscopic, microscopic, and thermal-emission relationships for low-k surfaces

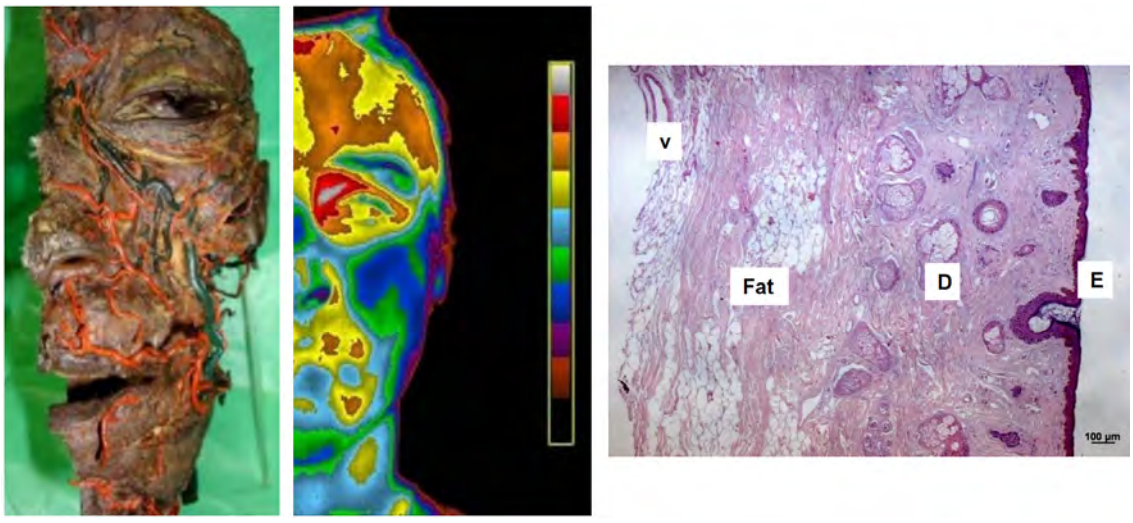

(**B**) Vasculature, thermal emissions, and histology of malar region (angular vein). Left: Formalinized hemiface injected with red neoprene (arterial system) and blue (venous system) to show large-caliber arterial and venous facial networks. Middle: Thermal emissions from the

hemiface (28-year-old male), showing lower temperatures throughout the face and forehead (blue-green-yellow) compared to the $SMOS_{BTT}$ (gray), which exhibits the maximal thermal emissions. Right: Photomicrograph of malar region, showing the thick dermis and SC fat layers with a blood vessel (V) beneath the fat layer; this results in low thermal emissions owing to the histology (thick dermis and fat), despite the large-caliber vessels. Scale bars denote 100 micrometers.

Figure 2C

Macroscopic, microscopic, and thermal-emission relationships for low-k surfaces

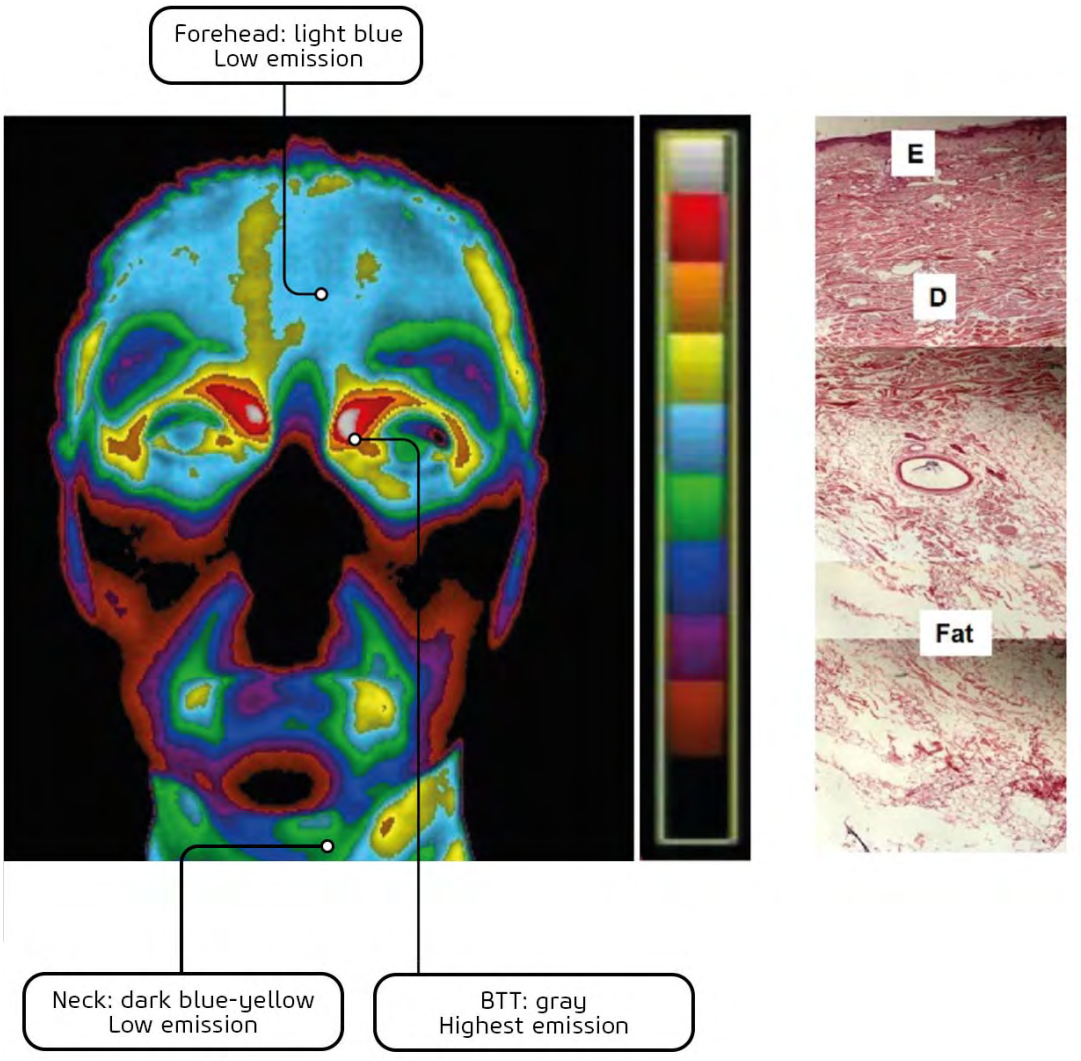

(**C**) Thermal emissions and neck histology. *Left*: Facial thermal emissions, showing low emissions from the neck, despite its large jugular vein and carotid artery. Note the very cold forehead (shown in blue-green), in contrast to the high-intensity eyelid emission at the BTT (cone shape), which features a center of maximum intensity (gray) surrounded by a lower-intensity region (red). *Right*: Photomicrograph showing thick dermis and fat layers, which produce a low-*k* barrier in the neck (Table #2). The infrared image was captured according to the criteria in Table 4. Data were acquired in a controlled ambient temperature of ~22 °C.

Figure 2D

Macroscopic, microscopic, and thermal-emission relationships for low-k surfaces

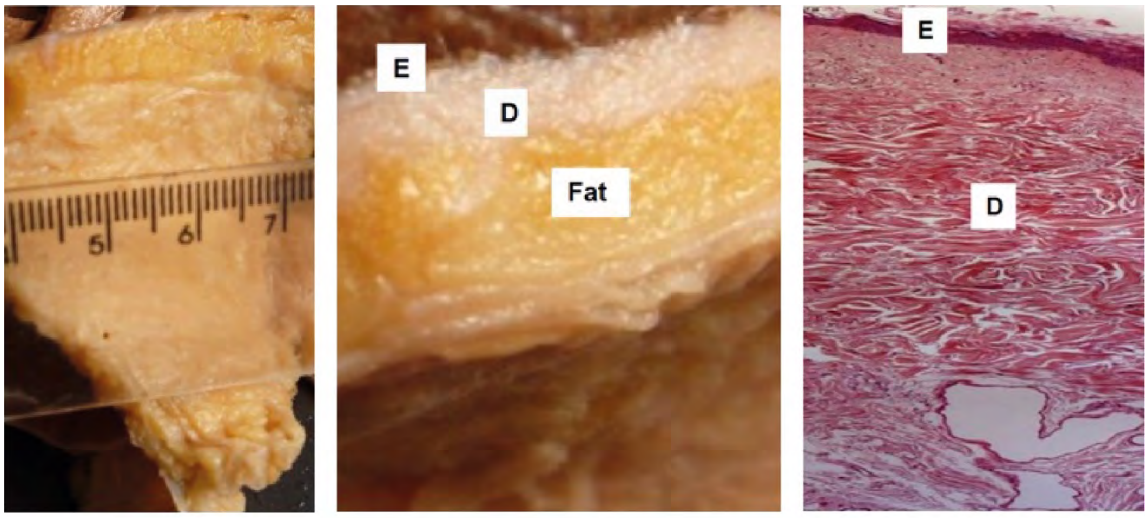

(**D**) Axilla: gross sections from two corpses (left and middle panels), showing thick dermis and sizeable variability in dermis and fat layer thicknesses (Table #2). The adipose tissue measures from 3 mm (in certain regions) up to 8 mm (where considerable fat remains in the axilla of the corpses, between the blood vessels, nerves, and lymphatics). The right panel depicts a photomicrograph showing the histology of the dermis (2500 µm) in Corpse #2, corresponding to the white area in the gross section.

Section 3. Quantification and models of inter-site distinctions for BTT, core, and forehead temperatures.

In all subjects, sites outside the $SMOS_{BTT}$ (e.g., the forehead) were "silent" for high thermal emissions, as further evidenced in **Movies #1–3 (see Supplemental Information)**. These show a single beam of light being generated at the $SMOS_{BTT}$ (represented by red pixels) and uniquely present in the eyelid there. These findings confirm that the intra-orbital blood/fat tunnel configuration (**Abreu et al., 2020a**) and external high-*k* skin surface (**Figure 1D**) facilitate the

emission of two high-intensity light beams in each of the upper medial eyelids (right and left) (**Figures 1A–C, 2C**), and these are thermally connected with the brain's thermoregulatory center (**Abreu et al., 2020a**). However, no other facial or body region produces the high-intensity beams that characterize the emission found in the $SMOS_{BTT}$ eyelid skin.

Inter-site quantification. To more effectively quantify the inter-site distinctions identified by thermal imaging and thermometry, we assessed 59 data points obtained from 16 volunteers seated in a temperature-regulated room (mean temperature: 22 °C). BTT° was recorded as the highest temperature obtained by a sensor (without correction factor) positioned over the $SMOS_{BTT}$ for 5 s (device shown in Section 8). Forehead temperature (FH°) was assessed with the same sensor, to capture the maximum temperature over 5 s at a nonspecific site above the brow on the ipsilateral forehead. Body core temperatures were measured as sublingual (SL°); via a thermometric catheter placed under the tongue for 3 min. Each subject was tested once daily for 2–5 successive days at the $SMOS_{BTT}$ (BTT°) and sites of core (SL°) and surface (FH°) measurement.

Mean (± SD) values were: BTT°, 36.29 ± 0.4 °C; FH°, 34.29 ± 0.8 °C; and SL°, 36.11 ± 0.5 °C. The difference between FH° and SL° (2.02 ± 0.7 °C) was significantly greater than that between BTT° and SL° (-0.21± 0.5 °C) ($p < 0.001$ by paired t-test). As seen in the comparative Bland-Altman plots (**Figures 3A and 3B)**, FH° was greater than SL° in every comparison. Bias (95% limits of agreement) for SL°-BTT° were -0.21 °C (-1.16, 0.73). In contrast, bias (95% limits of agreement) for SL°-FH° were 2.02 °C (0.53,3.51).

The variability among FH° readings and their failure to record temperatures equivalent to SL° and BTT° were consistent with our thermal-emission investigations (**Table #1**). These distinctions are attributable to the vascular tone and varying thicknesses of forehead fat and dermis layers within and between individuals (**Table #2**). Even at its most transmissive point, the forehead temperature remained below that of the BTT and oral mucosa (core). Unless corrected, forehead thermometry for individuals—as well as forehead thermal imaging for mass screening—will produce underestimations, which may occur even if correction or "fudge" factors are added when measuring very low-*k* surfaces with variable thicknesses and variable vasomotor tone. This is illustrated by the subject of **Figure 2C**, who has a very low forehead temperature that would prevent a potential SARS-CoV-2 infection being detected even if adding a correction factor (shown below). Likewise, overestimation can occur, as exemplified by the direct reapplication of the artificial correction factor used for the subject of **Figure 2C** to a subject with a forehead temperature ~1.5 °C higher (i.e., the subject of **Figure 1B**). This forehead measurement causes an individual with a true temperature of 37 °C to be falsely diagnosed with one of 38.5 °C, leading to a false fever diagnosis and placement of healthy individuals in quarantine with infected individuals. Asides from causing injury to healthy individuals, this misinformed action can promote the spread of COVID-19.

Correction factors can confound assessments (individual and mass screening), because applying the same correction factor to correct temperature interferences recorded by the body's thermal barrier introduces an error when the factor is too high or low for a given patient, in accordance with the wide range of inter-site differences shown in **Table #2** and **Figures 1A–C, 2C**.

Integrated anatomo-histological and thermal-emission models. We combined our histo-morphometric and thermal-emission findings to generate a schematic image of the tunnel that connects the high-*k* skin to the hypothalamus, to illustratively and numerically represent the sizeable detrimental impact of adding a correction factor to body thermal status measurements

obtained across low-*k* surfaces (e.g., the forehead), as shown in **Figures 1B, 2C** (algorithms and correction factors tend to add 0.7–1.4 °C; here, we adopt a value of 1.0 °C for illustrative purposes). FH° is equivalent to measuring the temperature of various types of wood, owing to the sizeable and unmeasurable variability in the quantity and thicknesses of fat and dermis layers (**Figure 1D**). This can be observed from the large variability of thermal emissions (**Figure 1B, 2C**).

Here, false-negative readings are produced because the thick fat layers, which generate low thermal emissions (**Figure 2C**), cause the true temperature of 38.2 °C to be underestimated to 37.0 °C under the forehead (or any surface) thermometry procedure (even when adding a correction factor of 1.0 °C to the true measured value of 36.0 °C; **Figure 3C**). In contrast, the fat-free and thin dermis layers overlying a high-heat-capacity tunnel allow the true thermal status of the body to be captured and fever temperatures (38.2 °C) to be detected, thereby facilitating the prevention of virus spread. Likewise, false-positive readings occur through surface anatomies (e.g., foreheads, wrists, fingers) featuring thin fat and dermis layers; these are represented as a thin, flat slab—corresponding to a thin fat layer—which generates higher thermal emissions (**Figure 1B**). This causes the true temperature of 37.1 °C to be overestimated to 38.1 °C using forehead thermometry (owing to the correction factor of 1.0 °C added to the measured forehead value of 37.1 °C; **Figure 3D**). In contrast, the high-*k* fat-free skin of $SMOS_{BTT}$ combined with stable high volumetric heat capacity does not require a correction factor; thus, it validly captures the true thermal status of the body (**Figure 1D; Supp. Fig. 44**); in contrast, a false fever is obtained by low-*k* thermometry combined with correction factors (**Supp. Fig. 42**). Hence, temperature measurements at highly variable low-*k* surfaces can facilitate spreading, thereby increasing the likelihood of mutations. This further emphasizes the need for temperature measurements that require no correction and invoke physical and biological principles for undisturbed heat transfer, to help interrupt human-to-human transmission in the context of the COVID-19 pandemic.

Figure 3. Quantification and models of inter-site distinctions for BTT, core, and forehead.

Figure 3A

Quantification and models of inter-site distinctions for BTT, core, and forehead

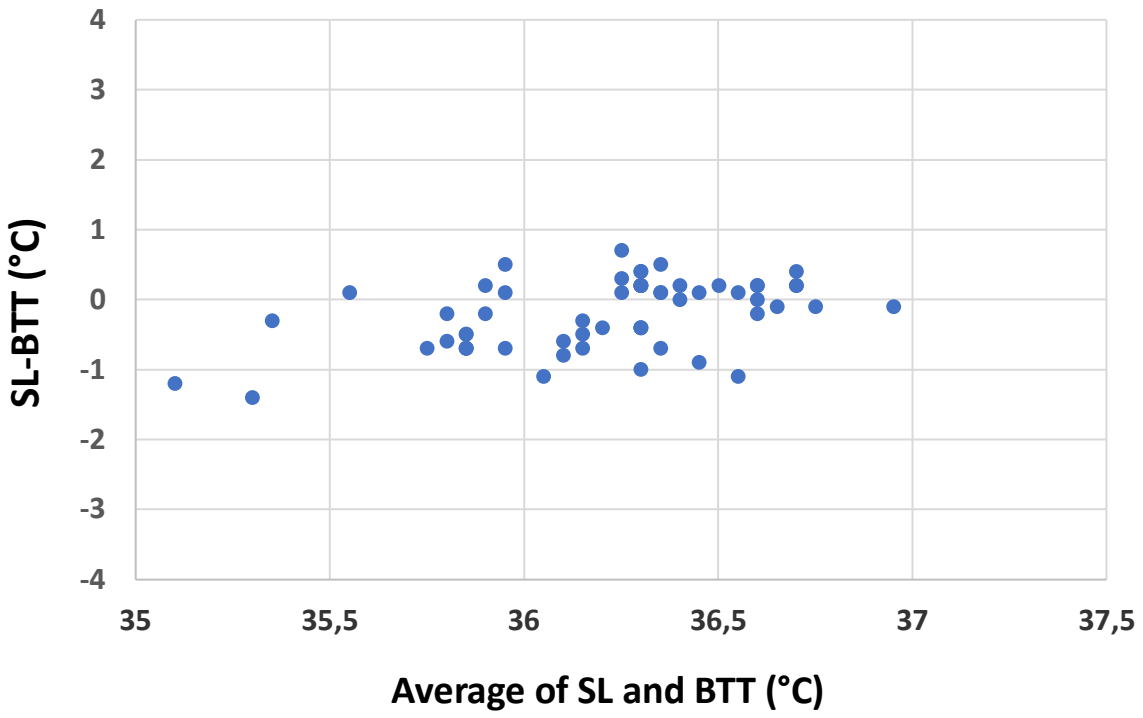

(A) Bland-Altman plot comparing Core° (obtained with thermistor placed under tongue for 3 min) and BTT° readings in healthy volunteers, on up to five different days (per text). Bias (95% limits of agreement) for SL°-BTT° were -0.21 °C (-1.16, 0.73). Temperature in Celsius (°C).

Figure 3B

Quantification and models of inter-site distinctions for BTT, core, and forehead

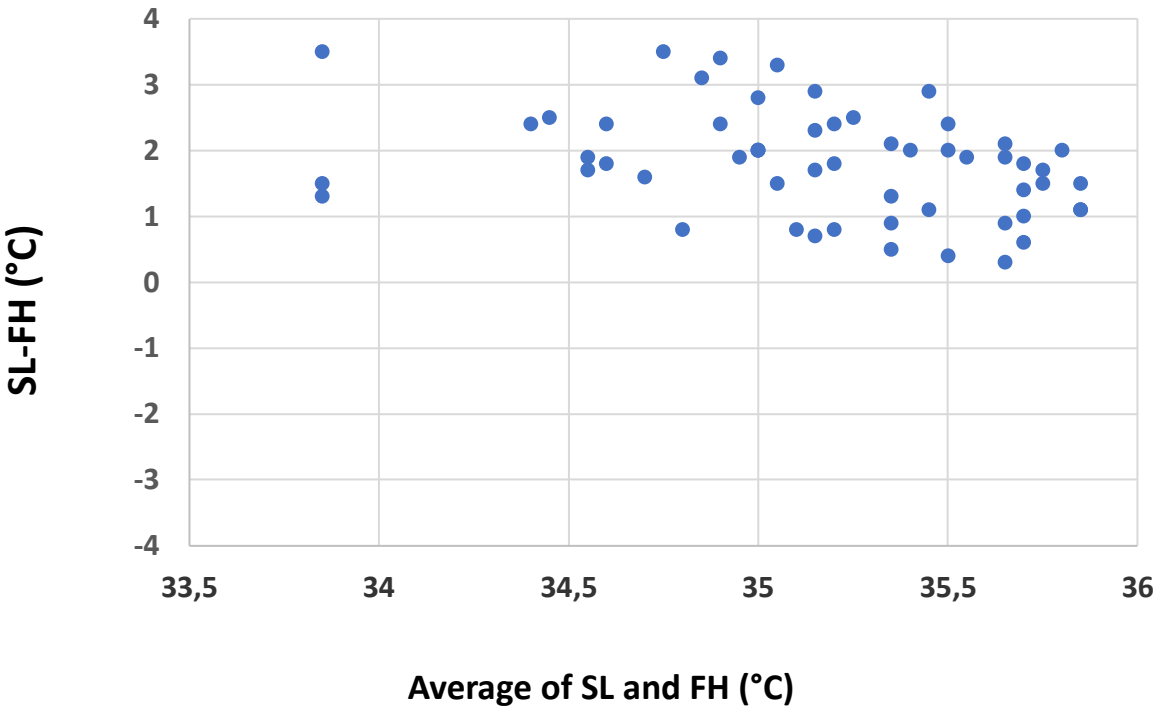

(B). Bland-Altman plot comparing Core° (SL°) and FH° readings in healthy volunteers (per 2 text) on same axes as Figure 3A. Bias (95% limits of agreement) for SL°-FH° were 2.02 °C 3 (0.53,3.51).

Figure 3C

Quantification and models of inter-site distinctions for BTT, core, and forehead

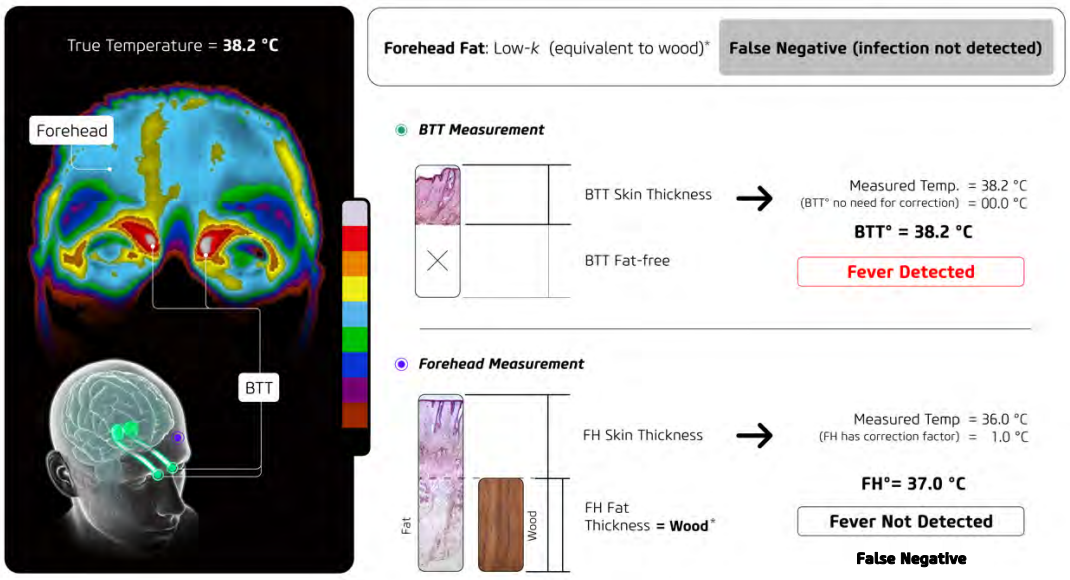

(**C,D**) Schematic construction and combination of thermal-emission and histo-morphometric information, with numerical thermometry values extracted from thermal imaging values (illustrated for a model adding an average correction of 1.0 °C). Colored bars denote the emission levels, from highest (gray-red) to lowest (black-brown). The left panel shows (upper) a colored thermal image of the $SMOS_{BTT}$ at the eyelid, forehead, and periocular regions; and (lower) the BTT external terminus, which is connected with the hypothalamic region at the BTT internal terminus (green). The BTT site (gray-red color) in the thermal image is illustratively connected to the infrared light source in the brain (hypothalamus). Variable and low-*k* values for FH produce different thermal emission zones of FH, in contrast to the single area of maximum light emission observed in the eyelid at the $SMOS_{BTT}$. Microphotographs: (i) (upper) fat-free thin dermis histology, which corresponds to the $SMOS_{BTT}$ and area of highest thermal emission in the image; and (ii) (lower) FH skin characterized by thick, variable fat and dermis layers, corresponding to areas of low and variable thermal emission. The thick fat and dermis layers in (B) and thin fat layer in (C) show a variable low *k* value between different specimens. Numerical values: (upper) BTT° without correction factors, corresponding to true undisturbed temperature and (lower) forehead measurements obtained with current thermometers, using a correction factor. See text for numerical details.

(**C**) Left panel: FH thermal image showing very low emissions (blue-green), in contrast to the highest emission of at the eyelid $SMOS_{BTT}$ (horn shape shown in gray-red color). The different thicknesses between the BTT and FH skin can be observed. The thick fat layer (thermally equivalent to thick wood) and dermis leads to underestimation of the true temperature, and to false-negative readings.

Figure 3D

Quantification and models of inter-site distinctions for BTT, body core, and forehead

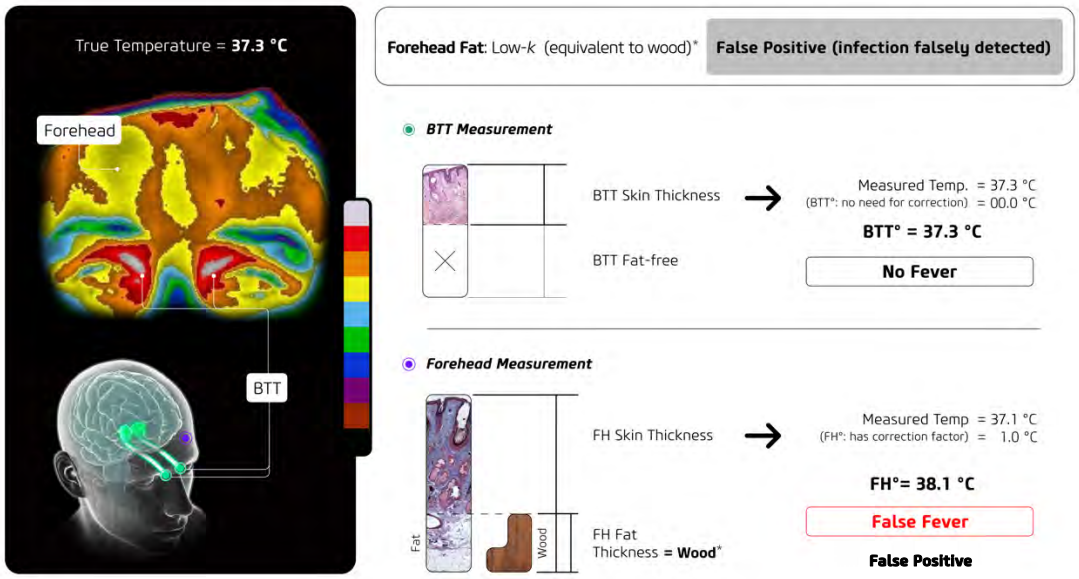

(**D**) Left panel: Thermal image of FH, showing low emissions (orange-yellow), in contrast to the highest emission at the eyelid $SMOS_{BTT}$ (gray-red). The FH of (C) produces a higher emission than (B) because of the thinner fat layer; this results in a higher FH°. The thickness differences between the BTT and FH skin can be observed: the thin fat layer (thermally equivalent to thin wood) produces an overestimation of the true temperature, leading to false-positive readings.

Section 4. Impacts of vasomotor tone and low thermal conductivity on temperature measurements; epidemiologic implications for infection spread.

To further characterize the effects of low-*k* thermometry on COVID-19 spread and the influence of the environment, countercurrent heat exchange, and reactive vascular zones upon temperature measurements taken through low-*k* skin, we assessed the thermal-emission response of the BTT and face to the externally induced vascular tone activation and cooling.

We tested the impacts of dynamic confounding factors upon thermal emission during facial fanning (speed: ~5 cm/sec; 13–15 °C). The thermal imaging assessment showed that the underlying facial vasculature (including the forehead) was incapable of maintaining consistent thermal emissions. BTT emissions were also—though to a lesser extent—affected (**Figure 4A**) by

the lack of skin insulation; this led to surface cooling at the $SMOS_{BTT}$, as detailed in **Section 5**. The temperature of all facial regions decreased significantly over time (a → d → h → l), reaching ~4.0 °C in the last of the 12 frames (2 min/frame). Even the SPV values fell markedly, and FH° was reduced by 2.0 °C after only 6 mins (Frame **c**), reaching 3.5 °C below the baseline by the end of the study. Such dramatic temperature changes under vasoconstrictive stimulation are consistent with the vaso-responsiveness of cutaneous vasodilation, which occurs in response to local pharmacological confounding factors; this produces a 3.3 °C increase in skin temperature (**Silverman et al., 1987**).

The surface temperature increase of 3.3 °C in the thigh, induced by a topical drug that causes vasodilation, matches the 3.5 °C decrease in forehead skin temperature generated by external thermal confounding factors that induce vasoconstriction. Notably, these large temperature variations occurred in distinct anatomic regions, revealing large variations of the cutaneous thermal response across the body surface. This marked and unpredictable response of cutaneous perfusion—induced by the myogenic effect—cannot be predicted by algorithms or correction factors, owing to the considerable variability in (a) the cutaneous vascular response and (b) the quantity of fat within a single individual over time and between individuals (from thick, multilayered layers to single, flat thin ones, as shown histologically in **Figure 1D)**.

Fanning-generated thermal confounding factors reduced BTT° by ~0.9 °C with respect to the baseline, owing to the lack of insulation covering the $SMOS_{BTT}$. The need for an unobstructed view during thermography means that environmental changes significantly influence the assessment and hinder the detection of febrile states. This leads to a reduced BTT° and confirms that insulation of the $SMOS_{BTT}$ is required for accurate BTT temperature measurements. As shown in previous studies and herein (for exercise in a hot chamber), the resilience of BTT° to environmental impacts results from the use of highly insulated high-resolution sensors (**Abreu et al., 2020a**; **Abreu et al., 2020b**), which is consistent with isolated head cooling (but does not lead to brain cooling), as measured invasively via intra-brain catheter (**Mariak et al., 1999**) and by acoustically evoked brain-stem potentials (**Jessen & Kuhnen, 1992**). This is in contrast to the reduced BTT° obtained by thermal imaging, confirming that insulation of the BTT site and its periphery is mandatory for acquiring accurate measurements via BTT, which in turn are necessary for early COVID-19 detection.

The rapid 2.0 °C reduction of FH° (**Figure 4A**) may cause the true temperature of 38.2 °C to fall to 36.2 °C in only 6 minutes (through variable vascular perfusion); this can lead to false-negative readings, causing the virus to go undetected. This rapid (6 min) thermal change, coupled with an unpredictable 6.8 °C variation of body-surface temperature (except for the eyelid $SMOS_{BTT}$) and a baseline thermal status 3.0 °C lower than the true thermal status (**Figure 2C**), prevents the forehead and any low-*k* skin site with reactive vascularity (e.g., wrist, finger, arm, chest, etc.) from providing reliable temperature measurements. This creates a challenge for the detection of early febrile states at the $SMOS_{BTT}$ if the BTT site is left uninsulated. However, as discussed later, the Abreu-BTT Brain-Eyelid Thermometry Technique allows standard noncontact infrared thermometers to obtain clinically useful temperature measurements for COVID-19 screening at the $SMOS_{BTT}$.

Accurate thermometry is more critical than ever because failure to address children—who may freely spread the virus (including the more transmissible variants—can lead to perpetuation of the pandemic, resulting in surges such as the world is currently experiencing. Furthermore, because COVID-19 may rival the 1918 pandemic (**Gates, 2020**) that killed 100 million people and destroyed economies (**Johnson & Mueller, 2002; Tomes, 2010)**, it is vital to implement infection

detection in children and determine the epidemiological aspects of rapid virus spreads such as that of 1918.

Notably, the 1918 outbreak occurred in military camps in Europe, and the final trigger for the devastating pandemic was the interaction of troops with the general population (**Oxford et al., 2002; Oxford et al., 2005**). The same risk is present today for uncontrolled COVID-19 spreading through large crowd settings; these include military bases and civilian gatherings that contain thousands of people in close proximity. The risk of virus entry and spread in military facilities—which also exposes military personnel to disease and death—is increased by the efforts to protect lives, which are decidedly commendable, but that are, unknowingly, relying on low-*k* thermometry in highly reactive vascular zones, as shown exemplarily in military bases and checkpoints, illustrated in China, Israel, Russia, and the U.S. (**Table #3** and **Supp. Figs. 1–7)**.

Preventing human-to-human transmission in military bases and posts (**Supp. Figs 1–7**) and military ships (**Baldor, 2020; Kasper et al., 2020**; **French Armed Forces, 2020; Simkins, 2020**) may prevent the widespread infection of communities observed in previous pandemics (**Oxford et al., 2002; Oxford et al., 2005**), whilst also preventing loss of military personnel as occurred (**LaGrone, 2021**), with spreading more likely at this stage owing to more transmissible variants (**Sheikh et al, 2021**).

Civilian settings containing large crowds also rely on low-*k* thermometry; thus, they may fail to detect COVID-19, thereby providing another environment for SARS-CoV-2 spreading, as exemplified by an indoor concert in Germany (**Supp. Fig. 8**), a hotel and casino in the U.S. (**Supp. Fig. 9**), a construction site in China (**Supp. Fig. 10**), a factory in France (**Supp. Fig. 11**), and a large U.S. amusement park (**Supp**. **Fig. 12**). Considering the current more contagious variants, even outdoor settings (e.g., stadiums) that rely on low-*k* thermometry and variable vascular activity may promote spreading, illustratively shown in settings in Australia, Japan, and the Netherlands (**Supp. Figs. 13–15**). This supports the conclusion that effective brain-based high-*k* thermometry practices are urgently required for both indoor and outdoor venues around the world.

Low-*k* thermometry-based efforts to screen for COVID-19 are also commonplace in high-risk locations for COVID-19 spreading, including healthcare environments (**Supp. Figs. 16, 17**) and schools, as shown in Indonesia, Russia, U.K., and the U.S. (**Supp. Figs. 18–22)**. This is even more critical because children can present with high viral loads and potentially become major mutation reservoirs.

Reliance on low-*k* measurements of highly reactive vascular surfaces in ports of entry [illustratively shown in Austria, China, Hong Kong, Italy, Mexico, Nigeria, Pakistan, and the U.S. (**Supp. Figs. 23–30**)] may cause passengers to readily spread dangerous variants around the globe. Effective infection detection is even more important in these scenarios because "vaccine passports" may allow the free movement of infected populations, and these fully vaccinated individuals can spread COVID-19, as reported by the U.S. Government authorities (**CDC, 2021a; CDC 2021b**).

An epidemiologically crucial scenario occurs at sea, as evidenced by previous widespread SARS-CoV-2 infections on military ships (**Baldor, 2020; Simkins, 2020**) and cruise ships **(Mallapaty, 2020)**. Reliance on low-*k* thermometry in reactive vascular surfaces (**Supp. Fig. 31**) or thermal imaging (covered in Section 5) for infection screening prior to boarding may fail to detect infection, resulting in uncontrollable spreads, as occurred onboard the Diamond Princess (**Dahl, 2020**). However, surges at sea might now be caused by more harmful variants and carried by fully-vaccinated people **(CDC, 2021a; CDC 2021b**), further emphasizing the need for fever-

detection procedures in concert with physical and biological principles, both prior to boarding and during travel.

Locations such as restaurants and stores in which people congregate in proximity for long periods of time and which rely on low-*k* thermometry are at risk of COVID-19 spreading, as observed around the world, and exemplified here in South Korea, the U.S., Brazil, and Israel (**Supp. Figs. 32–35**). Even government facilities—which rely on thermometry practices not in concert with physics and biology—are at risk of a single infected host entering a government building and infecting people inside, whether unintentionally or intentionally, exemplarily shown in facilities in Russia, Thailand, Ukraine, and the U.S. (**Supp. Figs. 36–39**). This is exacerbated by the fact that infections can be spread by individuals with "vaccine passports," because the fully vaccinated can spread COVID-19, as reported by the U.S. authorities (**CDC, 2021a; CDC, 2021b**).

All this emphasizes the vital importance of appreciating insulating barriers and highly reactive vascular zones, which are critical as the COVID-19 pandemic moves toward a new unknown and unpredictable phase in late 2021. A potential false sense of protection could unknowingly result in SARS-CoV-2 entry and *spreading within* large crowds and/or high risk settings (e.g., airplanes, amusement parks, casinos, cruise ships, factories, hotels, military bases, restaurants, schools, stadiums, and stores), and from there *spreading to* communities at large, despite consistent current temperature checks (**Table #3**) and vaccination programs.

Tympanic thermometry (**Supp. Fig. 40**) is not in concert with physics and biology for optimal and unobstructed heat transfer either, and may also lead to virus spreading. Something as trivial as ear wax can insulate the heat source; this has been indicated by several studies confirming the unreliability of ear thermometry for measurements (**Geijer et al., 2016; Mogensen et al., 2018; Niven et al., 2015; O'Brien et al., 2000**). Furthermore, cerumen must be removed for proper temperature measurement; this is impractical and risks COVID-19 contagion. Interestingly, non-thermally-configured sites such as the ear canal also conflict with protective biology because removal of wax impacts the natural protection offered by cerumen's antifungal and antibacterial functions (**Lum et al., 2009**).

We report the anatomo-histologic (Sections 1 and 2) and vascular physiology of surface regions (used by current thermometry) that shows low-*k* and unpredictable thermal variability. The persistence of worldwide reliance on temperature measurements in these low-*k* and highly variable regions from the beginning of the COVID-19 pandemic to the present date—and its crucial epidemiological implications of potentially hastening spread and thereby promoting mutations—is illustrated and evidenced by measurement of forehead temperatures at schools in the U.K. in 2020 (**Figure 4B**), which was repeated at the entrance of a theater in London in May 2021, a year later, during the Delta variant surge there **(Figure 4C**); the same low-*k* and highly reactive vascular thermometry practice was also recently repeated (on July 2021) in India during the surge COVID-19 (**Figure 4D**).

The practice of low-*k* thermometry and highly variable reactive surfaces for COVID-19 screening has been extended to other body regions, including the finger (**Smarr et al., 2020**) and wrist. Efforts to detect infection and prevent COVID-19 spreading via wrist thermometry is shown exemplarily at the entrance of a US Army Command Center **(U.S. Department of Defense, 2020, Figure 4E)**. These measurements over variable low-*k* surface areas with unpredictable and variable vasomotor activity may significantly compromise—if not entirely prevent—attempts to obtain clinically useful temperature measurements. The variable low-*k* and variable volumetric heat capacity that characterizes wrist morphology and physiology creates a biological and thermophysical barrier for achieving detection of the body's thermal status necessary in the context

of COVID-19, and these measurements may be impacted not only by environmental but also emotional factors, potentially leading to false negative and false positive readings (**Supp. Fig. 41**). The unpredictable combination of multiple and variable thermophysical features, ranging from thermo-conductivities and volumetric heat capacitances under variable vascularity—which prevent clinically useful body temperature measurements—present across the body surface (except at $SMOS_{BTT}$) is shown representatively here for the forehead and wrist (**Supp. Fig. 42**); all are vulnerable to the impact of environmental and even emotional factors, which may hasten COVID-19 spreading and thereby facilitate mutations. In sharp contrast, the stable volumetric heat capacity of the SOV—which is shielded inside the skull (shown in radiologic image of Section 5) and therefore immune to environmental impacts—is present in the high-*k* radiant eyelid skin uniquely found at the $SMOS_{BTT}$; furthermore, the use of an appropriate methodology [i.e., the Abreu-BTT Brain-Eyelid Technique (**Supp. Fig. 43**)] can produce clinically useful measurements and accurate detection of the body thermal status, applicable to standard infrared thermometry without correction factors (**Supp. Fig. 44**), which can be immediately implemented freely by any country or community employing standard thermometers.

Table 3. Global reliance on low-*k* temperature measurements

Supp. Fig.	Country	Location	Source
	Military Base and Checkpoint		
Supp. Figure 1	China	Armed Forces Checkpoint	Chiu, K. (South China Morning Post, 2020)
Supp. Figure 2	Israel	Military Base	Davis, R. (AJN, Times of Israel, 2020)
Supp. Figure 3	Russia	Military Base	Reuters Staff (Reuters, 2020)
Supp. Figure 4	U.S.A, Hawaii	Air Force Base	Military Health System (health.mil, 2020)
Supp. Figure 5	U.S.A, North Carolina	Marine Base	US Dept of Defense (Finerty M, 2020)
Supp. Figure 6	U.S.A, South Carolina	Army Base	US Dept of Defense (Shea A, 2020)
Supp. Figure 7	U.S.A, Virginia	Navy Checkpoint	Werner, B. (USNI News, 2020)
	Large Indoor Entertainment Venue		
Supp. Figure 8	Germany	Indoor Concert	Associated Press (CBC, 2020)
	Hotel		
Supp. Figure 9	U.S.A, Nevada	Hotel/Casino	Gilbertson, D. (USA Today, 2020)
	Workplace		
Supp. Figure 10	China	Construction Site	Kun, Z., & Wenting, Z. (China Daily, 2020)
Supp. Figure 11	France	Factory	Hindustan Times (Agence France-Presse, 2020)
	Large Outdoor Entertainment Venue		
Supp. Figure 12	U.S.A, Florida	Amusement Park	Walsh, B. (Barrons, 2020)
	Outdoor Setting		
Supp. Figure 13	Australia	Outdoor Setting	Jalal, A. (ABC, 2020)
Supp. Figure 14	Japan	Outdoor Setting	Mori, K. (UPI, 2020)
Supp. Figure 15	Netherlands	Stadium	Reuters (Daily Sabah, 2020)
	Healthcare settings		
Supp. Figure 16	U.S.A, Arizona	Hospital	Voa News (VOA News, 2020)
Supp. Figure 17	U.S.A, Nevada	Medical School	Brandt, J. (NBC Philadelphia, 2020)
	School		
Supp. Figure 18	Indonesia	School	Rauhala, E. (The Washington Post, 2020)
Supp. Figure 19	Russia	School	Golovkin, P. (AP News, 2020)
Supp. Figure 20	United Kingdom	School	Roxby, P. (BBC, 2020)
Supp. Figure 21	U.S.A, California	High School	Caroll, L. (NBC News, 2020)
Supp. Figure 22	U.S.A, Texas	High School	CBS Austin, & Associated Press (CBS Austin, 2020)
	Port of Entry		
Supp. Figure 23	Austria	Travel Checkpoint	Rauhala, E. (The Washington Post, 2020)
Supp. Figure 24	China	Airport	Xinhua (Xinhua Net, 2020)
Supp. Figure 25	Hong Kong	Travel Checkpoint	Today Online (Today Online, 2020)
Supp. Figure 26	Italy	Train Station	Bendix, A. (Business Insider, 2020)
Supp. Figure 27	Mexico	Airport	McDonnell, P. J. et al. (Los Angeles Times, 2020)
Supp. Figure 28	Nigeria	Airport	Nordling, L. (Science Mag, 2020)
Supp. Figure 29	Pakistan	Train Station	Shams, S. (DW, 2020)
Supp. Figure 30	U.S.A, Alaska	Airport	Baxtrer, A. (KTOO, 2020)
	Cruise Ship		
Supp. Figure 31	Sri Lanka	Cruise Ship	Dalton, M. & Barton, K. (W NYC Studios, 2020)
	Restaurant		
Supp. Figure 32	South Korea	Cafe	Sang-Hun, C. (The New York Times, 2020)
Supp. Figure 33	U.S.A, California	Restaurant	Repko, M. (CNBC, 2020)
	Store		
Supp. Figure 34	Brazil	Retail Store	Associated Press (VOA News, 2020)
Supp. Figure 35	Israel	Store	TOI Staff (The Times of Israel, 2020)
	Government Building		
Supp. Figure 36	Russia	Election Polling Station	Tass (Alamy, 2020)
Supp. Figure 37	Thailand	Government Building	Moritsugu, K. (AP News, 2020)
Supp. Figure 38	Ukraine	Presidential Office	Rauhala, E. (The Washington Post, 2020)
Supp. Figure 39	U.S.A, Washington, D. C.	White House	Superville, D. (The Washington Times, 2020)
	Ear-temperature measurements		
Supp. Figure 40	Germany	Airport	Agencies (The New Indian Express, 2020)

Figure 4. Impact of vasomotor tone and thermal conductivity on temperature measurements; epidemiologic implications for spreading COVID-19. Bars denote the nine light-emission grades (0.5 °C/color), from highest (gray) to lowest (brown-black).

Figure 4A

Vascular response of high-k BTT and low-k surfaces; their epidemiological impacts

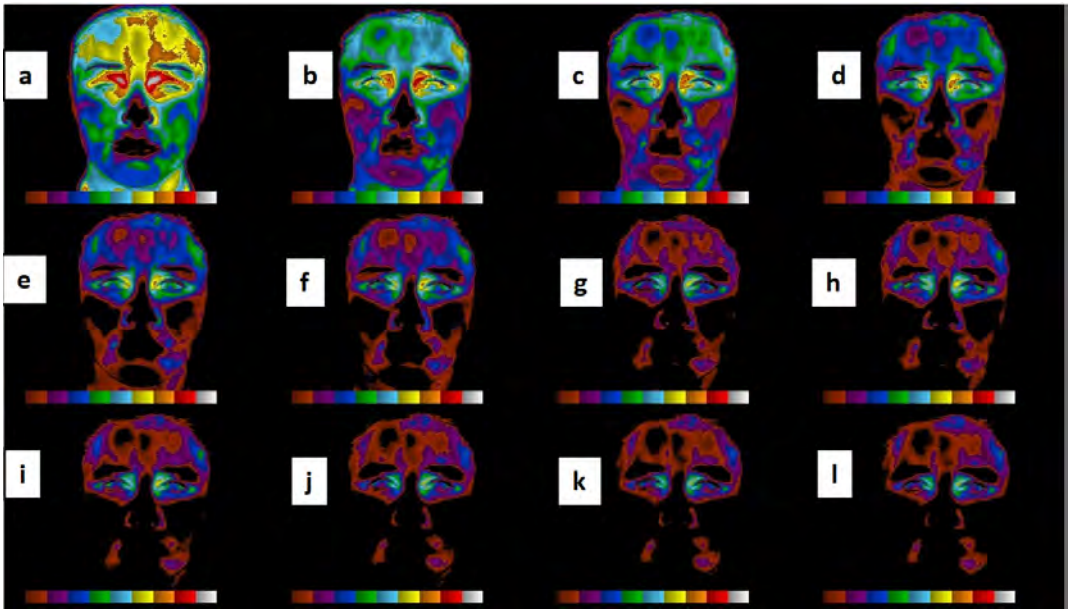

(**A**) Serial thermograms obtained during fanning show progressive facial cooling, from baseline (a) to coolest (l). BTT° also decreases but remains close to the baseline; other sites (e.g., the forehead) decline dramatically, even to very low absolute levels (< 3.0 °C; brown-black region). FH° and SPV decrease to low temperatures despite the large STA (Figure 1C) and identical fat-free histology to the BTT (Figure 2A), respectively. See text for details.

Figure 4B

Low-k highly reactive vasculature thermometry and its epidemiological impacts in 2020

(**B**) In 2020, during COVID-19 screening, a child has her temperature checked with a digital thermometer at a school in the U.K. – by Roxby, P. (BBC, 2020).

Figure 4C

Low-k highly reactive vasculature thermometry and its epidemiological impacts in 2021

(B) In 2021, low-*k* reactive vasculature thermometry was used during the COVID-19 surge in the U.K. This image shows temperature scanning underway at a London theater in mid-May, as Britain began easing several coronavirus restrictions – by Colchester M. (WSJ, 2021), photo by Vickie Flores.

Figure 4D

Low-k highly reactive vasculature thermometry and its epidemiological impacts in 2021

(C) In April 2021, the same low-k reactive vasculature thermometry was used during the Delta variant surge in India. Here, a healthcare worker checks the temperature of a rice mill worker during a COVID-19 vaccination drive at Bavla village on the outskirts of Ahmedabad, India, April 13, 2021 (Pic: Amit Dave/Reuters).

Figure 4E

Wrist: low-k highly reactive vasculature thermometry and its epidemiological impact

(**D**) Wrist temperature check at Military Command Center in the U.S. Temperature checks of the wrists of military personnel were conducted at the entrance of the headquarters buildings for the U.S. Army Reserve Command and the U.S. Forces Command, Fort Bragg, North Carolina. Image provided by the U.S. Department of Defense (Master Sgt. Michel Sauret, October 2020).

Section 5. Applications and impediments of thermal imaging and thermometry (aligned and unaligned with physical and biological principles) for infection screening.

At present, the standard thermometry and thermal-imaging practices are not in concert with biological and physical principles regarding effective and undisturbed heat transfer; this may lead to COVID-19 spreading and facilitate mutations, despite diligent temperature checks. Moreover, infrared thermal imaging must fulfill strict criteria to detect the thermal status and possible febrile states from the emission at the BTT. Here, we discuss the criteria necessary to improve thermal-imaging-based fever detection, in which an increased temperature is observed at the $SMOS_{BTT}$; furthermore, we illustrate potential impediments in the context of the mass screenings required to combat the COVID-19 pandemic.

Several factors limit the effective use of infrared thermal imaging for large numbers of people, including—but not limited to—the impacts of ambient temperature, air-current velocity, humidity, incident light, the detector's distance from the $SMOS_{BTT}$, and the requirement for the subject to remain completely motionless; other criteria are summarized in **Supplementary (Supp.) Table 1**. However, when all criteria in **Supp. Table 1** are concomitantly satisfied—including

subjects' acclimatization for 15 minutes in a confined, low-humidity room with ambient temperature carefully controlled to between 22–23 °C, without interference from artificial lighting or sunlight, and under an ambient air velocity of < 0.2 m/s [as described in research by the John B Pierce Foundation of Yale University (**Gagge & Nishi, 1977**)]—infrared thermal imaging can potentially provide useful measurements for fever detection, by using the $SMOS_{BTT}$.

The $SMOS_{BTT}$ temperature is not subject to the vascular reactivity that affects neighboring sites [including the forehead and SPV (**Sections 3 and 4**)]; nevertheless, we tested whether the BTT signals captured via thermal imaging were affected by external factors such as changes in environmental temperature or air velocity; these factors were confirmed in a normal 37-year-old female subject. The emission from the $SMOS_{BTT}$ was impacted by environment temperature between the skin (at the $SMOS_{BTT}$) and the detector of the thermal infrared camera. The remainder of the face was even more significantly affected by external factors, owing to the highly reactive and unpredictable response of facial vasculature, as reflected by the progressive darkening of the gray-scale thermal image (i → ii → iii) in **Figure 5A**. Under an ~3.0 °C change in environmental temperature and an air velocity of > 0.2 m/s, an ~0.7 °C initial reduction of $SMOS_{BTT}$ temperature was observed, followed by an additional 0.5 °C decrease during thermal equilibrium [denoted by the red arrow in the bar of **Figure 5A**, which proceeds leftward (representing cooler temperatures)].

The reduction of the $SMOS_{BTT}$ emission area indicates that the non-insulated capillary network at $SMOS_{BTT}$ reacts to ambient temperature and air velocity, producing a vasoconstrictive effect in the thermal emission area of the subject. The impact on the non-insulated $SMOS_{BTT}$ depends on the specific density of the capillary bed; and this results in large intra- and inter-subject variability for non-contact, non-insulated measurements taken via thermal imaging (extensive data to be presented in the next manuscript of the series). The temperature difference (as captured by thermal imaging) between the $SMOS_{BTT}$, which represents the highest temperature (red), and the facial site with the second-highest thermal emission (green) increased progressively from 0.69 °C at the baseline to 0.93 °C upon exposure to the cooler environment. This was followed by a difference of 1.15 °C at the equilibrium, which is consistent with a significantly higher vasomotor effect on areas outside the $SMOS_{BTT}$, attributable to environmental changes such as ambient temperature and air velocity. This supports our previous findings (**Abreu et al., 2020b**) and confirms the need for sensor insulation and skin contact at the $SMOS_{BTT}$ to realize accurate brain-temperature measurements.

We further evaluated the impact of local climate on thermal camera measurements of BTT emission (in a 22-year-old healthy male subject). A reduction of ~0.25 °C was observed, associated with an external temperature change of ~2.5 °C (**Figure 5B**); this is in contrast to the subject of **Figure 5A**, indicating the considerable individual variability of local climate, and therefore an impact which may prevent non-contact detectors from effectively capturing thermal emissions. In contrast, BTT sensors placed in contact with the skin [e.g., as patches, eyeglasses, or headgear (**Section 8**)] achieve a specific insulation coverage, which is robust against environmental influences; consequently, the typical acclimatization to the environment is not necessary prior to measurement by insulated BTT sensors.

In addition, our anatomical findings reveal features of BTT emergence at the $SMOS_{BTT}$ which may seriously compromise routine thermal imaging for fever screening. As seen in our thermo-anatomical studies (**Abreu et al., 2020a**), the SOV extends around the anteromedial eyeball such that the light beam emerges with a slight lateral orientation between the eyeball and nasal bridge beneath the—potentially obscuring—brow ridge. Video documentation of infrared

light emissions from the $SMOS_{BTT}$ (**Movies #1–3**) clearly shows the vital importance of aligning the camera with the $SMOS_{BTT}$ to obtain the measurements necessary to detect fever at the eyelid $SMOS_{BTT}$. Without this alignment and adherence to the criteria of **Supp. Table 1**, a thermal imaging camera will not detect a satisfactory thermal signal at the $SMOS_{BTT}$; thus, it may fail to detect febrile states.

Movies #1–3 show the disappearance of the infrared signal under slight movements of the subject's head. Hence, to properly evaluate thermal emission at the $SMOS_{BTT}$ using thermal imaging, the subject must remain *completely motionless* (i.e., not walking or moving) whilst looking directly at the camera after 15 min acclimatization in a confined temperature-controlled room with an air current of < 0.2 m/s. Thus, we suggest that, to reduce inaccuracies when conducting fever screening with infrared imaging, the criteria shown in **Supp. Table 1** should be strictly adhered to. These criteria include—among many other factors—acclimatization in a confined environment with a controlled ambient temperature of 22–23 °C, a low humidity, and an air velocity of < 0.2 m/s. Failure to follow these criteria may result in failed fever detection and increased COVID-19 spread; and this may lead to more prevalent disease, death, and increased viral replication, thereby facilitating the emergence of mutations. Poor detection practices may have significant consequences in environments in which large numbers of people congregate, such as entertainment venues, schools, factories, cruise ships, military ships, airplanes, hotels, and other large, crowded environments, as well as places in which people remain in close proximity for extended periods of time (> 30 minutes), such as restaurants, stores, and businesses (described in Section 4).

When all aforementioned criteria in **Supp. Table 1** are methodically followed, thermal imaging provides a useful quantitative analysis of the thermal statuses of bodies, particularly during high fever, as exemplified for an 8-year-old child (**Figures 5C**) and 22-year-old adult (**Figure 5D**). The highest emission in the 8-year-old subject was measured at the $SMOS_{BTT}$, indicating that BTT emissions in children accord with the highest emissions found (at the $SMOS_{BTT}$) in adults. The highest temperature was found at the $SMOS_{BTT}$ in both subjects, further corroborating the findings shown here (**Table 1**) and reported elsewhere (**Abreu et al., 2020a; Abreu et al., 2020b**). This indicates $SMOS_{BTT}$ to be the most thermally-emissive region on the surface of the human body across different age groups.

The utility of thermal imaging for fever screening within controlled and confined environments (e.g., hospital rooms) was further confirmed by a report on infrared thermography, which achieved reliable measurements in the fever screening of hospitalized patients (**Chan et al., 2004**). Furthermore, although difficult for mass fever screening necessary in a pandemic such as COVID-19, technological advances may help to better assess thermal changes associated with vascular reactivity Nonetheless, use of infrared thermal imaging for COVID-19 may be challenging if problems remain unaddressed in mass screenings; this is because useful measurements require each subject to be individually measured in a dedicated room, without interference from incident light and under controlled temperature (22–23 °C) and air velocity (< 0.2 m/sec) conditions; furthermore, images must be acquired from motionless subjects who have been acclimatized for ~15 min, alongside all other criteria in **Supp. Table 1**.

Limitations of non-contact infrared thermometry were recently reported (**Foster et al., 2021**); and barriers regarding fever detection by infrared thermography have been corroborated by other studies, which show that thermal imaging fails to identify infected individuals during mass screenings (**Priest et al., 2011**). Moreover, temperature results of the inner canthi—a common measuring site in infrared thermography—were shown not to correspond to core temperature

(**Teunissen & Daanen, 2012**). Nevertheless, the critical period for SARS-CoV-2 infectivity is characterized by the afebrile state (**He et al, 2020**), and continuous temperature monitoring is necessary to detect such early thermal changes. Hence, thermal imaging (which detects infections via thermal emission increases) may be unable to identify temperature kinetics, owing to thermoregulatory dynamics in the early infection stages. This renders thermal imaging (and standard thermometry) liable to failure during the high-infectivity period of COVID-19. Standard temperature measurements are more able to detect infections after peak viral shedding has occurred; thus, standard thermometry and thermal imaging may be too late to practically prevent peak viral shedding by the host, as well as replication within the host; as a result, it may fail to mitigate mutations.

The BTT is characterized by a high volumetric heat capacity, and the $SMOS_{BTT}$ is relatively large (~10 mm) (**Abreu et al., 2020a**); however, only one central light beam (approximately ≤ 2 mm in diameter) is used (**Figure 5E**); this contains the narrowly focused emission required to precisely capture brain thermal signals and effectively detect RNA viral infection (**Section 8**). **Figure 5F** shows computerized tomography results, highlighting the contrast of the orbit and associated vasculature; these radiologically show that the critical central point of the $SMOS_{BTT}$ (red circle) represents the central narrow light beam of **Figure 5E**. This narrow beam denotes the convergence point of three high-heat-capacity media: the blood from the (1) frontal (downward arrow) and (2) angular (up arrow) veins, which joins (3) the blood in the SOV (double arrow), which exhibits the highest heat volumetric capacity, is in thermal continuity with the hypothalamus (**Abreu et al., 2020a**), and is externally located in the high-*k* skin of the eyelid. This produces the highest-intensity infrared light emission, as shown in **Figure 2C**.

As noted in our previous radio-morphological studies, this pathway between the brain and surface is narrow (**Abreu et al., 2020a**), and the corresponding thermal transmission from the BTT (exemplified in **Figure 5E)** may produce a pinpoint emission at the $SMOS_{BTT}$. The signal intensity decreases significantly from the main center of the $SMOS_{BTT}$ (which has the highest emission and surroundings associated with unpredictable thermal emissions); however, signal capture outside this central and narrow path may reduce the procedure's ability to detect the thermoregulatory dynamics required to identify afebrile and early febrile infection.

This peak intensity is present only in one radiative center; and this corresponds to the central area (red circle) of **Figure 5F**, which is surrounded by areas of lower thermal intensity (denoted by the yellow ring). Accordingly, we present technical solutions (based on previous methods) to detect the maximum thermal intensity at the $SMOS_{BTT}$ (**Abreu, 2012**) and ensure detection of the highest-thermal-intensity zone, including the pinpoint dimension area. This resulted in the development of a smart-sensing system for detecting the peak thermal intensity. The system consists of an intelligent automatic topographic locator (IATLo) **(Supp. Fig. 45**) and self-calibrating high-resolution thermal sensor (0.001 +/- 0.003 °C), which is key for achieving early detection and was developed from collaborative research undertaken using U.S. Navy technology (**Lagakos & Bucaro, 2010**).

The IATLo performs insulated contact-sensing topography to detect thermal emissions; these are shown in previous thermal images as areas of high thermal intensity surrounded by broad regions of much lower intensity. Thus, to ensure detection of the peak intensity point (shown in **Figures 5E, F**), IATLo includes an intelligent quadro-absorbing ring (iQAR) that contains four high-resolution thermal sensors (positioned at the cardinal points of the ring) that measure temperature simultaneously and jointly with the central sensor, thereby providing at least five simultaneous thermal inputs (**Supp. Fig. 45**). If the temperature in any of the sensors in the iQAR

exceeds the central temperature, the intelligent system is activated to automatically detect the thermal topography from the highest iQAR signal and central temperature, to determine the location of the peak-intensity signal. This generates a tridimensional thermal map of the $SMOS_{BTT}$ (not shown), which is used to obtain peak brain thermal signals in this topography, as required to distinguish thermoregulatory brain patterns.

Additionally, skin-temperature changes induced by forced or passive convection—caused by air currents of > 2 m/s or direct cooling—are eliminated by using insulated BTT contact sensor assemblies (**Section 8**). The limitations of infrared thermography (e.g., the need for acclimatization and the other criteria shown here) are thereby eliminated by wearable, highly insulated BTT microsensors, which automatically and continuously capture thermal signals—that are normally shielded inside the skull—using the unique antero-posterior axis of the brain tunnel (as shown in **Figure 5F**). This allows brain thermoregulatory dynamics to be distinguished without interference from external environmental factors.

As shown in **Figure 5E**, certain confounding biological factors may prevent acquisition of clinically useful measurements by thermal imaging cameras at the $SMOS_{BTT}$; these include the proximity of the skin of the $SMOS_{BTT}$ to the lacrimal (tear) duct, the caruncle area in the inner canthi, and the conjunctiva. Because infrared thermography detects maximum temperatures, inflammation of the tear duct, conjunctiva, and inner canthi region—fairly common occurrences (e.g., produced by allergy or infection)—may lead to spurious detections of an increased temperature unrelated to the thermal status of the body or brain. Hence, measurement of a high-temperature area adjacent to the eyelid skin of the $SMOS_{BTT}$ may simply reflect local inflammatory changes. These morphological characteristics further support our previous finding: that diagnostic light beams from the natural waveguides of the BTT are present in the skin of the eyelids between the eyes, rather than in the eye or mucosal sites (e.g., the inner medial canthus) (**Abreu et al., 2020a**). The BTT site does not involve the tear duct, inner canthi of the eye, or the eyeball itself; furthermore, conjunctival or mucosal linings may produce false-negative readings (due to dry eye) and false-positive readings (due to allergic, infectious, and inflammatory conditions).

The combination of the aforementioned technical features with the necessary insulation realizes the sensing capabilities required to detect pre-febrile stages and thereby prevent asymptomatic COVID-19 transmission, whilst also overcoming the impediments of thermal imaging methods. Because thermal image capture depends entirely upon an unobstructed view of the area being assessed, it does not benefit from the advantages of insulation; thus, thermal imaging will invariably be impacted by the uncertainties of local climate and reactive surface vasculature (**Figure 5E**). In contrast, insulated-contact-sensing topography provides the accuracy required to detect COVID-19, by capturing high-k signals in thermal continuum with the brain thermoregulatory center, as demonstrated by our radio-morphological studies (**Abreu et al., 2020a**).

Figure 5. Applications and impediments of thermal imaging (aligned and non-aligned with physical and biological principles) for infection screening.

Figure 5A

Applications and impediments of thermal imaging for infection detection

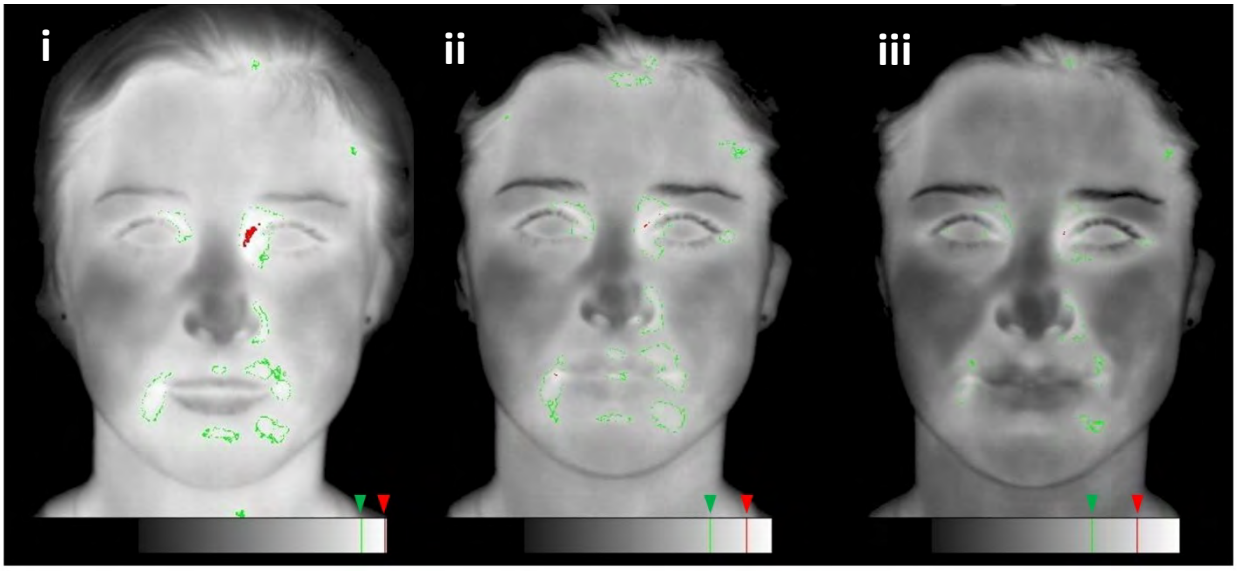

(**A**) Bars represent grades of infrared light emission, from highest (white) to lowest (black). Red arrows corresponds to maximal temperatures (consistently found at the $SMOS_{BTT}$); green arrows correspond to the second-highest emission zones. Serial facial thermal imaging capture (gray scale) during an ~3.0 °C decrease of ambient temperature shows the progressive facial and $SMOS_{BTT}$ cooling, from baseline (i) to initial cooling (ii) and thermal equilibrium (iii). This results in pinpoint emissions at the $SMOS_{BTT}$. Although BTT° decreased, thermal emissions in the remainder of the face fell much further (darker image and reduced green isotherm). Furthermore, the difference between the $SMOS_{BTT}$ temperature (red arrow) and that of the second-highest emission region (green arrow) increased over time, owing to more intense cooling and vascular-reactive effects outside the $SMOS_{BTT}$. Numerical values given in text.

Figure 5B

Applications and impediments of thermal imaging for infection detection

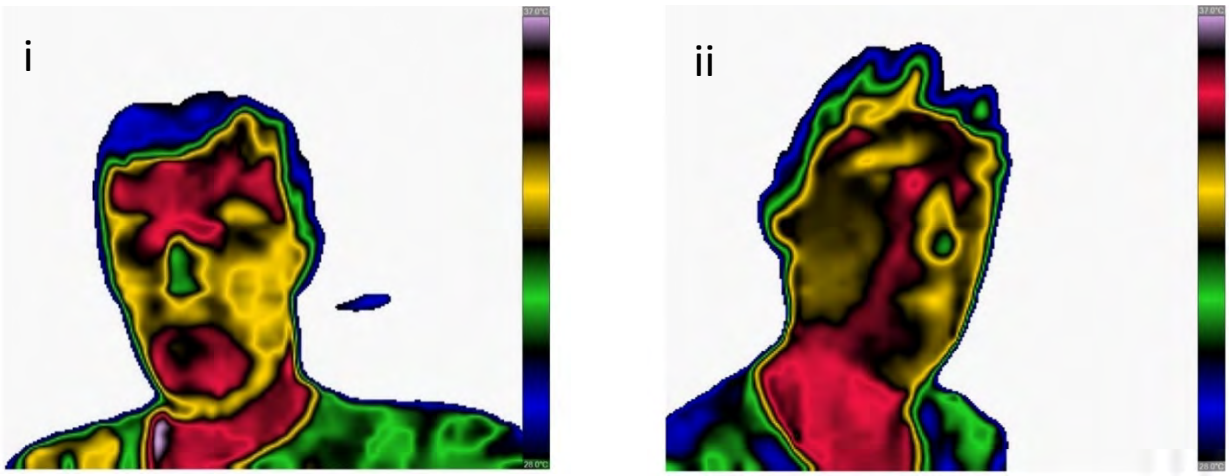

(**B**) Bars represent grades of infrared light emission, from highest (red) to lowest (blue). The thermal emission capture exhibits interference due to ambient temperature, lack of acclimatization, and air currents of > 0.2 m/s. This reduces the temperature from the baseline (i) to post-exposure in a cold room (ii). The absence of red on FH post-exposure (ii) indicates the impact of ambient temperature on the infrared thermography of the forehead. Temperature levels are provided in text.

Figure 5C

Applications and impediments of thermal imaging for infection detection

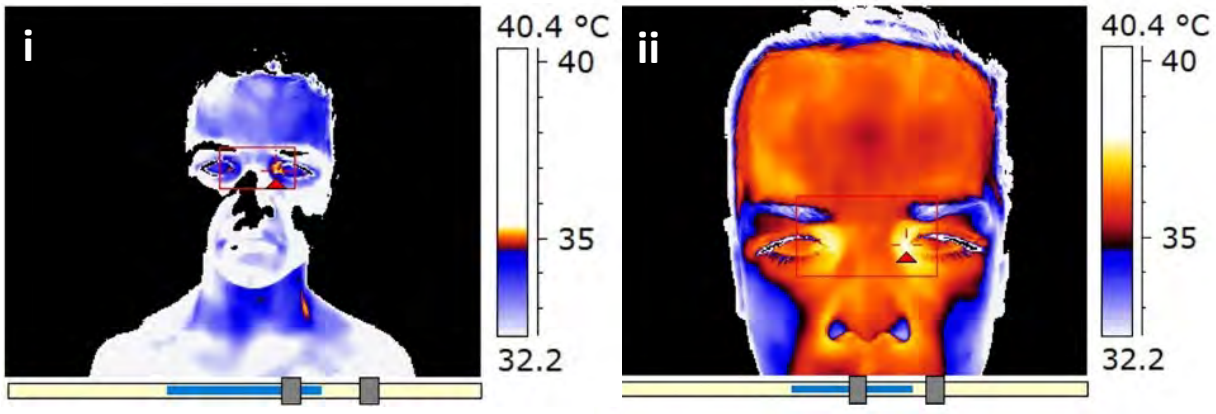

(**C, D**) Fever detection with thermal imaging. Bars represent grades of infrared light emission, (**C**) from highest (white-red) to lowest (purple), and (**D**) from highest (red) to lowest (blue). Thermal emissions at the $SMOS_{BTT}$ using proper criteria (**Supp. Table 1**), including acquisition of images in a confined room with a temperature of 22–23°C, no incident light, an air current of < 0.2 m/sec, and 15 min subject acclimatization. (**C**) For the 22-year-old male patient, the baseline $SMOS_{BTT}$ temperature was 35.3 °C (i) for pre-febrile emission and 37.8 °C (ii) during fever.

Figure 5D

Applications and impediments of thermal imaging for infection detection

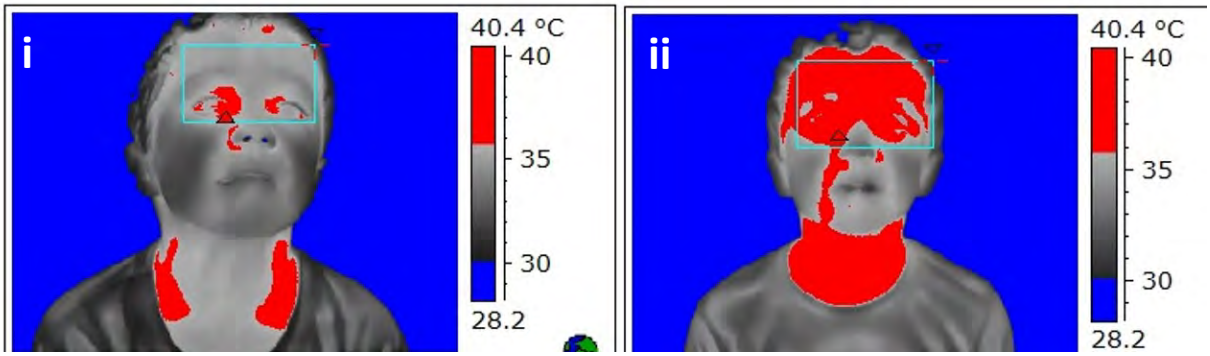

(**D**) For the 8-year-old patient (see text), the baseline emission was 36.3 °C (i) for the pre-febrile state and 38.6 °C (ii) during fever. Red triangles denote maximum facial temperatures, which occurred at the BTT site in both pre-febrile and febrile states.

Figure 5E

Applications and impediments of thermal imaging for infection detection

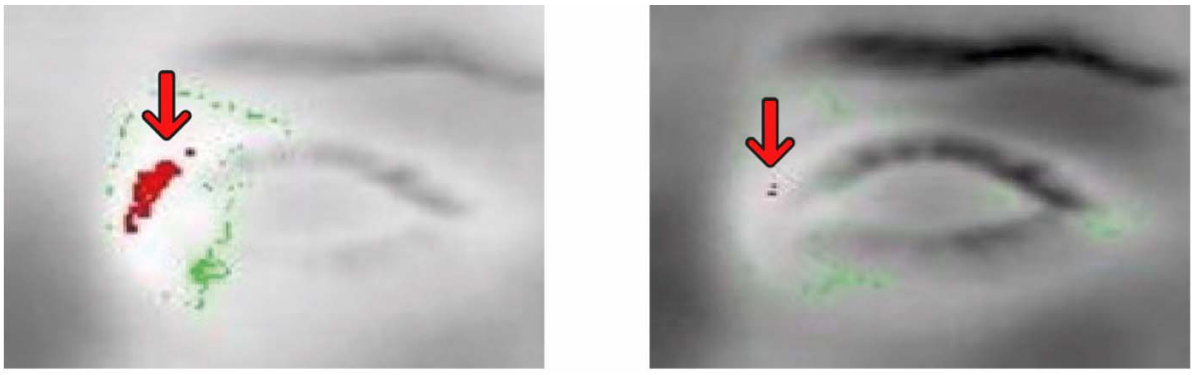

(**E**) Close-up thermal image of the orbital region, showing the reduction of the broad baseline light beam (left panel) to one central narrow (pinpoint) light-emission region (right panel), as well as the associated overall decrease in periocular temperature (darker and reduced green zone) attributable to environmental factors.

Figure 5F

Applications and impediments of thermal imaging for infection detection

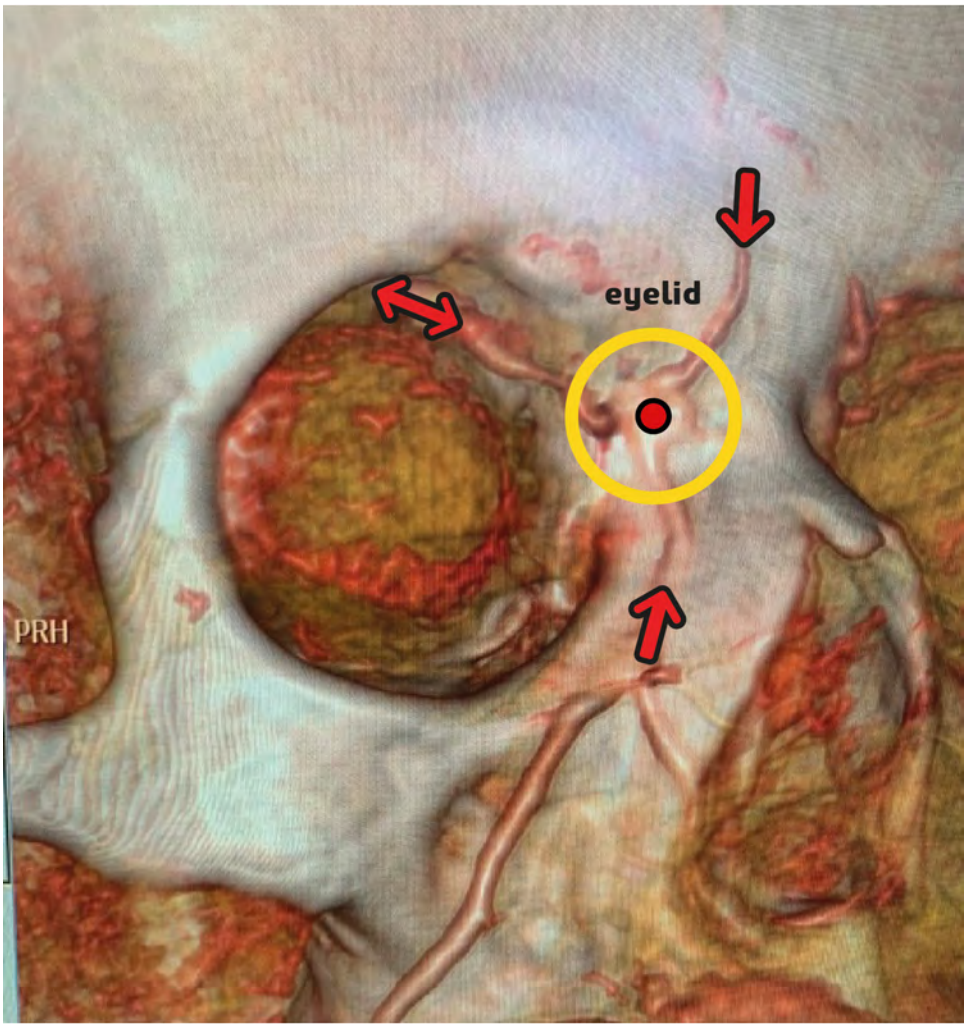

(**F**) Computerized tomography image showing contrast of orbit, with right anterolateral view showing right-upper-medial eyelid region (3D reconstruction realized by a volume-rendering technique—see Material and Methods for details). Convergence of the angular (upwards arrow) and naso-frontal (downwards arrow) veins forming the superior ophthalmic vein (double arrow) is observed and demarcated with a yellow circle, which contains (in the center) the blood

convergence area corresponding to the narrow area of the light beam (red circle); this carries the signals associated with the hypothalamic thermoregulatory response.

Section 6. Resting and dynamic thermal transmissions from BTT, core, and periocular sites; implications for COVID-19 detection

We corroborate the findings of Section 2 and show that without an underlying tunnel, thermal emissions on the body surface (besides the eyelid region of the $SMOS_{BTT}$) do not correspond to the internal (brain or core) thermal status of the human body. After satisfying all criteria of **Supp. Table 1**, we performed further resting and dynamic assessments of thermal transmission at the BTT, oral mucosa (representing core temperature), periocular skin (i.e., the SPV region), and mucosal (i.e., caruncle and inner canthi) sites.

As seen in **Figure 6A**, neither the SPV nor caruncle (inner canthi) exhibit emissions equivalent to those of the eyelid skin at the $SMOS_{BTT}$ (red isotherm), because of the high-*k* skin overlying the tunnel. Emissions from the BTT and oral mucosa exhibit the highest intensity. In contrast, the caruncle and inner canthi region (green isotherm) fail to produce thermal emissions such as those present at the $SMOS_{BTT}$ and oral mucosa (Core°). These findings further suggest that heat transfer from the superficial mucosal vessels reflects local temperatures, as found in the inner canthi and tear duct. The temperature of mucosal-type surfaces is strongly influenced by humidity, wind, and even simple inflammatory process in the eye (e.g., conjunctivitis). Thus, measurements of the inner canthi (e.g., by thermal imaging) during screening for COVID-19 may deceptively overestimate the temperature, owing to emissions resulting from a local infection or inflammation; alternatively, they may underestimate it because of reduced blood flows, which can occur under vasoconstriction and humidity changes. Moreover, eye drops—which alter vascularity—may result in inconsistent heat transmission, because conjunctival vessels and caruncles are characterized by highly reactive vascular responses. Additionally, lack of a direct connection from the brain to the inner canthi and mucosal areas prevents detection of early thermal changes. This has been corroborated by a report showing that the thermal emissions of the inner canthi during infrared thermal imaging did not correspond to core temperature (**Teunissen & Daanen, 2012**).

Such suboptimal screening techniques may be insufficient to accurately detect febrile states, which may lead to COVID-19 spreading. In contrast, BTT thermal emission during resting was equivalent to the oral mucosa emission. The correspondence of BTT° to Core° at rest was further supported by the results of our anesthesia studies, which showed that BTT° matched Core° (represented by pulmonary artery temperature) during the pre-bypass phase of cardiothoracic surgery (**Abreu et al., 2020b**). We also assessed the impact of the body-core thermal confounding factors upon BTT thermal emission, by immersing the subject's hand and forearm in iced water (**Figure 6B**) and simultaneously assessing the thermal emissions from the core (oral) and facial surface (skin and mucosa). Notably, $SMOS_{BTT}$ emissions were uniquely maintained during cold immersion; emissions from other facial regions (including nearby SPV skin, inner canthi, and oral mucosa) were observed to decline, confirming our previous findings regarding brain/core discordance (**Abreu et al., 2020b**).

Figure 6. Resting and dynamic thermal transmissions from BTT, core, and periocular sites; their implications for COVID-19 detection

Bars represent grades of infrared light emission, from highest (white) to lowest (black). After satisfying the criteria of **Supp. Table 1**, facial thermal images taken at rest and during immersion in ice water were compared. These displayed distinct emissions from the BTT, oral mucosa, ocular mucosa (inner canthi, caruncle), and skin surface (SPV and forehead) results; thus,

we could distinguish the right and left BTT as sites of maximal light emission, both under resting conditions and in the presence of extreme-cold confounding factors.

Figure 6A

Resting and dynamic thermal transmission from BTT, core, and periocular sites

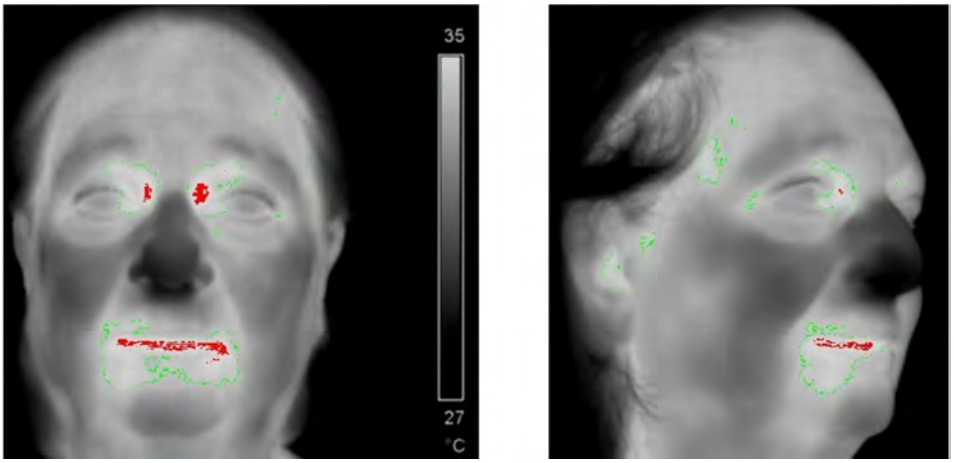

(**A**) Gray-scale facial thermal emissions. *Left*: Oral cavity reflects Core° and exhibits similar emissions to BTT (both sites feature red isotherm of maximal thermal intensity, surrounded by a green isotherm of lower intensity). Right and left BTT show the highest surface emissions. Outside BTT and oral mucosa, emissions varied considerably in intensity and location. *Right*: Side view shows lack of high emission at the FH, caruncle and SPV [green isotherm (with no red) indicates absence of high thermal emissions, as found at BTT site]. It should be noted that pinpoint emission changes are produced by changes in head position, further confirming findings in Section 5.

Figure 6B

Resting and dynamic thermal transmission from BTT, core, and periocular sites

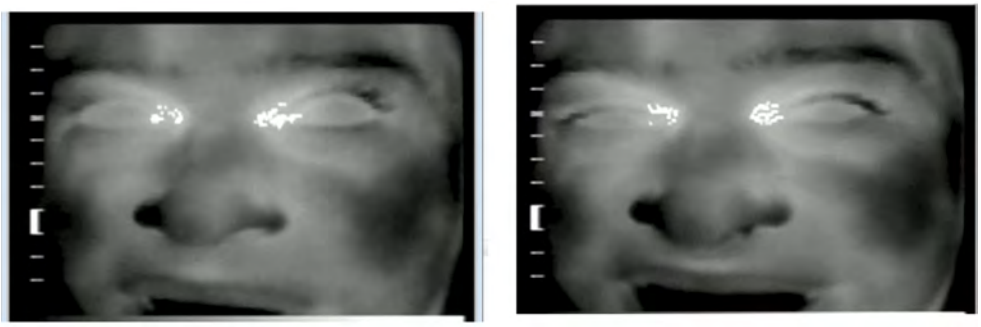

(**B**) Initial (left) and final (right) frames of experiment video (upper-arm immersed in ice water). At the baseline, similar emissions were found at the caruncle and BTT sites. During immersion, the forehead, superior palpebral, and caruncle (inner canthi, tear duct) emissions decreased, whilst those at the BTT site remained virtually unchanged from the baseline value under identical light emissions. The oral cavity (black) has a much lower emission rate than the BTT; this suggests cooling of the core but not of the BTT (i.e., the brain temperature), as corroborated in previous studies (Abreu et al., 2020b) and investigations herein (Section 8).

Section 7. Consistency of BTT thermal emissions across different races

The skin histomorphometry results at the $SMOS_{BTT}$ revealed uniform dimensions and structures across different races (**Abreu et al., 2020a**). However, considering the common anatomic (specifically, topographical and vascular) variability, we investigated emissions across different races for the high-*k* region and axial vessel (SOV) of the $SMOS_{BTT}$. Thermal emissions, shown in representative Asian, Black, and White subjects (**Figure 7A**), confirmed that the morphological features were consistent with findings from our large database (not shown). BTT emission was consistently identified in the upper medial eyelid at the $SMOS_{BTT}$ (red area); meanwhile, the forehead and other facial areas were silent in high-thermal-emission areas. Thus, BTT° uniquely facilitates consistent temperature measurements across different races, which is essential for tackling the COVID-19 pandemic on a global scale.

Figure 7A

Consistency of BTT thermal emissions across different races

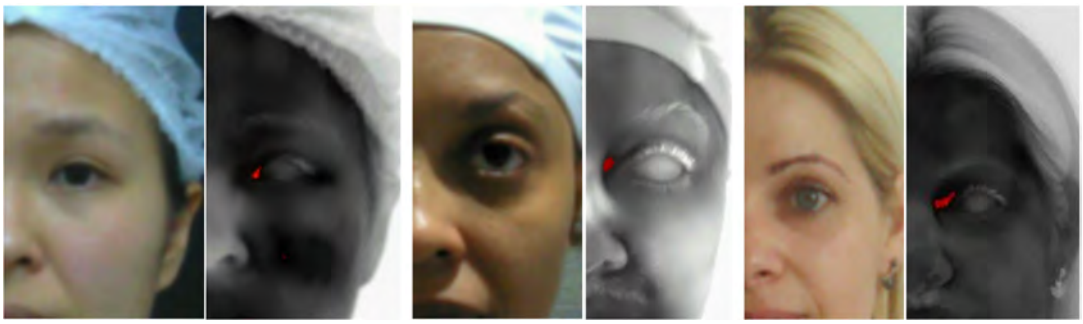

Infrared light emissions across different races, showing highest thermal intensity at the $SMOS_{BTT}$ (red zone at medial eyelid) and lack of equivalent thermal energy on the FH and face in all subjects.

Section 8. BTT° (in concert with physics and biology) exhibits specificity for thermoregulatory brain activity and detection of afebrile asymptomatic RNA viral infection.

To establish a basis for the brain-temperature-kinetics-based detection of thermoregulatory activity prior to the febrile state of RNA viral infection, we tested whether BTT°—in concert with physical and biological knowledge for optimal heat transfer—could detect the brain's thermal status and thermoregulatory dynamics in clinical and experimental scenarios during brain/core discordance; furthermore, we investigated the associated relationships between BTT° and Core°

as well as the surface temperature (Surface°) measured on forehead skin (FH°). Using a series of both wired and wireless high-resolution thermal sensors (mounted on adhesives, eyeglasses, frames, and headgear) configured to noninvasively measure temperature at the $SMOS_{BTT}$ (**Figures 8A–E**), we evaluated brain temperature kinetics (A) during neuronal depression (sedation, anesthesia, and sleep), (B) after traumatic brain injury, (C) in pediatric patients during suspected fever, and (D) in afebrile asymptomatic RNA viral infection patients whilst awake and asleep.

(A) Pharmacological and Physiological Brain Neuronal Depression.

1. Pharmacologically-induced brain neuronal depression and recovery. Brain depression was induced in patients—who consented to BTT° monitoring via noninvasive thermal sensors (**Figure 8A**)—whilst under sedation and general anesthesia, as part of their clinical care.

(i) *Sedation*: This study was performed to determine whether temperature measurements at the BTT site (performed in concert with physics and biology) could be used to detect decreased brain thermogenesis and hypothalamic activity under increasing propofol sedation during monitored anesthesia care (MAC) surgery, to thereby provide further evidence of the specificity of BTT° for brain temperature, which is fundamental for the early detection of viral infection.

An infusion of propofol was administered to induce sedation (titrated by the care provider) during surgery; this was performed under a field block in 12 patients (7 female, 5 male; ages 26–70). BTT° – SL° was determined prior to propofol infusion, at the start of infusion, 10 mins thereafter, the 30th minute of propofol infusion, when the infusion was stopped, and 30 min thereafter. The sedation level was recorded at each time point (0 = none, 1 = minimal sedation, 2 = moderate sedation, 3 = deep sedation, 4 = general anesthesia). BTT° declined from 36.5 ^{o}C at onset of propofol infusion to 36.09 ^{o}C after 30 minutes (when all patients had sedation scores of 3) ($p < 0.0001$ by paired t-test). SL° also decreased from 36.56 ° to 36.48 ° ($p = 0.02$), attributable in part to the surgical area's exposure to room temperature (without use of the warming blanket commonly provided during general anesthesia). However, the decline in BTT° was notably more dramatic: BTT° – SL° increased from -0.03 ^{o}C to -0.40 ^{o}C ($p < 0.0001$; one-tailed paired t-test) in response to the propofol infusion; this revealed selective brain depressions uniquely captured by BTT°. Each of the 12 patients who achieved a sedation score of 3 after 30 mins of infusion—and the single patient who reached this level at 10 min—had a BTT° – SL° difference beyond -0.2 ^{o}C.

The results reveal a progressive, statistically significant decrease in brain temperature, as measured noninvasively by BTT° after propofol infusion for MAC surgical cases. The ability to monitor sequential BTT° changes that correlate with the sedation level suggests that BTT° can distinguish the sequential thermal changes that occur during hypothalamic activation in infectious processes (**McCann et al., 2000**), such as the viral infection caused by SARS-CoV-2.

(ii) *Anesthesia:* Next, we conducted pilot studies to explore the brain's thermoregulatory response under immunosenescence [60+ years old (**Ma & Fang, 2013**)] during general anesthesia, because delineating changes during complete brain neuronal depression will further indicate that BTT° can detect subtle initial thermoregulatory changes—such as those found at infection inception in immunocompromised populations—and will confirm that thermal measurements aligned with physical and biological principles can detect thermal status characteristics undetectable under other techniques. Asides from the elderly, immunosenescence also arises in the immature immune systems of children, who are unable to mount an effective immune response; this further indicates that BTT° can capture brain thermal responses in both of these age groups, who are typically characterized by blunt thermal responses.

Consistent with the degree of cerebral metabolic depression observed during general anesthesia (**Sessler, 2000**), BTT° – Core° during general anesthesia (as managed by the care provider

independently of our data collection) exceeded that during sedation. Core° tended to remain constant, owing to the use of a warming blanket (to prevent the otherwise common development of hypothermia). In the first patient (60-year-old female) (**Figure 8F**), Core° was measured using an equally calibrated esophageal thermistor (Esg°), which was placed at the rear of the tongue when the patient was awake and relocated to the esophagus after the induction of general anesthesia. At the baseline, BTT° – Esg° was ~0 °C; this difference increased to -0.9 °C after induction of anesthesia and activation of the warming blanket (Point 5 on the x-axis). BTT° decreased from 37.2 °C at onset of anesthesia to 36.3 °C at induction; for the same period, Esg° decreased from 37.1 °C to ~36.75 °C. However, when anesthesia was reduced (Point 10), BTT° gradually increased (from 36.3 °C to 36.75 °C), facilitating detection of the depth of anesthesia; this was not detected by Esg°, which remained at approximately the same thermal level as Point 3 (Induction). BTT° was increased to match Esg° (36.75 °C). Increasing the anesthesia depth decreased BTT° to ~1.0 °C (Point 13); meanwhile, Esg° only decreased by ~0.55 °C. BTT° subsequently remained below Esg° until extubation and awakening (Point 26). Notably, BTT° remained below Esg° upon extubation, indicating persistent thermoregulatory changes in the hypothalamus (and brain), attributable to anesthesia; however, these were not detected with Core° (Esg°). The persistent brain hypothermic status (with a difference of 0.8 °C between BTT° and Esg°) is of considerable clinical importance, because anesthesia-induced hypothermia inhibits phosphodiesterase A2 and has been associated with the development of Alzheimer's disease through tau hyperphosphorylation (**Planel et al., 2007; Planel et al., 2009**); this explains the association between anesthesia and Alzheimer's disease, which can then be prevented by proper brain thermal management.

In a second patient (68-year-old male) (**Figure 8G**), the intraoperative measurement of Core° also included a nasopharyngeal probe equivalently calibrated with BTT° (NP°) until awakening. This corresponded more closely with blood traveling toward the brain than Esg°; however, the readings were virtually identical to those of Esg°. Induction of anesthesia produced a 0.6 °C decrease in BTT°, causing BTT° – Core° to increase from -0.1 °C at the baseline to -1.0 °C at the BTT° nadir (Point 5). The relative reduction of anesthesia caused BTT to gradually increase from 35.0 °C to 35.7 °C; however, the change in the anesthesia depth was not detected by Esg° or NP°, both of which were only reduced by 0.1 °C. Extubation and awakening caused BTT° to increase such that BTT° – Core° was only -0.2 °C (Point 11). Subsequently, the patient was no longer stimulated by the endotracheal tube, and the warming blanket was discontinued. Measurement of Core° in the post-anesthesia care unit (PACU) was achieved using Esg° (taken at the rear of the tongue); furthermore, as dictated by the PACU clinical routine, a forehead scan (FH°) was obtained, which revealed that FH° measurements overestimated both Esg° and BTT°, most likely because of correction factors that artificially increased the temperature readings to offset the body's low-*k* wood-like thermal barrier. For COVID-19 screenings, this inaccurate forehead measurement would have produced false-positive readings, leading a healthy person at a port of entry to be placed in the high-temperature group, which may include truly infected individuals. The selective response of BTT° to the lingering impacts of general anesthesia and analgesics was demonstrated by a BTT° – Core° of approximately -1.0 °C, which was maintained for several hours (Points 13–17); this difference had returned to the baseline by the following morning (Point 18). This subject's results further corroborated the uniform post-anesthesia hypothermic status of the brain, which leads to the inhibition of phosphodiesterase A2 and the potential development of Alzheimer's disease (**Planel et al., 2007; Planel et al., 2009**).

Findings in these patients further confirmed the correspondence of BTT° to brain neuronal depression under anesthesia, the ability of BTT° to delineate cyclical changes correlating with

levels thereof, and the peak and decline of hypothalamic thermal changes in these subjects, as similarly observed during hypothalamic activation in infectious processes (**McCann et al., 2000**). The BTT° detection of brain-temperature variations in immunocompromised patients (due to immunosenescence) under anesthesia are aligned with BTT° detection abilities in children (due to immature immune system). Besides children and the immunosenescent, numerous medical conditions are associated with immunocompromised states and have been shown to increase SARS-CoV-2 replication, leading to high mutation rates (**Choi et al., 2020**). This is critical in the context of mutation emergence in immunocompromised patients (**Choi et al., 2020; Hensley et al., 2021; Khatamzas et al., 2021; Truong et al., 2021)** because—as observed in the immature immune systems of children—such patients' inability to mount a post-vaccination immune response can potentially lead to intra-host viral evolution and mutations.

2. Physiologically-induced brain neuronal depression (sleep) and arousal. The specificity of BTT° for brain-temperature measurements during the pharmacologically-induced decrease of cerebral neural activity prompted us to investigate the cerebral metabolism changes—including both increased and decreased brain activity—physiologically represented by sleep (and natural awakening), to investigate brain-temperature kinetics during non-infectious processes. This preliminary study provides a baseline for comparison between asymptomatic and symptomatic viral infection, with a view towards continuous RNA viral infection detection, to be administered during sleep. **Figures 8H** and **I** depict simultaneous recordings (at 15–60 s intervals) obtained using identical thermal sensors for BTT°, FH°, and rectum (Rct°) in a dimly lit (< 10 lux) room, during "Sleep Onset," transient "Arousal," and morning "Awakening," as part of a large sleep study.

(i) *BTT° vs. Rct°.* A healthy 28-year-old male volunteer member of our research team was continuously monitored (from sleep onset to awakening) using BTT frames (**Figure 8B**). A thermal sensor was placed noninvasively at the BTT site, and simultaneous temperature measurements were also obtained using an equally calibrated thermal probe inserted (10 cm) into the rectum (Rct°) (**Figure 8H)**. At sleep onset, BTT° decreased further and more rapidly than Rct° (1.28 °C and 0.67 °C, respectively), consistent with the preferential cooling of the brain as an integral component of sleep. During sleep, Rct° was primarily characterized by minimal thermal changes and homogeneity. In contrast, BTT° readings displayed active thermodynamics (despite being below Core°). During brief arousal (n = 2 episodes), BTT° increased by 0.64 ± 0.06 °C, whilst Rct° increased by only 0.08 ± 0.002 °C, demonstrating the selective sensitivity of BTT° to increased brain activity and the inability of Rct° to identify such brief periods of selectively increased cerebral activity. The BTT° vs. Rct° difference was also large upon awakening (increases of 2.3 °C and 0.4 °C from the baseline, respectively). Hence, the BTT° capture of discordance between Brain° and Core° was also confirmed during natural sleep.

(ii) *BTT° vs. FH°.* In addition to Core° (represented by Rct°, as noted above), we investigated BTT° vs. surface temperature (FH°) during sleep, by continuously monitoring a 60-year-old male volunteer of our team **(Figure 8I)** using the same BTT equipment used for Core° testing. Prior to sleep, BTT° exceeded FH°; however, consistent with the reduced brain metabolism that accompanies sleep onset, BTT° steadily decreased, with a mean reduction of 1.60 ± 0.2 °C. In contrast, FH° was inconsistent because of its remoteness from the brain and its susceptibility to changes in vascular tone (e.g., vasodilation due to sleep-associated decrease of sympathetic control). The overall decline in FH° at sleep onset was 0.42 ± 0.09 °C ($p < 0.000001$ vs. BTT°; two-tailed paired t-test) and often delayed. Hence, even though BTT° began at a higher temperature than FH°, it fell to a lower level, such that BTT/FH crossing occurred; this conflicts

with findings obtained under periods of increased cerebral activity, such as during electroconvulsive therapy (**Abreu et al., 2020b**). During arousal and upon awakening, the BTT° again reflected the change in brain activity, increasing by 0.92 ± 0.29 °C and 1.26 ± 0.37 °C, respectively. This was overlooked by FH°. Changes in FH° were delayed and of low magnitude: 0.19 ± 0.15 °C ($p < 0.00001$ vs. BTT; two-tailed paired t-test) and 0.38 ± 0.36 °C ($p = 0.018$ vs. BTT) for arousal and upon awakening, respectively. This is consistent with the local thermal changes of forehead skin, which varied independently of cerebral metabolism. Upon awakening, crossing occurred again, with BTT° exceeding FH°. The geometry of the plots was also revealing: BTT° exhibited a more heterogeneous geometry than either FH° or Rct°, reflective of the rapidly changing cerebral metabolic activity. Results confirm that the BTT° can delineate thermoregulatory activity during sleep in subjects from the age groups associated with immunosenescence and immunocompromised states (**Ma & Fang, 2013**).

B. Brain Injury. The use of an invasive brain temperature catheter during brain injury provides an additional clinical setting for assessing the specificity of BTT° for brain temperature in the presence of brain/core discordance, as well as the detection of cytokine activity in the injured brain. The continuous non-invasive monitoring of brain temperature (with high-resolution BTT sensors) was achieved through a BTT° head-mounted sensor assembly (**Figure 8D**), which transmitted a signal wirelessly to a mobile phone equipped with a BTT application (**Figure 8J**). Tests were conducted in two patients who required an invasive intraventricular catheter as part of their medical care in the intensive care unit (University of Sao Paulo School of Medicine, Brazil).

(i) *Traumatic brain injury*. The first patient (7-year-old male) suffered a traumatic brain injury (TBI) as a result of a motor vehicle accident [resulting in a Glasgow score of 8 (**Figure 8J**)]. His invasive intracranial catheter read 37.8 °C, whilst the initial ipsilateral and contralateral wireless BTT° readings were 37.05 °C and 37.75 °C respectively. Over the course of 22 seconds, these metrics increased to 37.21 °C and 37.79 °C, respectively, as shown by the mobile application (Time: 0:26 and 0:48). The BTT° region revealed a remarkable velocity of 0.73 $°C \cdot 100s^{-1}$ for the side ipsilateral to the injury, compared to 0.18 $°C \cdot 100s^{-1}$ for the contralateral side. This fast response and remarkable four-fold increase in velocity in the injured side was consistent with the BTT°-detected brain thermodynamics findings. These characteristics may result from inflammatory processes and an increased interleukin release in severe brain injuries (**Dimopoulou et al., 2004**). The experiment further indicates the specificity of BTT° for brain temperature and its ability to monitor thermal kinetics in a child's brain. This led to our large-scale (100 pediatric patient) study to identify hypothalamic thermoregulatory activity during infection; this is key to the COVID-19 response, because it addresses a large population that may become a key source and reservoir for mutations (because children cannot respond to vaccinations, owing to their immunogenicity).

(ii) *Stroke.* A second patient (60-year-old female) was monitored via wireless streaming (using the same device as in **Figure 8D,J**). She had suffered a massive right-sided generalized fronto-temporal ischemic stroke. The right BTT° (33.79 °C) differed from the ipsilateral intraventricular catheter reading (34 °C) by 0.21 °C, and both were more than 2.0 °C below Core° (Esg° = 36 °C). This further corroborated brain/core discordance and the specificity of BTT° for brain temperature, which accords with the reduced brain temperature (albeit of lower magnitude) found during our noninvasive impeding stroke investigations (**Abreu et al, 2020b**). These findings further supplement the validation of our previous comparison of BTT° to invasive brain temperature monitoring (**Abreu et al., 2020a**). Furthermore, they confirm BTT° as an appropriate measure of brain thermal status in elderly patients; this is of considerable relevance to the COVID-

19 pandemic, considering the immunocompromised states produced by immunosenescence **(Ma & Fang, 2013**).

C. Brain Hyperthermia: Exercise in Hot Climate Chamber. This initial study was performed to determine whether the temperature measurements (aligned with physical and biological principles) at the BTT site could detect the increased brain thermogenesis, hypothalamic activity, and heat production and absorption levels that occurred during exercise in a 40 °C chamber, to provide further evidence of the specificity of BTT° for brain temperature during hyperthermia. To determine whether the BTT° identified the brain/core discordance during exercise, we compared the BTT° and Core° (obtained with a thermal capsule [Capsule°] ingested eight hours prior to the exercise]) readings in a healthy male co-investigator (M.F.B.) during continual exercise (slow jogging) on a treadmill in a warm (40 °C) environmental chamber. The difference between BTT° and Core° was 0.35 °C at the baseline, increased transiently to 0.7 °C, and subsequently remained constant at $\geq$ 0.25 °C throughout the exercise (**Figure 8K**). After 40 min, the BTT° exceeded 39.1 °C (vs. 38.8 °C for body core temperature), and the exercise was terminated. Despite the heat absorbance from the environment and the muscle-activity induced thermogenesis, there remained a difference of at least 0.25 °C between the BTT and Core temperatures, as detected by BTT°. The differences between BTT° and Capsule° were consistent with the arterial and venous temperature differences reported in subjects with thermocouples placed (invasively) in the aorta and internal jugular vein, where the average brain temperature during exercise was calculated to be ~0.2 °C higher than that of the core (**Nielsen & Nybo, 2003**). Within 3 min of exercise termination, the BTT° had been reduced by 0.35 °C, whilst the Capsule° continued to rise (0.13 °C). This brain/core discordance may help address the diagnostic differences between hyperthermia and fever, a key issue in COVID-19 mitigation, as previously addressed in *Temperature* (**Daanen et al, 2021**).

D. BTT° Identification of Selective Hypothalamic Activation and Detection of Afebrile Asymptomatic RNA Viral Infection

We performed a series of tests to establish a basis for identifying hypothalamic activation and disturbance, including heretofore-unobserved thermoregulatory responses during the pre-febrile phase of a viral illness. These experiments entailed identifying changes in the hypothalamus temperature and thermodynamics during scenarios in which the vital ~4 g structure at the internal terminus of the BTT natural thermal waveguide was altered (**Abreu et al., 2020a**). The subsequent studies revealed changes in BTT° and the activation of hypothalamic autonomic activity, which has typically remained undetected in the absence of major modifiers of body temperature [e.g., intravenous body cooling that produces shivering (**Lopez et al., 1994**)].

Intra-hypothalamic normothermic thermoregulatory activity (IHNTA) is predominantly below the febrile threshold (herein also referred to as the fever threshold), which was established as 38.0 °C by the U.S. Center for Disease Control (**CDC, 2017**). IHNTA is typically not accompanied by a detectable change in Core°. This motivated several proof-of-concept assessments, initially examining the impacts of the "extra-hypothalamic" influences of biochemical compounds (e.g., cytokines during traumatic brain injury) originating from outside the afferent and efferent hypothalamic neuronal circuitry, changes impacting thermoregulatory dynamics (e.g., anesthesia, sedation, and sleep), intracerebral changes (e.g., brain injury), and changes originating from core (e.g., myothermogenesis) and whole-body warming during exercise in a 40 °C chamber. We applied these findings to the relationships between BTT° and Core° for data obtained from 100 emergency room pediatric patients with suspected fever; BTT° was found to reveal hypothalamic thermoregulatory activity. These findings provided the foundation for

tracing the assessments of three subjects, who were unknowingly in the incubation phase of influenza virus infection during testing of the BTT° sensors. In these subjects, the thermoregulatory disturbance was the probable consequence of cytokine inhibition of the hypothalamic parasympathetic-induced modulation during sympathetic thermogenesis. The findings represent a probe of hypothalamic thermoregulatory activity and compromise thereof, which may be valuable for the detection, diagnosis, and treatment of multifarious related conditions, including hypothalamic and related brain injuries, hormonal disturbances, autoimmune diseases, sleep disorders, neurodegenerative diseases, and disturbance of brain/core integration (e.g., peripheral cardiovascular disturbances). Most importantly for COVID-19, these findings facilitate detection of SARS-CoV-2 during the virus' incubation (afebrile asymptomatic) period, where it has the unique ability to spread within the body and be silently shed to the environment. Analysis of three datasets shows that the pre-febrile phase can be identified by sequential BTT° measurements and/or concurrent measurements of BTT° and Core°.

(1) BTT°-based Hypothalamic Activity Detection in Pediatric Patients with Potential Fever

We conducted studies upon 100 pediatric patients with potential fevers, based on a continuous delineation of brain temperature kinetics via BTT; this was achieved by inserting an intra-brain thermal sensor into a pediatric patient (**Figure 8J**), and it corroborated the ability of BTT° to detect the brain thermal statuses of children for early infection detection. Detection of COVID-19 in children is crucial to controlling the pandemic and preventing a potential catastrophic resurgence that—as studies already indicate (**Davies et al., 2021**)—will likely inflict more severe damage in 2021.

Children are particularly liable to misdiagnosis by thermometry practices unaligned with physical and biological principles during the COVID-19 pandemic, because of parents' reliance on fever as the main objective warning sign for COVID-19 (or Kawasaki disease). The other signs of infection in children are subjective and difficult to interpret. Lack of infection detection in children may lead to accelerated viral evolution.

Accordingly, the BTT°-based detection of early infection in children addresses a critical problem: children represent major reservoirs for the accumulation of mutations, because their immature immune systems facilitate uncontrollable virus replication, and this higher replication rate can cause intra-host viral evolution. Thus, children are a major source for more dangerous and deadly variants, thereby perpetuating the pandemic. This is supported by (i) studies of infants with COVID-19, who exhibited exponentially (over 50,000 times) higher viral load concomitants following emergence of a variant (**LoTempio et al., 2021**); (ii) investigations showing children and adolescents to be more infective than adults in household settings (**Li et al., 2021**); and (iii) the recent spike in infections in children, which is associated with new variants (**Day, 2021)**.

We sought to determine whether BTT° can identify the effects of infection on the hypothalamus, by examining a population of 100 pediatric patients in the emergency department of a major New York hospital. As per routine clinical practice, Core° was obtained for each patient using a digital oral thermometer (SL°). BTT° was obtained (for investigational purposes) by recording the highest value obtained (over a 5 s period) by a hand-held non-contact BTT detector held over the eyelid at the $SMOS_{BTT}$ (BTT Abreu Brain-Eyelid Thermometer 3.1, BTTCorp, Aventura, FL), representatively shown in **Figure 5E**. Linear regression identified clinically troubling disparities, resulting in an equation of SL° = 20.19 + 0.4529 (BTT) with $R^2 = 0.344$ and a 95% confidence interval of ± 1.0 °C (unpublished data).

We appreciate that the inter-device difference exceeded (and opposed) that generated under resting conditions in healthy subjects, where BTT° – SL° averaged -0.06 ± 0.5 °C. In contrast, BTT° – SL° increased to 0.46 ± 0.7 °C in the 100 emergency department patients. Moreover, in line with the equation, the distribution of BTT° – SL° differences was not homogeneous at different temperatures (**Figure 8L**). When the average BTT° and SL° temperatures exceeded 37 °C, BTT° exceeded SL° in 60/72 patients, and the average difference in those 72 patients was 0.62 ± 0.7 °C ($p < 0.001$; paired t-test). In the subgroup above 37.5 °C, BTT° exceeded SL° in 30/32 patients. At or below 37 °C, BTT° exceeded SL° in only 15/28 comparisons ($p < 0.001$ vs. above 37.5 °C and $p = 0.003$ vs. above 37.0 °C; chi-square analysis), and BTT° – SL° averaged 0.06 ± 0.7 °C ($p < 0.001$; unpaired t-test for difference vs. group above 37 °C). In the subgroup below 36.5 °C, BTT° exceeded SL° in only 1/5 patients; this was attributable to their not having a febrile (or imminently febrile) condition (as opposed to the febrile state of an incubating condition).

The relative increase in BTT° readings above 37 °C, obtained in the absence of a visible characteristic capable of producing such changes, suggests an extra-hypothalamic factor. In contrast to exercise in a heated chamber, this did not require precipitation (via increases of Core°) or sympathetic withdrawal and activation to attain the necessary cardiovascular responses. Alternatively, we attributed the "loss" of IHNTA to the infection-induced release of cytokines. These affect the hypothalamus by increasing the setpoint to parasympathetic activation, which subsequently suppresses sympathetic thermogenesis. This increased the hypothalamic and systemic temperatures, as manifested in BTT° and Core°. The increased BTT° – Core° difference was attributable to the initial effect at the hypothalamus, which, being a disinhibitory process, produces multiple stages within the organ and can accelerate the depolarization of multiple hypothalamic neurons. The consequent increase in hypothalamic temperature precedes an increase in Core°; hence, the development of Brain°-Core° discordance may identify infection before it becomes clinically evident. This expands temperature from being a vital indicator of symptomatic infection to the only available indicator of preclinical infection.

The increase in BTT° readings above 37 °C also indicated the BTT° detection of hypothalamic activation in the aforementioned IHNTA range. It appears that BTT° captures the equilibrated temperature of the hypothalamic-pituitary axis (HP axis) and neighboring brain regions adjacent to its terminus in the cavernous sinus (**Abreu et al., 2020a**); furthermore, by measuring the temperature of the body's thermoregulatory region, BTT° can also capture the heat of the increased hypothalamic thermogenic activity of the hypothalamus and/or HP axis and neighboring brain regions, thereby offering an aggregate measurement, as first suggested by the fact that, during a hypothermic cardiopulmonary bypass study, the BTT° value exceeded the temperature of all Core° measures at the end of the rewarming period (**Abreu et al., 2020b**). Below, we address how, in the context of COVID-19, this may provide a vital early detection tool and thereby prevent spreading, by targeting specific populations and prompting early treatment of individuals before significant intra-victim spread and community shedding.

The major effect of hypothalamic thermoregulatory activity above 37.0 ℃ is consistent with the reported 95th percentile for normothermia: 37.1 °C and 37.6 °C at 6 am and 6 pm, respectively, in 700 measurements obtained from healthy volunteers, as measured by digital SL° (**Mackowiak et al., 1992**). Regression modeling involving 150,280 temperature measurements between 2007 and 2017 generated 95th percentiles ranging from 36.64 °C (in black men) to 36.77 °C (in white women) (**Protsiv et al., 2020**). The 95th percentile for our 80 BTT° data points during measurements of healthy volunteers was 36.81 °C.

The present data suggest that, in many cases, by measuring the cumulative metric of systemic fever and regional activation, BTT° can identify the otherwise-undetectable presence (or imminence) of systemic fever. Fifty-five patients in the present series of patients exhibited SL° readings between the [recently cited (**Protsiv et al., 2020**)] mean for normothermia (36.67 °C) and the threshold [reported by the United States Centers for Disease Control and Prevention (**CDC, 2017**)] for fever (38.0 °C); hence, these patients would be deemed afebrile. However, BTT° was ≥ 38 °C in 20/55 patients, such that BTT° – Core° indicated a 36.4% lack of SL° detection for a potentially fever-generating condition when SL° lay within this data range (**Figure 8M**). The more sensitive aggregate measure provided by BTT° captures the impact of cytokine release before it induces a comparable and appreciable change in the hypothalamic setpoint and Core°.

Another observation within the 100-patient dataset further supports the conclusion that BTT° is sensitive to hypothalamic thermoregulatory activity and that monitoring BTT° may help to identify the sites of action and impact for certain putative agents (e.g., antigens and excessive cytokines), as well as the effectiveness of treatment. Four of the patients received an antipyretic ("acetaminophen" or "ibuprofen," based on clinician preference, which was not specified). In each of the four patients, BTT° – SL° was reduced, such that the mean ± SD decreased from 0.46 ± 0.6 °C to 0.04 ± 0.6 °C ($p = 0.11$). The pattern observed in this preliminary assessment is consistent with the recognized action of these anti-pyretics along the prostaglandin-enabled pathway associated with hypothalamic activation. The site of impact may help identify the expressed advantages/disadvantages of a given therapy (e.g., the inhibitor of PGE2 or interleukin) in practical contexts. Reduction of the post-treatment BTT° – SL° may indeed represent a valuable metric for the early detection of cytokine activity, because BTT° is uniquely responsive to therapeutic anti-inflammatory effects at the level of the hypothalamus. This small subset reveals another potential indicator of incipient fever. It included two measurements of BTT°, facilitating the evaluation of drug-induced changes without the need for an accompanying Core° measurement. BTT° was reduced by 0.55 ± 0.8 °C after therapy. We appreciate that successive readings would also exhibit variability in untreated patients. As shown below, changes in BTT° may indicate increased thermoregulatory activity during the incipient asymptomatic phase of RNA viral infection. The aforementioned findings reveal that BTT° uniquely detects hypothalamic thermoregulatory activity.

2. BTT°-based Thermal Patterns of Asymptomatic Afebrile RNA Viral Infection.

2.1 *Disturbed BTT°$_{normal}$ / BTT°$_{afebrile\ infection}$ during otherwise-undetected afebrile state whilst awake.*

Considering our 100 patient study, which found that BTT uniquely detected hypothalamic thermoregulatory activity, we conducted further investigations to detect thermoregulatory changes in the context of asymptomatic afebrile (here used interchangeably with pre-febrile) RNA viral infection. To determine whether BTT° could detect unique thermoregulatory brain dynamics (which may identify thermal patterns consistent with the potential signatures of asymptomatic influenza infection and thereby promote our ongoing studies into asymptomatic COVID-19 patient monitoring), we compared BTT° plots from the same subject whilst uninfected (BTT°$_{normal}$) and during the pre-febrile and asymptomatic stage of infection (BTT°$_{prefebrile\ infection}$). The subject (35-year-old male, referred to as "Prefebrile-1") was tested with wireless sensors designed for long-term use (> 1000 mins); these were built into the frames of eyeglass (**Figure 8C**), and they streamed data to a mobile application, as shown in **Figure 8J** (BTT Intelligent Eyeglass, IATLo 3.0, BTT Corp, Aventura, FL). The subject was asymptomatic for ~48 hours after completing the

sensor tests, was subsequently diagnosed with influenza, and then developed classic influenza symptoms, with a fever of > 38 °C.

We compared continuous brain temperature kinetics between the baselines for the normal (non-infected) state and for asymptomatic infection (including thermal levels, variability, and maximum temperature). Once the BTT° monitoring began, a 500 s time window was stored; and this was sequentially compared to the previous window, to identify thermal changes over time. In addition, a comparison was also conducted against a stored normal baseline for the subject under evaluation; this was supported by our machine-learning-based data training for fever detection (**Microsoft, 2017**). Comparison of a 500 s segment of a seemingly "flat" interval (**Figure 8N**) during asymptomatic infection against a 500 s seemingly "flat" segment when the subject was free from infection and wearing an identical BTT sensor revealed that, in addition to a higher mean (36.50 °C vs. 35.94 °C, respectively) and maximum temperature (36.55 °C vs. 35.96 °C, respectively), the subject's pre-febrile state exhibited greater variability (standard deviation: 0.020 °C vs. 0.013 °C, respectively; 10^{th}–90^{th} percentile: 0.05 °C vs. 0.03 °C, respectively).

During our tests of the noninfected state (which did not include Core° measurements), $BTT°_{\mathbf{normal}}$ remained equal to or below 35.96 °C, again below the fever threshold. During the first 7 h of testing, $BTT°_{\mathbf{prefebrile\ infection}}$ varied from 35.40 °C to 37.05 °C. This corresponded to a $BTT_{maximum}° - BTT_{minimum}°$ difference of 1.65 °C during the afebrile asymptomatic phase of RNA viral infection, compared to 0.6 °C in the non-infected state. The large variation in BTT°, as identified during afebrile asymptomatic RNA viral infection in the awoken state, was also found during sleep (shown below). When the subject was healthy and using previously tested identical BTT sensors, his maximum $BTT°_{\mathbf{normal}}$ during the 500 s interval was 35.96 °C, compared to a $BTT°_{\mathbf{prefebrile\ infection}}$ of 36.55 °C during the infected state.

These comparative thermal levels provide an initial basis for a proposed thermoregulatory activity pattern capable of detecting asymptomatic RNA viral infection; this includes a change of > 0.60 °C from the mean BTT° baseline during the pre-febrile state and a greater variability (> 0.020 °C) than the non-febrile state. The greater variability and > 0.60 °C change arising during asymptomatic viral infection revealed sympathetic activity aligned with an early thermogenic response. A third comparative characteristic employed to detect asymptomatic infection involves comparing the maximum temperature difference between the baseline temperature in the euthermic (non-infected) state and after infection, as shown in the 500 s window. Asymptomatic infection exhibits a maximum BTT° higher than the temperature of the noninfected state. The maximum $BTT°_{\mathbf{prefebrile\ infection}}$ during the 500 s interval was 0.59 °C higher than $BTT°_{\mathbf{normal}}$. Hence, the first essential feature for delineating the autonomic thermodynamic signatures of asymptomatic RNA viral infection involves capturing the baseline brain temperature kinetics and variability as well as the maximum temperature, and comparing these with the new baseline and new variability generated once an individual becomes infected; this reveals hypothalamic activation moving toward predominantly sympathetic activity.

2.2 Disturbed BTT° – BTT° and BTT° – Core° during otherwise-undetected afebrile illness whilst awake.

The confounding—and remarkably diagnostic—impact of sympathetic cytokine release on BTT° recordings was further documented by the plot from a 38-year-old male member of our technical staff, who underwent a comparative test of BTT° and SL° to examine BTT° sensors mounted in eyeglass frames (**Figure 8C**). This subject had been unknowingly incubating influenza virus. Asides from a mild drowsiness, the subject (herein called "Prefebrile-2") appeared healthy at the time of testing and was afebrile. However, he developed symptomatic influenza (including a fever

of > 38 °C) and was diagnosed with influenza ~24 hours after completing the test. **Table 4** summarizes the BTT° plots (19–44 s in duration) at each of the five comparative measurements over the 94 min testing interval (recorded as the value at the onset of the given segment) and the corresponding SL°. Analysis of the data reveals that, although BTT° and SL° both remained below the fever threshold (38 °C), a pronounced variation between BTT° readings and a prominent BTT° – Core° discordance occurred during the paired readings.

The potential diagnostic value of serial BTT° was evidenced by the range of BTT° (37.33–37.97 °C). The BTT° increase of 0.64 °C, as measured 82 min after the lowest temperature level at onset (37.33 °C), shows the gradual disinhibition of sympathetic thermogenesis, attributable to a cytokine-autonomic input from the brain's thermoregulatory center. The level was comparable to the aforementioned -0.55 ± 0.8 °C reduction of BTT° in response to therapies affecting PGE2 synthesis in the four febrile emergency department patients.

Further evidence of the unusually pronounced IHNTA during the pre-febrile phase was provided by the BTT° – Core° discordance, which was as high as 2.25 °C (**Table 4**). This greatly exceeded the discordance in any of the aforementioned testing models presented in this manuscript. However, 9/91 pediatric patients (with mean temperature between BTT° and SL° of ≥ 36.6 °C) exhibited BTT° – Core° > 1.5 °C. We attributed the discordance in "Prefebrile-2" and in the nine febrile and sub-febrile emergency room pediatric patients to cytokine-induced disruption of the hypothalamic thermoregulatory control, which stimulated unrestrained increases of sympathetic thermogenesis and hypothalamic temperature before a comparable impact was registered by Core°; this supports the "brain sees before the body feels" conclusion. In accordance with the subsequent activation of the sympatho-immunologic response at fever onset, Core° of "Prefebrile-2" primarily increased over the remainder of the testing period. The large changes and variable relationships are likely attributable to the interacting neural, chemical, and thermophysical stimuli during incipient infection (**Schieber & Ayres, 2016; Soto-Tinoco et al., 2016**), many of which are extra-hypothalamic in origin.

Table 4. Comparison of BTT° and SL° during incipient influenza

Time (min) since first measurement	BTT (°C)	SL (°C)	BTT – SL (°C)
0	37.65	35.4	2.25
12	37.33	35.9	1.43
+ 23	37.83	36.3	1.37
+ 34	37.94	37.4	0.54
+ 25	37.97	37.2	0.77

Thus, the aforementioned findings indicate that assessment of BTT° – BTT° and/or BTT° – Core° discordance can provide heretofore-unattainable thermoregulatory information and hypothalamic-based thermal signatures for early viral infection; this can be used to identify the afebrile (or pre-febrile) phases of infection when neither Core° nor BTT° has reached the fever threshold. We anticipate that widespread testing will not only benefit individual patients and their communities but also facilitate future investigations of BTT° and Core° comparisons in various contexts.

2.3 Asymptomatic afebrile RNA viral infection detection during sleep.

To determine whether BTT° can detect unique brain thermal kinetics (suitable for identifying the thermal signature of asymptomatic infection) during sleep, we analyzed the plots

of a 33-year-old male, who was continuously monitored whilst testing the BTT sensing headgear (**Figure 8D**) and data streaming (to a mobile application, as shown in **Figure 8J**) operation during sleep. The subject was asymptomatic prior to sleeping; however, he was later diagnosed with influenza and developed classic symptoms (including a 38 °C fever) ~48 hours after monitoring. **Figure** 8O shows the pre-febrile plot from sleep onset until awakening, which reveals a normal initial sleep pattern presenting a gradual BTT° decrease in the first 3000 s, as observed in the subjects of **Figures 8H** and **I** and in our large database of brain thermodynamics studies conducted during sleep (not shown). However, a sudden sympathetically-driven surge of BTT° occurred at ~4 hours. This had a velocity of 0.06 °C·100s^{-1}, which was consistent with the thermodynamics (0.07 °C·100s^{-1}) of "Prefebrile-1," who was awake. Likewise consistent with Prefebrile-1, the predominantly sympathetic input was followed by a predominantly parasympathetic tone and a sudden reduction of BTT° (-0.14 ºC·100s^{-1}). These changes suggest the thermoregulatory center's ability to maintain autonomic responsiveness to infection during sleep, as captured by BTT°. Testing of "Prefebrile-3," was performed for ~25,000 s during sleep; we detected a $BTT_{maximum}$° – $BTT_{minimum}$° of 1.85 °C (36.20–34.35 °C), which is consistent with the large thermal variation of (1.65 °C) during the awoken state. In contrast to the $BTT_{maximum}$° – $BTT_{minimum}$° difference of 1.85 °C during afebrile infection, the noninfected state during sleep showed a < 0.9 °C variation (**Figure 8H,I**); this was confirmed by data in our large sleep database (from the Yale Sleep Center), which documents these narrower variations in non-infected states (not shown). As shown here, the large variation in brain tunneling temperature, identified during afebrile asymptomatic RNA viral infection in the awoken state, was also found during sleep.

Wireless monitoring via a mobile application (**Figure 8J**) during sleep (**Figure 8D**) facilitates the widespread acquisition of data—not only for individual assessment (including children) but also for cumulative analysis at a central monitoring center—in accordance with the aforementioned machine learning approach; this facilitates effective and timely isolation and quarantine for interrupting human-to-human transmission.

Our findings represent a proof-of-concept for the feasibility of monitoring during sleep to detect early RNA viral infection. This may be especially valuable for detecting intermittent quantal changes, as well as patterns of impulses, fluctuations, and shifts; furthermore, overnight testing provides a convenient setting for detecting incipient infection and delineating patterns of activity, to identify changes (e.g., the frequency and nature of fluctuations and thermal changes secondary to disease progression) and assess the impact of therapy.

The problem of identifying and monitoring asymptomatic RNA viral infections resulted in a small sample (n = 3), which has been largely expanded by monitoring individuals exposed to COVID-19 (see the second manuscript of the series). Nevertheless, our fever study involving 100 pediatric patients reveals that BTT° can be used to detect hypothalamic activity, and the thermal patterns detected during asymptomatic infection are consistent with the thermoregulatory response to infection and sympathetic release; taken together, this provides a foundation for detecting asymptomatic RNA viral infection via BTT°.

The urgent need for a timely SARS-CoV-2 infection detection (continuous monitoring and/or spot check) operating in concert with physical and biological principles and cooperatively with vaccines as a "detection–vaccination" pair solution is clearly evidenced by the comparison of case numbers in the U.S. on September 3rd, 2020 (pre-vaccination) and 2021 (post vaccination): 46,397 daily new cases in 2020 vs. 191,298 daily new cases in 2021 (more than a 4-fold increase) despite ~207 million people having received one dose of the vaccine and 176 million people being fully vaccinated in the U.S. (**Supp. Fig. 46**).

Figure 8. BTT° brain-temperature kinetics monitoring and brain/core discordance detection

Figure 8A

BTT° noninvasive brain temperature monitoring and brain/core discordance detection

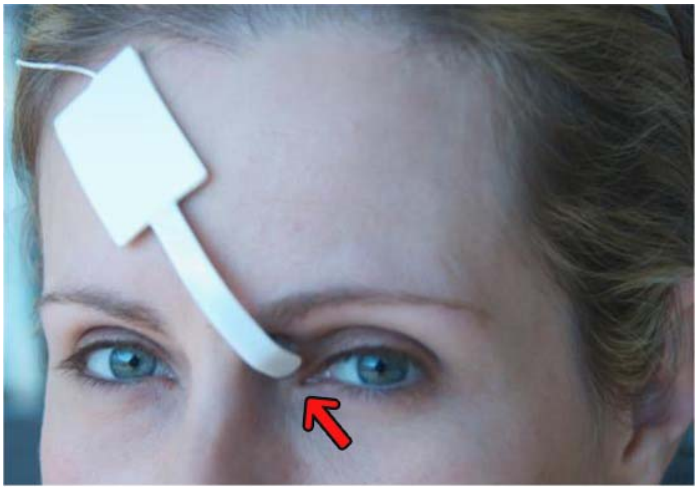

(**A**) Wired anchored sensor for noninvasive, surface-based brain temperature measurement based on FDA-approved Abreu BTT 700 System and C1 sensor (FDA, 2010), which was used during anesthesia. Left BTT sensor on the left eyelid at the BTT site (see text and Methods for details).

Figure 8B

BTT° noninvasive brain temperature monitoring and brain/core discordance detection

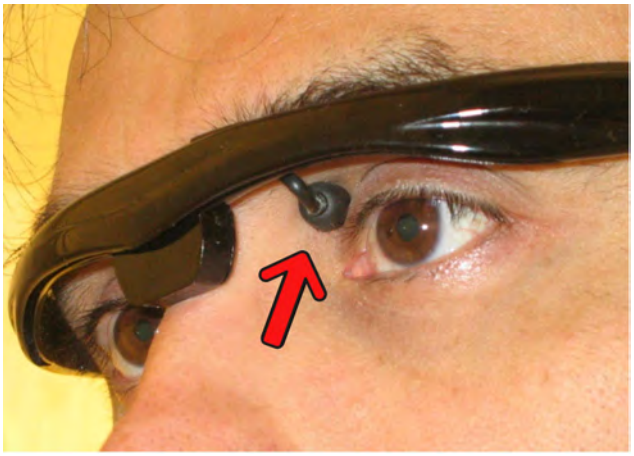

(**B**) BTT thermal sensor integrated in frame with wireless signal transmission to a remote device (BTT Intelligent Frame 2.0, BTT Corp, Aventura, FL). Side view of the user's face, showing location of left BTT sensor on the left eyelid at the BTT terminus. The wireless device and battery are located in the center of the frame.

Figure 8C

BTT° noninvasive brain temperature monitoring and brain/core discordance detection

(D) Eyeglass frames with high-resolution thermal sensor integrated in the frame and wireless signal transmission to a remote device (e.g., the mobile phone application shown in **Figure 8I**), used to detect asymptomatic viral infection (**Figure 8K**). Side view of the user's face, showing location of right BTT sensor on the right eyelid at the BTT terminus (see text and Materials and Methods for details).

Figure 8D

BTT° noninvasive brain temperature monitoring and brain/core discordance detection

(D) BTT wireless headgear with high-resolution thermal sensor (primarily for monitoring during sleep) for ICU monitoring of traumatic brain injury and stroke, shown here being used by an infant (and in **Supp. Fig 47** by an adult). This system facilitates continuous brain temperature monitoring and multiple data capture, storage, and analysis; furthermore, it transmits signals to a computer or cell phone, which enables automated early detection of brain thermal disturbances when subjects are awake or asleep. Values can be viewed locally or streamed as continuous measurements to a remote (e.g., centralized) platform (see text and Materials and Methods for details).

Figure 8E

BTT° noninvasive brain temperature monitoring and brain/core discordance detection

(E) Measurement of brain temperature of a child with non-contact infrared-based detection using the Abreu-BTT Brain-Eyelid technique (Supp. Figs. 43,44) in a 45° angle aimed toward the left upper medial eyelid (left BTT) (BTT Abreu Brain-Eyelid Thermometer 3.1 (BTTCorp.com, Aventura, FL) is used.

Figure 8F

BTT° noninvasive brain temperature monitoring and brain/core discordance detection

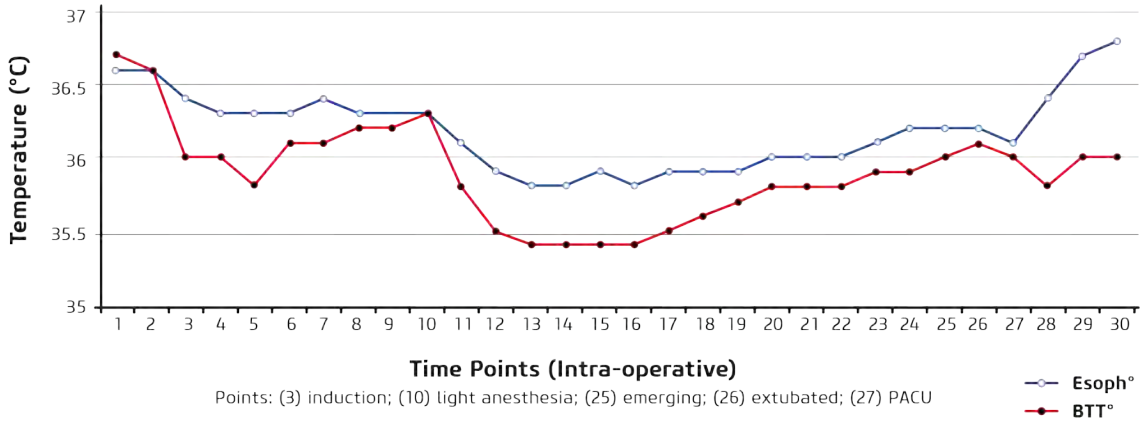

(F) Brain thermodynamics during general anesthesia, reflecting depression and activation during hypothermic state of general anesthesia. x-axis: intraoperative time points. y-axis: temperature, BTT°, and Esg°. Brain activity corresponding to depression and subsequent hypothermia was detected only by BTT°. Core° (Esg°) measurements failed to detect the depression and depth of anesthesia.

Figure 8G

BTT° noninvasive brain temperature monitoring and brain/core discordance detection

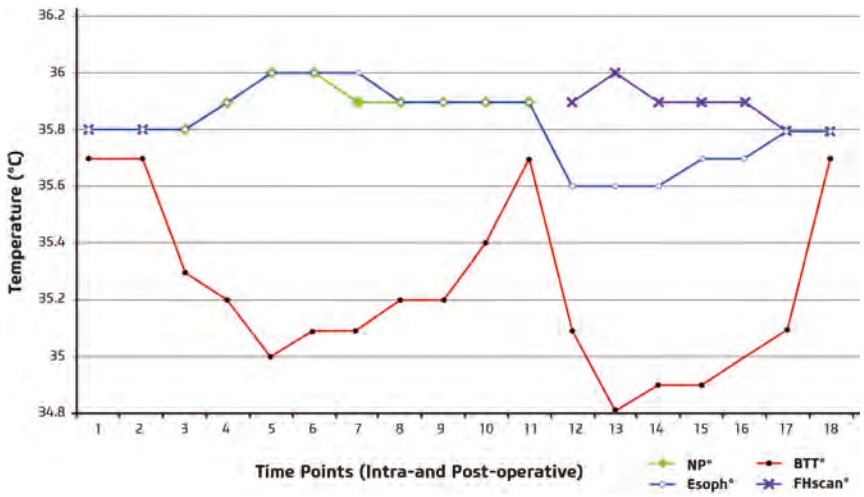

(**G**) Brain thermodynamics during general anesthesia for intra-operative and post-operative periods, reflecting depression and activation during hypothermic state of general anesthesia. x-axis: time points, intra- and post-operative. y-axis: temperature, BTT°, Esg°, NP°, and FH°. Brain activity identifying hypothermia was detected only by BTT° during intra- and post-operative periods. Measures of Core° (Esg°, NP°) and Surface° (FH°) failed to detect the depression and depth of anesthesia.

Figure 8H

BTT° noninvasive brain temperature monitoring and brain/core discordance detection

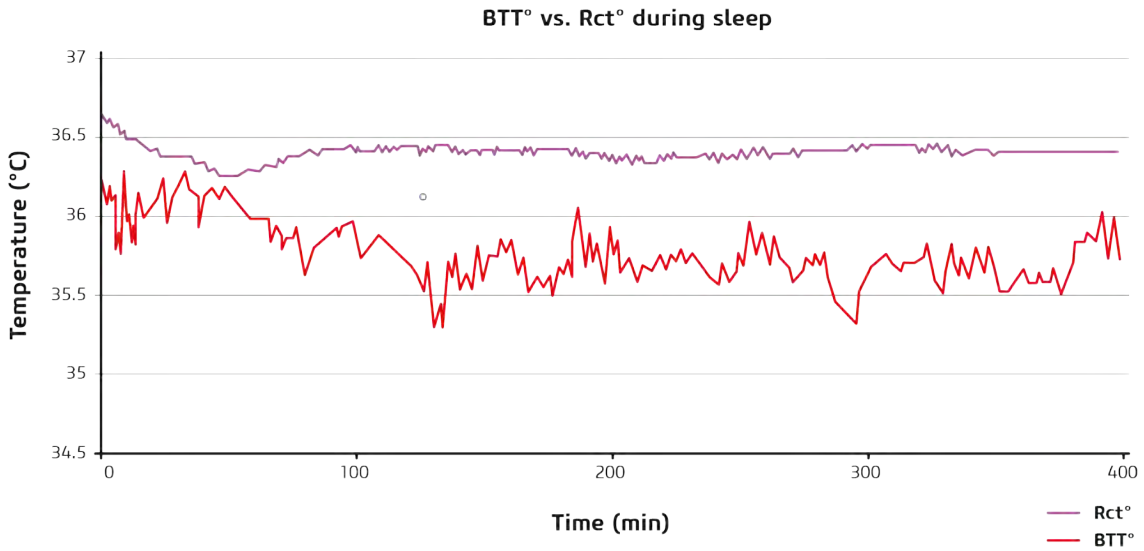

(**H**) BTT° (blue) vs. Rct° (magenta) for a sleeping volunteer. BTT° changes during sleep are consistent with brain temperature changes associated with neuronal depression. BTT° fell from ~36.3 °C to 35.3 °C, whilst Rct° decreased from 36.6 °C to 36.3 °C (see text).

Figure 8I

BTT° noninvasive brain temperature monitoring and brain/core discordance detection

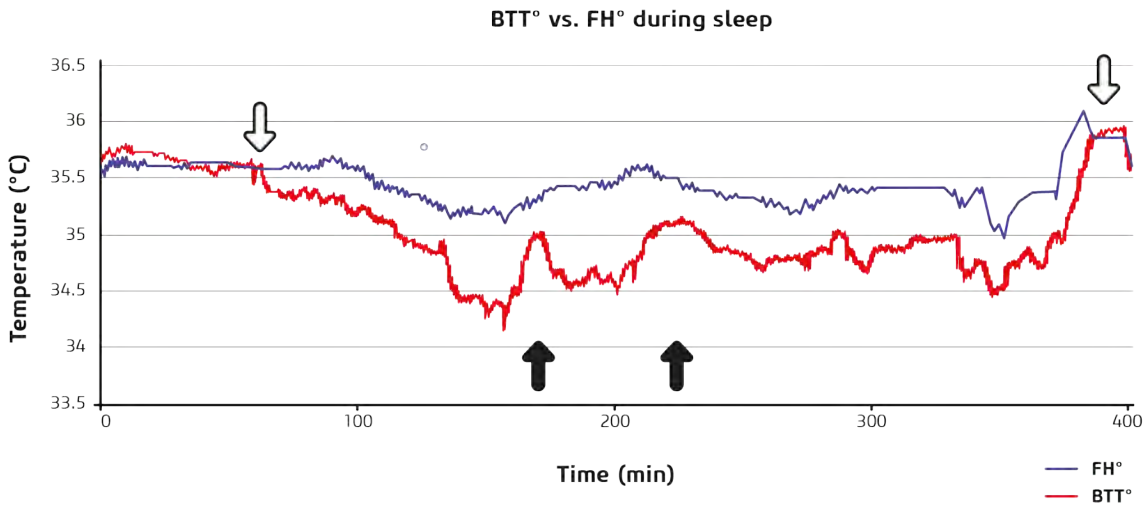

(**I**) BTT° vs. FH° for a sleeping volunteer. The BTT° during sleep is consistent with brain temperature changes. BTT° decreased by 1.60 °C relative to the baseline, whilst FH° decreased by 0.42 °C during the same period (see text).

Figure 8J

Specificity of BTT° for brain temperature and hypothalamic activity

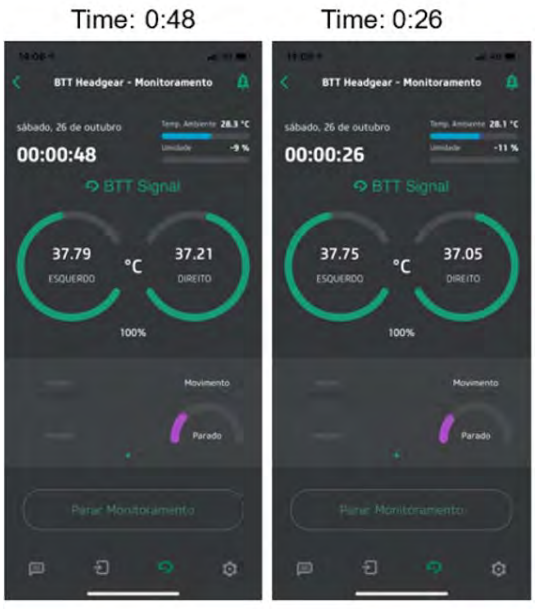

1

(J) *Top*: BTT wireless headgear (Figure 6D) positioned on the face of a patient after TBI. Magenta arrows denote intraventricular temperature-monitoring catheter. Red arrows denote BTT° monitoring devices with right and left BTT sensors. *Bottom*: Continuous BTT° readings were recorded via wireless signals to a cell phone equipped with an application. BTT° at the left ("esquerdo") and right ("direito") sides, showing values of 33.55 °C and 33.79 °C, respectively, with a temperature of 34 °C measured by the right-side intraventricular catheter (cited in text).

Figure 8K

BTT° noninvasive brain temperature monitoring and brain/core discordance detection

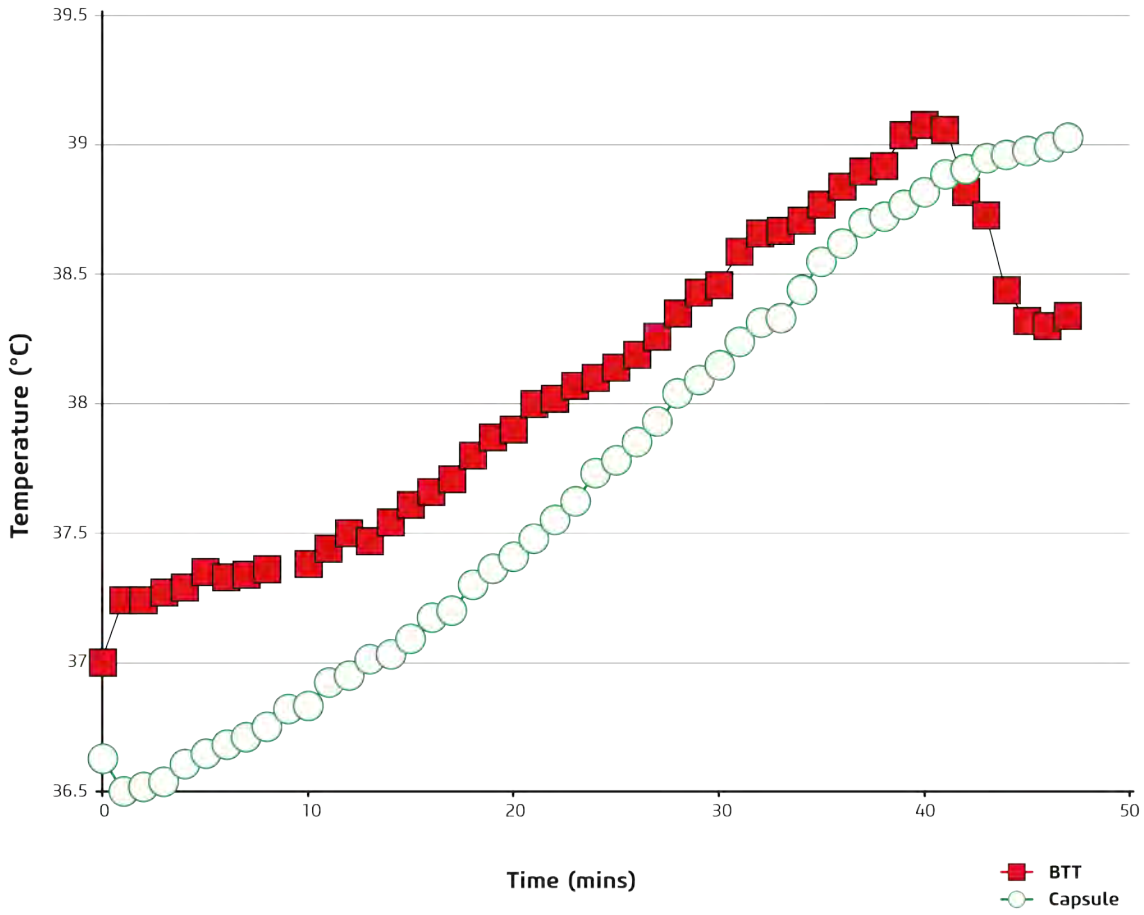

(**K**) BTT° vs. Core° (measured via ingested thermal capsule) for volunteer standing and exercising in a 40 °C chamber. The BTT° – Core° discordance observed during standing (Time 0) persisted during the exercise, despite the increased heat absorption from the environment and heat production caused by muscle thermogenesis. Upon cessation of exercise (black upwards arrow), BTT° immediately fell and then stabilized whilst Capsule° continued to rise, thereby allowing the BTT° to be used to immediately differentiate (within 3 min) fever from the hyperthermia induced

by physical exertion and the use of protective equipment. This is an extremely important issue in the context of healthcare personnel, who may exhibit increased temperatures caused by heat stress (and not fever due to SARS-CoV-2 infection), as previously reported (**Daanen et al., 2021**). BTT (°C) (range: 36.5−39.5) and time (min) (range: 0−50).

Figure 8L

Specificity of BTT° for brain temperature and hypothalamic activity

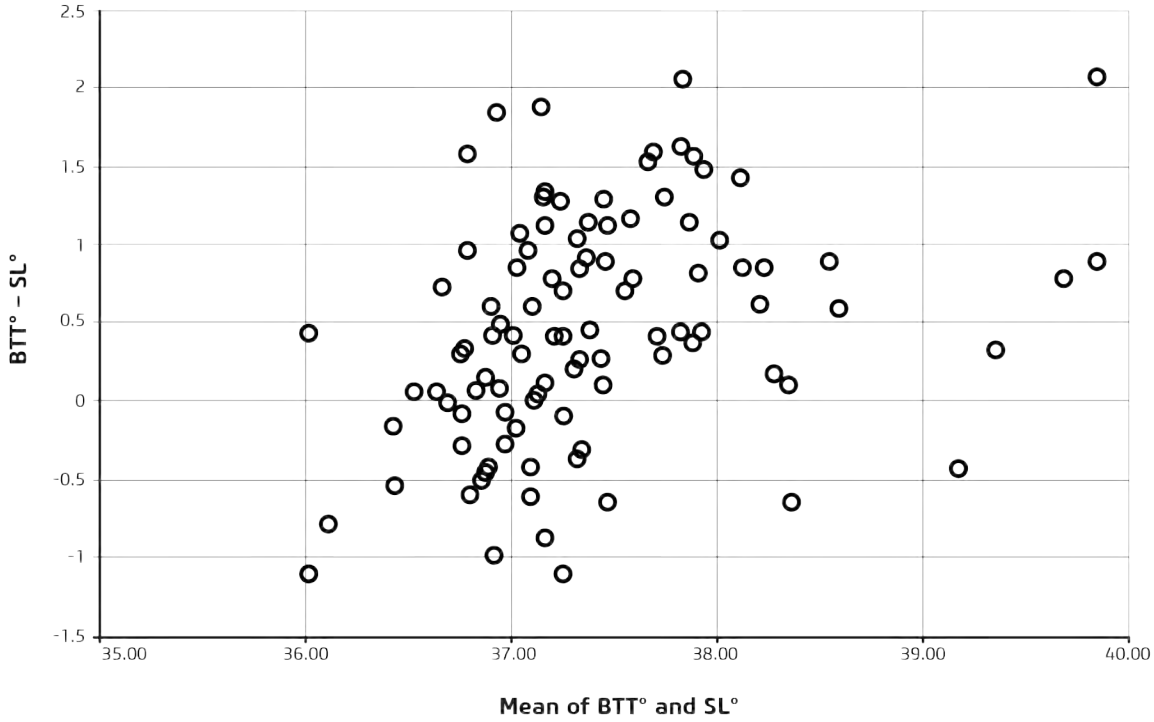

(**L,M**) Comparison of single BTT° and SLdigital° readings for 100 pediatric patients (ages 3–17) presented to the emergency room.

(**L**) Bland–Altman display of the 100 pairs of BTT° and SL° readings (see text).

Figure 8M

Specificity of BTT° for brain temperature and hypothalamic activity

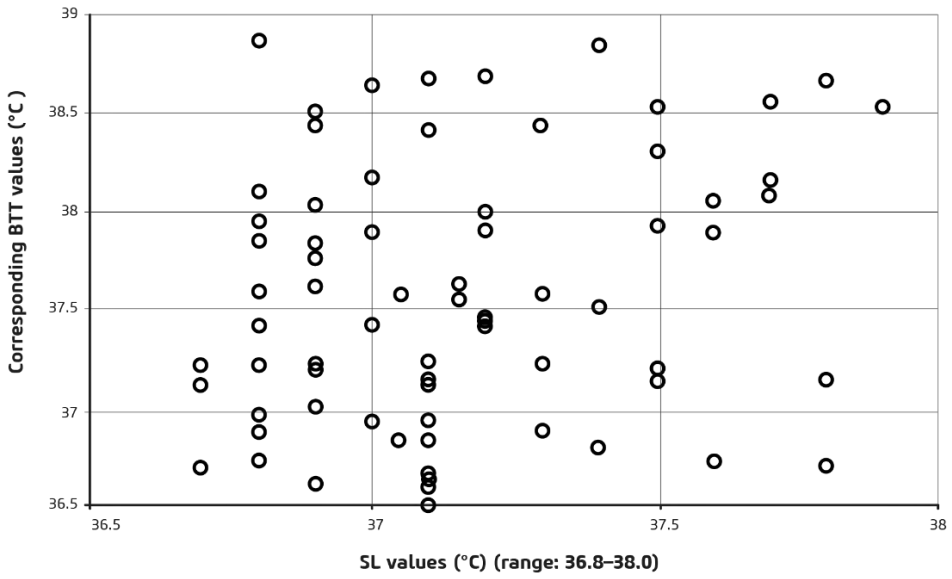

1 (**M**) BTTº values when SL° was within 36.7–38 °C (see text).

Figure 8N

Brain thermodynamics and waveform analysis of BTT° for infection detection

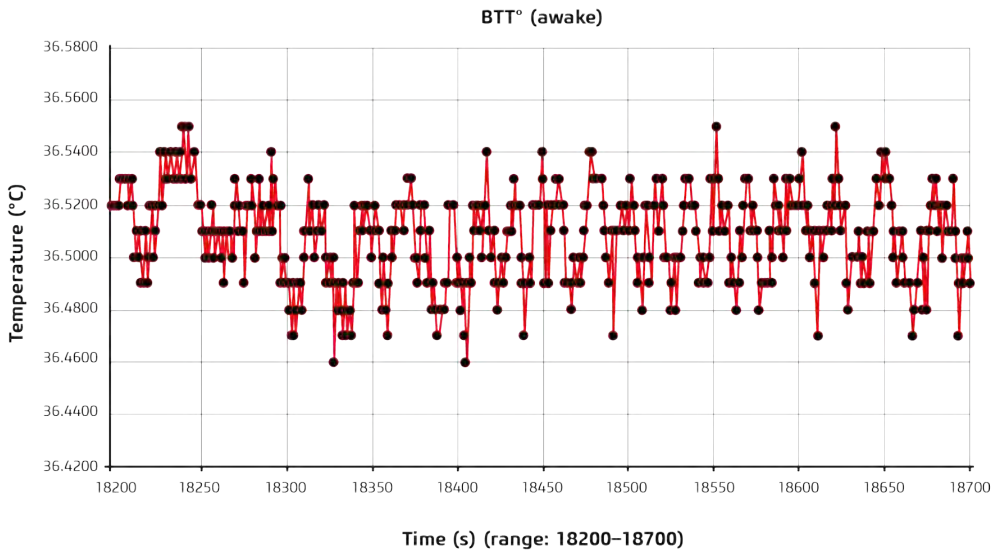

(**N**) Seemingly flat 500 s interval from continuous temperature-monitoring plot, starting at 18200 s; this determines the baseline for comparison with afebrile noninfectious measurements (see text). BTT (°C) (range: 36.42−36.58) and time (s) (range: 18200−18700).

Figure 8O

Brain thermodynamics and waveform analysis of BTT° for infection detection

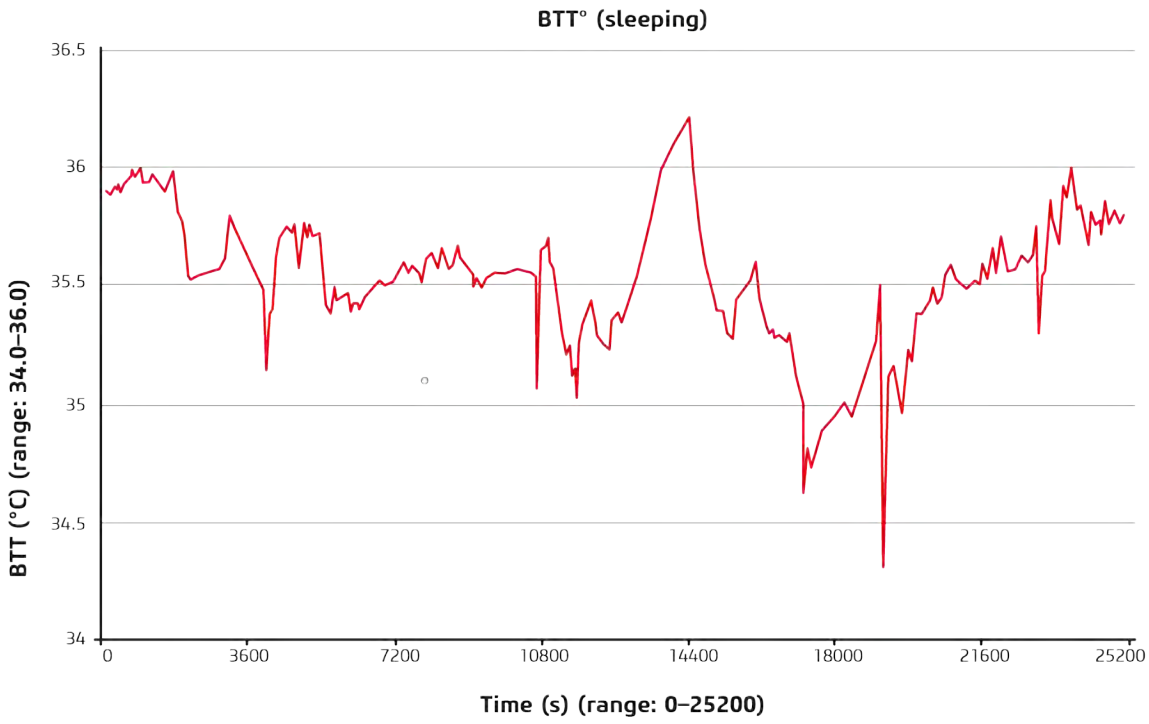

(**O**) BTT° during sleep for Prefebrile-3, a male volunteer who (unknowingly) was in the incipient phases of influenza. As noted in the text, Prefebrile-3 produced an apparent sympathetic surge and progressive parasympathetic inhibition, attributable to cytokines; this facilitated sympathetic predominance, leading to fever. BTT (°C) (range: 34.0−36.0) and time (s) (range: 0−25200).

Discussion

Until now, efforts to tackle COVID-19 have been constrained by methods that measure body temperature through low-*k* wood-like surfaces, which are characterized by highly fluctuating vascular tones; notably, such measurements are not in concert with physical, morphological, and physiological principles for effective and undisturbed heat transfer; as a result, noninvasive brain temperature measurements are severely constrained (**Kiyatkin, 2019**).

From nature emerges the threat (the virus and its mutations)—and also from nature emerges the solution (the brain and its temperature kinetics).

Our findings demonstrate the efficacy and broad utility of a novel temperature measurement paradigm based on brain thermal signals, obtained via the natural brain-eyelid thermal tunnel (the BTT). This technology offers an innovative new approach for combating pandemics by harnessing natural engineering (instead of imposing human engineering onto nature), and it applies—for the first time in infection detection—an integrated approach combining thermophysical properties and cranio-facial morphologies to produce a natural brain-based thermal waveguide (**Abreu et al., 2020a**). The resulting undisturbed thermal signals from the brain, measured through the radiative eyelids at the $SMOS_{BTT}$, render feasible a brain-based wearable technology that is automated, noninvasive, harmless, invulnerable to (and not limited by) virus mutations, suitable for use on awake and sleeping subjects, and applicable to all races and ages. Here we show how the alignment of thermometry with physical and biological principles can mitigate the risk or even prevent the rebirth of a more harmful and uncontrolled COVID-19 pandemic.

For brain-temperature-kinetics-based methods to be effective in interrupting the COVID-19 pandemic (and/or its re-emergence) and complementing COVID-19 vaccines, the thermal signal and measurements must be in concert with physical and biological principles regarding optimal heat transfer. This is achieved by using the BTT, which consists of a thermophysical path that maintains thermal continuum between the brain's thermoregulatory center and the high-*k* eyelid skin, via fat-encircled high-volumetric-heat-capacity blood (**Abreu et al., 2020a**). Our findings show that wearable sensors can be adapted to noninvasively monitor brain-temperature kinetics, detect hypothalamic activity, and continuously detect negative-sense RNA viral infection; furthermore, we find that spot-check BTT-based thermometry can detect hypothalamic responses to infections. Hence, we provide two physically and biologically founded infection-detection methods: continuous automated monitoring and spot-check measurements. Taken together, these address a key reservoir for mutations: the bodies of children.

Need for temperature-based infection detection in children, to control a potential key source for mutations and high infectivity that cannot be easily addressed by vaccines.

Our temperature-based brain-enabled infection detection methods may be essential in the fight against COVID-19, through facilitating early fever detection—via hypothalamic thermoregulatory responses—in children, who represent the largest potential reservoir for virus mutations.

Infections in children will likely represent the most difficult challenge of the COVID-19 pandemic. This is because, owing to natural limitations, children cannot be easily protected by vaccines. Furthermore, previously developed safe vaccines have met considerable challenges from the fatal "enhanced diseases" that were triggered by vaccines for respiratory syncytial virus (**Acosta et al., 2015**), an RNA virus; although unlikely, this indicates the potential for fatal reactions to be triggered by SARS-CoV-2 (also a RNA virus) vaccines. However, even with a child-safe vaccine, the weak immunogenicity of children (due to their immature immune systems) may prevent effective vaccination, because children tend not to mount an effective immune response. Notably, a solution cannot go against nature, or it will invariably fail; thus, vaccinating children (and babies) may expose this defenseless population to harm from the vaccine's potential side effects, without achieving the goal of preventing infection and/or spreading. This can be clearly observed in the concerning evidence that children can carry extremely high viral loads, owing to undeveloped immune responses. For example, a 51,418-fold increase in viral load was identified in a baby, who also generated a novel spike protein variant (**LoTempio et al., 2021**). Although this represents an outlier, it reveals the potential for high intra-host viral replication

leading to accelerated viral evolution and mutations in infants. This case of an immature immune system represents the nature of children's immunological responses, and vaccines' dependency on effective immune responses results in a lack of efficacy, aside from issues with safety. Hence, even with an entirely vaccinated global adult population, children may propagate the COVID-19 pandemic and even infect fully-vaccinated adults, because—as reiterated twice by the U.S. government—"*Vaccinated people could potentially still get COVID-19 and spread it to others*" (**CDC, 2021a**; **CDC, 2021b)**.

This further emphasizes the need for immediate and—ideally—automated daily infection detection practices (as shown here). Arguably, concern for this defenseless population is made more pressing considering babies' and children's reliance upon parents for their daily needs (which demand close proximity and thereby produce an environment for viral spreading). Moreover, children—in particular babies (and toddlers)—tend to remove their masks, and the risk of sudden infant death syndrome further prevents the safe use of masks. Thus, infection detection is vital, even more given that the benefits of vaccines cannot be easily extended to children. This places children at risk of suffering and dying from COVID-19, further underscoring the need for early detection before viral replication and widespread organ damage occurs as a result of the virus or cytokines (e.g., multisystem inflammatory syndrome).

The higher infectivity of children as compared to adults **(Li et al, 2021**) also corroborates the need for infection detection in this age group, to protect children and adults (in particular, parents and teachers); this reveals another key target group for infection detection practices aligned with physics and biology, such as continuous automated monitoring or spot-check measurements. Like children, immunocompromised adults (e.g., cancer patients) may also promote accelerated viral evolution, resulting in the emergence of deadly mutations (**Choi et al., 2020; Hensley et al., 2021; Khatamzas et al., 2021; Truong et al., 2021**); however, in contrast to children, vaccines can be safely administered in this group (as discussed in the second manuscript of the series). Nevertheless, high viral loads in children may lead to mutations and the emergence of deadly variants; this demands immediate attention because more children are being infected, leading to the highest number of hospitalizations in the U.S. since the beginning of the pandemic (**Toy & Wernau, 2021**); this is further supported by the case of a fully vaccinated mother who was infected by her child: *"Our kids are Trojan-horsing us. They are the way in."* (**Brueck, 2021**). The need to protect children (and parents alike) via early infection detection is yet further corroborated by the steady increase in child cases reported by the American Academy of Pediatrics (**Thomas, 2021**) and a Mississippi report pleading "Save our babies" owing to recently increased numbers of fatalities attributable to COVID-19 (**Haselhorst, 2021**).

The critical impact of mutations on the COVID-19 pandemic reveals the vital need for noninvasive temperature-based infection detection in children.

The only way to eradicate SARS-CoV-2 is by addressing mutations; this can only be effectively achieved by addressing populations who may not effectively respond to vaccinations due to immunogenicity, particularly children. Unless effectively addressed, mutations emerging in the bodies of children (and babies) through intra-host-accelerated viral evolution may potentially cause SARS-CoV-2 to spread indefinitely.

As an RNA virus, SARS-CoV-2 is continuously mutating, producing mutations with increased infectivity (**Korber et al., 2020**) and a subsequently increased resistance to the therapeutic effects of monoclonal antibodies and convalescent plasma (**Wang P. et al., 2021**).

Vaccines can control COVID-19; however, mutations (e.g., the Delta variant) may reduce their effectiveness (**Sheikh et al., 2021**), and previous studies show that the two major RNA

vaccines in the U.S., BNT162b2 mRNA and mRNA1273, are 10.3 and 12.4 times less effective against the South Africa variant (Beta B.1.351), respectively (**Wang P. et al., 2021**); this indicates that all variants carrying the E484K "escape mutation" [e.g., the New York variant (**Lasek-Nesselquist et al., 2021**)] may reduce the effectiveness of vaccines. This reduced vaccine efficacy was further confirmed by studies from Israel showing that the South Africa variant B.1.351 and U.K. variant (Alpha B.1.1.7) are able to weaken protection from the BNT162b2 mRNA vaccine (**Kustin et al., 2021**). This was further corroborated by a study from Qatar showing the reduced effectiveness of the vaccine against the South Africa variant B.1.351; however, the vaccine was effective in preventing severe illness and death (**Abu-Raddad et al., 2021)**. Thus, if the B.1.351 or B.617 variant, or another new variant [which could be gestated in the bodies of children or the immunocompromised (e.g., cancer patients)] that evades vaccines becomes dominant, it could impact the protection of vaccines, further supporting the need for a "detection–vaccination" pair solution—assisted by nature via the brain-eyelid morphology—to effectively address the COVID-19 pandemic and potentially eradicate SARS-CoV-2.

The need for daily and automated early infection detection—to mitigate mutations—is clearly evidenced by the impact of the following mutations: (a) California, B.1.429 (**Zhang et al., 2021; Tchesnokova et al., 2021**), which seems more lethal (**Wardman, 2021**); (b) New York, B.1.526 (**West et al., 2021)**, which seems to evade vaccines **Lasek-Nesselquist et al., 2021**); (c) the U.K., B1.1.7 (**Kemp et al., 2021; Kidd et al., 2021**), which is highly transmissible and more deadly (**Bager et al., 2021, Challen et al., 2021)**; (d) Brazil, P.1, which seems to evade immune responses and is more transmissible (**Hoffman et al., 2021; da Silva Francisco et al., 2021; Souza et al., 2021**); South Africa, B.1.351, which is more deadly and resistant to the antibodies produced by vaccines and previous infections (**Hoffman et al., 2021; Tegally et al., 2021; Wang Z. et al., 2021, Wibmer et al., 2021***)*; and India, "double mutant" B.1.617 (the Delta variant), which is more transmissible, deadly, and has caused a catastrophic surge in India (**Ranjan et al., 2021**). These are in addition to the viral convergent evolution identified in the U.S. (**Hodcroft et al., 2021**) and in Europe, in which the mutated virus can evade antibody-mediated immunity without losing fitness **(Thomson et al., 2021**), and the New York variant, which includes three mutations: the E484K mutation, that allows the virus to evade vaccines and immune responses; the D235G mutation, that reduces the efficacy of neutralizing antibodies; and the S477N mutation, that increases infectivity (**Lasek-Nesselquist et al., 2021).** Concerning combinations of mutations are also occurring in the U.K. (showing that the virus is evolving further), where the original U.K. variant B.1.1.7 (which is more transmissible) has evolved and now incorporates mutation E484K, producing a more transmissible variant that now also may evade vaccines (**Wise, 2021**). According to dynamic models, mutations may cause 2021 COVID-19 hospitalizations and deaths across England to exceed those in 2020 (**Davies et al., 2021a**), further indicating the potential for an even more dangerous COVID-19 strike in 2021. This reiterates the importance of early infection detection in the immunocompromised and children, as well as people living in close proximity to these populations, including parents, teachers, and caregivers.

The importance of protecting children via the early detection of hypothalamic activity through the natural brain-eyelid morphology also arises from the challenge of identifying COVID-19 via nonspecific signs of COVID-19 infection in this age group (in addition to reducing transmission from children), because the number of infections in this group is currently climbing (**Toy & Wernau, 2021**). Early infection detection is further supported by previous investigations showing that schoolchildren drove influenza epidemics (another RNA virus similar to SARS-CoV-2) and played a leading role in transmissibility (**Worby et al., 2016**). Additionally, it has been

recognized that *"Children may play an important role in the transmission of infection and outbreak dynamics and could be a key target population for effective measures to control outbreaks" (***Rajapakse & Dixit, 2021**); this is yet further supported by the increase in the reproductive number during the 2009 influenza pandemic following the opening of schools (**Huang et al., 2014**).

Need for noninvasive temperature-based infection detection for fully-vaccinated and non-vaccinated parents and teachers, to protect children and mitigate infection and mutations.

According to the CDC warnings, *fully-vaccinated people can potentially contract and spread COVID-19* (**CDC, 2021a, CDC2021b**). As shown here, daily, harmless, and automated infection detection in children (via the BTT) is feasible, because it relies on completely noninvasive detection (continuous or spot-check) procedures; this protects both non-vaccinated and fully-vaccinated adults, who are at risk of contracting COVID-19 from infected children.

Daily and automated checking of this large population group [23 million (0–5 years) and over 48 million when including children up to 12 years of age in the U.S. alone (**US childstats.gov, 2021**)] can protect children (by early treatment) and adults from becoming infected, thereby halting the mutation cycle (children → adults → children). Likewise, the protection of children is crucial. Parents and teachers live and work in close proximity to children; hence, it is vital that they are monitored daily, to promptly detect infections and prevent children—whose immature immune systems make them more vulnerable—from contracting COVID-19 from adults. Furthermore, the early stage of SARS-CoV-2 infection corresponds to the period of highest infectivity (**He et al., 2020**). Hence, to avoid exposure to the largest extent of viral shedding, daily infection detection—which can be realized in an automated and noninvasive fashion through temperature-based methodologies—is necessary for children and the adults closely interacting therewith.

Three situations that expose children to COVID-19 infection from fully-vaccinated adults are associated with vaccine efficacy, immunity duration, and vaccine-resistant variants. The potential unimpeded spread of COVID-19 by fully-vaccinated adults (i.e., parents and teachers) not wearing masks or populations with "vaccine passports" permitting free interactions with children emphasizes the need for temperature-based, brain-enabled, noninvasive, daily automated infection detection, to protect children and adults alike. The three exposure scenarios are discussed as follows:

Vaccine efficacy: U.S. Government data indicate a 90% vaccine efficacy for the mRNA vaccines used in the U.S. (**Thompson et al., 2021**); hence, 10% of the vaccinated population may become infected and spread the virus. Furthermore, as of July 15, 2021 (CDC COVID Tracker), over 160 million people in the U.S. were vaccinated; hence, 16 million fully-vaccinated people in the U.S. remain vulnerable to infection and may spread COVID-19 to children. Moreover, ~3.0 billion vaccines have been administered worldwide (July 14, 2021), and their apparent 70% efficacy (**Mallapaty & Callaway, 2021**) indicates that ~900 million or more fully-vaccinated people worldwide may potentially become infected and spread the virus to children, perpetuating an environment amenable to mutations. BTT-based infection-detection procedures could be immediately implemented globally without undue burden or costs, through use of the BTT technique for spot checking (discussed below).

Immunity duration: Vaccines were approved in the U.S. in December 2020; hence, insufficient time has elapsed for the true duration of immunity in the general public (beyond ~8 months) to be verified. Based on completed published studies, an initial SARS-CoV-2 vaccine report revealed 119 days of protection for a mRNA vaccine (**Widge et al., 2020**). This limited immunity duration is supported by other previous coronavirus vaccine studies, which report a wide

range of immunity durations, lasting from several weeks (**Bisht et al., 2004; Zhou, 2005**) to 4 months (**Kapadia et al., 2005**) to ~12 months (**Deming et al., 2006**). Translated into current vaccination attempts, this shows that populations interacting with children will become vulnerable to infection at completely different times. Hence, vulnerable vaccinated populations may be infected by children, owing to the variable duration of vaccine protection; over time, they may in turn unknowingly spread the virus to children unless effective infection detection—by automated noninvasive continuous monitoring via brain temperature kinetics —is implemented.

Vaccine-resistant variants: The third scenario pertains to infection from variants that may be resistance to vaccines [e.g., B.1.351 (**Kustin et al., 2021; Lasek-Nesselquist et al., 2021; Wang P. et al., 2021**) and Delta B.1.617 (**Sheikh et al, 2021)**] as evidenced by key studies which conclude that: *" mutations … will erode the effectiveness of natural and vaccine elicited immunity, … mRNA vaccines may need to be updated periodically to avoid potential loss of clinical efficacy*" (**Wang Z. et al., 2021**) and "*data… foreshadows reduced efficacy of spike-based vaccines*" (**Wibmer et al., 2021**).

Thus, vaccines, although essential to combatting COVID-19, may face considerable challenges trying to defeat COVID-19. The proposed automated, harmless, noninvasive, and continuous brain-temperature-based early viral infection-detection procedure, combined with spot-check measurements and operating in concert with physical and biological principles, may play an essential role in containing COVID-19, by facilitating—though detection of hypothalamic responses—the early identification of vaccinated individuals infected with SARS-CoV-2. This can interrupt human-to-human transmission, including transmission from vaccinated adults to children and vice versa.

Our studies on children demonstrated the feasibility of automated monitoring, realized using wearable headgear (**Figure 8J, D**). A large percentage of children wear eyeglasses; hence, the use of sensors integrated into eyeglass frames (**Figure 8C**) may provide an automated, continuous, unobtrusive, and comfortable infection-detection methodology for children of all ages (including adolescents). This may prevent these potentially more infectious sources (**Li et al., 2021**) from spreading COVID-19 to a teacher, other children at school, or to family members at home. BTT° can be used to detect infection during sleep; thus, the development of the relevant artificial intelligence [which dates back to 2017 (**Microsoft, 2017**)] can protect the lives of children (and babies) via early infection detection (and early treatment if needed), as well as protecting the lives of family members in close proximity to the infected children (including babies).

Thermometric limitations and measurements not in concert with thermal physical and biological principles for optimal heat transfer hamper infection detection in children and adults alike.

The urgent need to address thermometric practices not in concert with physical and biological principles for optimal heat transfer is underscored by a photograph published (on May 29, 2021) in a major U.S. newspaper, which shows the U.K. COVID-19 surge being fought with temperature measurements on the low-*k* wood-like surface of the forehead (**Colchester, 2021**), as shown in **Figure 4C;** this is the same thermometry previously used by U.K. schools in 2020 to detect COVID-19 in children (**Figure 4B**) and also used in India during the surge in April 2021 (**Figure 4D**). The photograph documents the persistent use of low-*k* thermometry, which is likely hastening the spread of COVID-19 and the emergence of mutations in children and adults. Similarly, finger and wrist measurements suffer from numerous limitations, including low-*k* surfaces and unpredictable vascular reactivity, as well as being physically distant from the brain (**Supp. Figs. 41,42**). A recent review indicates that these sites are unsuitable for clinical assessment

because they do not comply with international guidelines (ISO13154) (**Foster et al., 2021**). The deficiencies in temperature-measurement practices have prevented practitioners from answering even the most fundamental questions regarding the presence or absence of fever, because one site indicates normothermia and another simultaneously identifies fever, leaving practitioners asking, "Can there be a standard for temperature measurement…?" (**Martin & Kline, 2004**).

Despite the invention of thermometers over 300 years ago, humans have for centuries invaded multiple orifices and used multiple sites in attempts to overcome the body's thermal barrier. Although electronic thermometers have been developed, biological and thermophysical challenges result in widespread deficiencies and misleading results from forehead measurements and other thermometric practices (e.g., tympanic, oral, and axillary); these have been widely documented by multiple authorities over the decades (**Farnell et al., 2005; Forrest et al., 2017; Geijer et al., 2016; Jensen et al., 2000; Kiekkas et al., 2016; Kiekkas et al., 2019; Kimberger et al., 2007 ; Latman et al., 2001; Modell et al., 1998; Mogensen et al., 2018; Niven et al., 2015; O'Brien et al., 2000; O'Grady et al., 2008; Patel et al., 1996 ; Suleman et al., 2002; Tandberg & Sklar, 1983; Teller et al., 2013; Varney et al., 2002)**. Here, we elucidated the thermophysical and biological bases for the limitations of skin-surface thermometry, and we showed that these deficiencies prevent surface thermometry from effectively detecting febrile states, let alone early febrile changes. Thus, they are not clinically useful in the current pandemic and are unable to assist in a vital element of its response: interrupting human-to-human asymptomatic and early symptomatic transmission, and the emergence of mutations.

Temperature monitoring has traditionally relied on sites not biologically configured for temperature measurement, thereby producing widely variable and unreliable results, and the measurements rely on artificially-generated correction factors. Our findings show that the skin sites employed are structured for thermal insulation (working as a wooden shield) rather than heat transmission. Except for the eyelid skin of the $SMOS_{BTT}$ (and adjacent SPV), the entire body is covered by a thermally insulating wall, including layers of largely variable structures and sizes, such as fat [k = 0.00004 Kcal/(s·N·C)] and dermis [k = 0.00009 Kcal/(s·N·C)], both of which have very low *k* values (**Wenger, 2002**). This prevents reliable skin-based measurement of brain (or body-core) temperatures, both at the individual level and in population settings. Corrective algorithms lack reliability, owing to variations in insulation layers across individuals, spatial variability between sites upon the same individual, and temporal variability at the same location, as well as vascular perfusion changes, which can produce a remarkable 6.8 °C variability of skin temperature (**Section 4**).

Internal sites (e.g., the mouth, esophagus, nasopharynx, ear, rectum, and bladder) are structured for ingestion, air exchange, auditory sensation, and excretion. Their contents—food, feces, liquid, air—may also hamper accurate thermometry readings. In addition, invasive procedures come at a great cost, including risk of injury (even potentially fatal complications in the case of esophageal and rectal perforation). Core° produces more reliable measurements compared to surface sites; however, it does not represent brain temperature, as has been documented for over a century (**Abreu et al., 2020a; Kawamura & Sawyer, 1965; Kiyatkin, 2007; Kiyatkin, 2019; Maloney et al., 2001; Mosso, 1892; Rampone & Shirasu, 1964)**. Furthermore, invasive procedures increase the risk of spreading COVID-19, which prevents the safe use of invasive thermometry during pandemics.

For centuries, scientists have struggled to access the brain. Nineteenth-century researchers relied on invasive brain-temperature measurements in animals (**Mosso, 1892**) and "experimenting on live dogs and chickens by plunging thermo-electrode needles into the substance of their

brain…" (**James, 1892**). In the 20th and 21st centuries, continuous brain-temperature measurements remained dependent on such invasive methods (**Kawamura & Sawyer, 1965; Kiyatkin, 2007; Kiyatkin, 2019; Maloney et al., 2001; Rampone & Shirasu, 1964; Yang et al., 2002**). Temperature monitoring in humans has been limited to procedures similar to those used in animals (i.e., a probe inserted through a hole drilled into the patient's skull) when treating life-threatening conditions; these remain in use today (**Foreman, et al., 2020)**. This has led a major review to conclude, resignedly, that "In contrast to other physiologic parameters, brain temperature in humans remains generally unknown because of an almost complete lack of direct experimental studies" (**Kiyatkin, 2007**). Whilst MRI can provide noninvasive assessments of brain temperature, it is not practically feasible, because the subject must remain inside a metal-free environment and be confined within a tight tube-shaped magnet; additionally, it lacks the crucial capacity for continuous measurement and simultaneous monitoring of multiple sites under variable conditions as well as during surgery, sleep, or exercise, as shown here and in our previous studies (**Abreu et al., 2020b**).

As documented here (with evidence from countries in all continents) for both adult and children and for all conceivable scenarios (ranging from military bases to civilian facilities, from government buildings to ports of entry, from cruise ships to entertainment venues and hotels), current measurements practices are not in concert with physical (i.e., by measuring on a low-*k* surface equivalent to wood, which varies topographically and temporally), morphological [i.e., by measuring body parts that contain fat, which varies within the same anatomical region, over time within the same individual, and across different populations (including the obese and underweight)], and physiological (i.e., by measuring skin surfaces characterized by a highly reactive vasomotor tone) principles. Moreover, all of these surface sites feature blood vessels running along the surface of the body [e.g., the temporal artery (forehead), ulnar artery (wrist), and dorsal digital artery (finger)]; this limits the accuracy of measurements, owing to external environmental influences. Thermal variability in skin surfaces outside the $SMOS_{BTT}$ can undergo a 3.3 °C increase due to dilation (**Silverman et al., 1987**) and a 3.5 °C decrease due to constriction, as shown in studies presented here (**Section 4**).

Forehead thermometry is suboptimal from both physical and biological standpoints; furthermore, it fails to detect early thermoregulatory changes, which are necessary to successfully detect COVID-19. Whilst BTT° monitoring captures undisturbed brain thermal signals without the need for a correction factor, the morphological and thermophysical barriers of the forehead (and other skin surface sites such as the finger, wrist, arm, axilla, and chest) require correction factors. This latter approach tends to overestimate temperature in attempts to offset the body's low-*k* barrier. Moreover, through exposure to ambient temperature, temperature measurements of the forehead, finger, wrist, and other body surfaces may simply represent the external temperature and/or the impact of the environment, producing false-positive readings in a hot environment [e.g., a hot day in the summer (due to the combined effects of unpredictable amounts of vasodilation and warm skin temperatures)] and false-negative readings in cool or cold environments [e.g., under exposure to air conditioning (in a car or facility) prior to temperature checks (due to the combined effects of unpredictable amounts of vasoconstriction and cold skin temperatures)]. In addition, variable fat layers, dermis thicknesses, vasculature quantities, and vasomotor tones in the forehead (and other regions such as the finger, wrist, arm, axilla, and chest) further exacerbate the over- and under-estimation of temperature, producing unreliable and inconsistent measurements. This is especially true near the fever threshold, and it occurs even when scanning and employing a correction factor during forehead temperature measurements, as extensively documented by

multiple authorities over the past two decades (**Abreu et al., 2020b; Forrest et al., 2017; Geijer et al., 2016; Kiekkas et al., 2016; Kiekkas et al., 2019; Kimberger et al., 2007; Mogensen et al., 2018; Niven et al., 2015; Patel et al., 1996; Suleman et al., 2002; Teller et al., 2013**).

The abovementioned biological and thermophysical limitations and impediments that prevent clinically useful measurements being obtained are particularly significant for temperature measurements in areas with highly reactive vascular beds (e.g., the finger and wrist, which are characterized by highly variable and intense vasoconstriction, as confirmed by the fingers' susceptibility to frostbite and vasodilators offering therapeutic benefits) (**Murphy et al., 2000**).

A recent report provided information pertaining to the monitoring of physiological parameters (including temperature) using wearable devices for fever detection; however, the proposed temperature-measurement method [i.e., a ring on the finger (**Smarr et al., 2020**)] may produce thermal signals corresponding to local thermal changes rather than the thermal status of the body. This is even more important during the COVID-19 pandemic because vasoconstriction—which frequently occurs in the fingers and wrist—may result in falsely low temperature readings (**Supp. Figs. 41,42**), thereby failing to identify infected individuals; this leads to COVID-19 spreading and consequently increases the likelihood of mutations. Likewise, significant vasodilation—also a characteristic of the finger vascular bed (**Murphy et al., 2000**)—produces false-positive readings, potentially causing a healthy individual to be placed with infected ones and further promoting COVID-19 spreading. Additionally, finger (and wrist) temperature measurements suffer from the same limitations and impediments associated with measuring temperatures through low-*k* wood-like surfaces; this, combined with the highly reactive vascular bed, precludes accurate assessment of the usual thermal status of the body, let alone the early febrile state produced by a viral infection. In sharp contrast, the BTT comprises a natural thermal pathway that includes the high-*k* eyelid skin at the $SMOS_{BTT}$ which is in thermal communication with a vein, which features a thin, smooth muscle layer and lacks external elastic lamina; thus, minimal variation occurs in the volumetric heat capacity of the tunnel; this, coupled with the intracranial course, protects thermal signals from any environmental impact upon the thermal signatures it exhibits (**Abreu et al., 2020a**).

The unpredictable extent of vasodilation and blood-vessel vasoconstriction in the finger, wrist, and forehead (and all other skin sites, except at the $SMOS_{BTT}$), which occur within the same individual over time and between different populations (even depending on the hydration status and blood pressure at time of measurement), virtually eliminates the possibility of using correction factors or algorithms to adjust for the quantity of fat, vasomotor tone, ambient temperature, hydration, blood pressure, or other factors (e.g., stress).

Variable and erratic vasomotor tones, associated with the unpredictable emotional status of an individual, may generate errors regarding the presence or absence of a febrile state. Hence, in addition to the wood-like measurement surface, even emotions can represent a further confounding factor during COVID-19 screenings, generating large thermal swings that may simply result from local tissue changes (up to 6.8 °C); these can produce false readings. Notably, stress can cause vasoconstriction; this reduces local temperatures, leading to falsely low temperature readings and thereby false negatives, thereby facilitating virus spreading and mutations and potentially precluding fever detection (e.g., during a stressful state).

Body temperature measurements that are not in concert with physical and biological principles may lead to the undue exacerbation and prolongation of the COVID-19 pandemic. Healthy individuals misdiagnosed as febrile (due to overestimation) can be unnecessarily quarantined and/or placed with infected individuals (in households, hospitals, or quarantine

facilities), leading to more contagion when healthy populations become infected. In addition to injuring healthy individuals and further spreading COVID-19, unnecessary quarantine or hospital visits represent an undisputable and costly strain to healthcare systems; they also reduce the workforce, with obvious socio-economic consequences. Conversely, underestimation with surface thermometers can occur, owing to the low-*k* skin surface and related vascular physiologies. Furthermore, blood vessels parallel to the surface are vulnerable to the uncertainties and impacts of environmental changes (e.g., ambient temperature and air velocity), further compounding the inability of current surface thermometry to provide accurate thermal assessments for COVID-19 screening.

Our morphological, thermal-emission, and clinical data indicate that diverse forehead fat layers across different individuals (**Figure 1D**) may lead to deficient fever detection. False-negative readings, that result from low-*k* thermometry (e.g., forehead and wrist), can lead to uncontrolled virus spread, even when temperature is monitored (**Suppl. Figs. 1–41, Table 3**); this potentially leads to rapid spreads in crowded facilities where individuals are in close proximity (e.g., schools, factories, cruise ships, military ships, entertainment venues, and military bases). Additionally, underestimation of the body core temperature delays the seeking of care, leading to increased mortality, morbidity, and sequelae. As noted above, current surface thermometry and thermal imaging practices are influenced by ambient changes and unpredictable and variable vasomotor tones. Mass screenings (by thermal imaging) also suffer from comparable deficiencies for infection detection (**Priest et al., 2011**), unless the strict criteria (shown in **Supplementary Table 1)** and guidelines (**Foster et al., 2021**) are met; these inaccuracies prevent infrared thermography from achieving the accuracy needed for effective fever screening in the context of the COVID-19 pandemic.

Measurement at nonthermally configured sites (e.g., ear thermometry or tympanic membrane) may also conflict with the body's natural protection, because cerumen—which has antifungal and antibacterial functions (**Lum et al., 2009**)—must be removed for proper measurement of temperature in the ear canal. Other non-thermally-configured sites suffer from similar limitations. Oral thermometry requires a minimum 30-minute wait after consumption of food or liquid; otherwise, measurements will be erroneous (**Quatrara et al., 2007**). This is particularly problematic when consistent fluid intake is recommended during viral infections, because hydration is key for preventing complications. Moreover, measurements in sites not biologically configured for thermal functions are in conflict even with the key physiological parameters during fever; for instance, tachypnea occurs during fever and falsely reduces oral temperature (**Tandberg & Sklar, 1983**), and bradypnea causes false temperature elevation (**Quatrara et al. 2007**). Thus, common changes in respiratory function during infection may lead to false-negative and -positive readings, creating further biological environments for the perpetuation of the pandemic.

The limitations of current thermometry are "built" upon a foundation of thermometric deficiencies that has led to "a confusing jungle of sites and technologies" (**Robinson, 2004**); we cannot combat an opponent as infective and deadly as SARS-CoV-2 by relying upon a confusing jungle characterized by an absence of measurements in concert with physics and biology. More than 50 years after the publication of the classic article regarding the etiologies of "*fever of unknown origin*" (**Petersdorf & Beeson, 1961**), inadequate thermometry remains a recognized reality, and we still face the dilemma of "*fever of unknown degree*". Doctors (and patients) have often been saddled with the basic—but nonetheless vital—question: "Does the patient have fever?" when different sites in the same patient present different values.

Children—the largest potential source for mutations—pose an even greater challenge, because the only key objective warning sign for COVID-19 (or Kawasaki disease) in children is fever (with further signs such as irritability, tachypnea, and other subjective indicators being difficult to interpret). Suboptimal thermometry during the COVID-19 pandemic jeopardizes children in two ways: lack of detection, which can lead to complications and, although not as common as in older people, even death; and false fever, which can expose children to diseases whilst they seek medical attention. In addition, an invalid reading can fail to identify infected children (from babies to adolescents), who are associated with the high infectivity levels (**Li et al., 2021**) and may become reservoirs for large viral loads and mutations (**LoTempio et al., 2021**).

A crucial question concerning BTT-based high-*k* brain-eyelid thermometry.

What differentiates BTT° from joining the stockpile of failed devices and body sites that has characterized the history of thermometry for over 300 years? We believe the answer is simple: whereas, since the invention of thermometers, thermometry at other sites—as used in all settings (from households and hospitals to schools and military bases)—must overcome physics and biology; in sharp contrast, BTT brain-eyelid thermometry is based on a natural thermal pathway with no function other than thermal; this produces a method operating in concert with physical and biological principles for the effective, consistent, and undisturbed transmission of thermal signals in the protected environment of the skull, as well as emission via high-*k* eyelid skin at the $SMOS_{BTT}$. The BTT represents the first biological thermal waveguide—comprising a natural blood/fat/skin thermophysical configuration—that integrates the *sudden presence* in the orbit of large low-*k* fat layers enveloping the tunnel containing a high-heat-capacity blood medium (with said specialized fat preventing heat from leaking in or out, resulting in undisturbed thermal transmission) with the *sudden absence* of low-*k* fat at the external interface of the tunnel in the eyelid; this satisfies the heat-dissipation equation to produce a uniquely radiant eyelid (**Abreu et al., 2020a**). From a physical standpoint, the BTT can be described as a brain thermal energy tunnel characterized by a high total radiative power and heat flow. The tunnel stores thermal energy in its high-heat-capacitance, -density, and -inertia medium, and it provides an undisturbed path for transporting thermal energy from one end of the tunnel (in thermal continuum with the hypothalamus) to a thin high-*k* interface, with a heat flow inversely proportional to the thickness of the interface. Moreover, BTT provides nature-based thermometry and the absence of an artery adjacent to the SOV prevents countercurrent heat exchange, and the unique axial configuration completely shields the heat-carrying medium (i.e., blood in the SOV) from environmental effects. The specialized thermo-mechanics and -dynamics of the unsaturated fat in the tunnel minimizes the impact from intra-orbital environs, including myogenic heat production from the surrounding highly active extraocular muscles (**Abreu et al., 2020a**).

The brain is a thermodynamic organ (**Collell & Fauquet, 2015**), and the BTT has no function besides a thermal one; that is, it operates as a brain-temperature indicator via a natural thermophysical path in concert with morphological (i.e., connected with the hypothalamus, shielded against environmental temperatures, and presenting a thin-skin-surface interface), physiological (i.e., stable blood volume and a signal insensitive to respiratory changes), and physical (i.e., low-*k* wall encircling a medium with high heat capacity, high density, and high inertia, as well as a high-*k* terminus) principles (**Abreu et al., 2020a; Abreu at al., 2020b**). The BTT (and brain tunneling temperature) measurements harness the engineering provided by nature, instead of imposing human engineering onto nature, as occurs by the use of correction factors, when invading body orifices with thermal probes or forcing the extraction of a thermal signal through a low-*k* skin surface.

Temperature measurements in concert with physics and biology (via brain thermal signals and hypothalamic activity) to mitigate mutations.

Our findings provide first-of-their-kind temperature measurements in concert with physical and biological principles for effective and undisturbed heat transfer; this is realized via the BTT and facilitates detection of hypothalamic activity in children (besides brain-temperature kinetics monitoring); thus, we provide a proof-of-concept for the feasibility of BTT°-based wearable devices for detecting asymptomatic and afebrile negative-sense RNA viral infections whilst awake and during sleep.

These results support multiple previous conclusions (abovementioned) that indicate the inability of surface thermometry and other thermometric methods (including thermal imaging) to accurately detect the thermal status of the body during initial stages of fever. Here, we clarify the basis for this recognized failure: the absence of temperature measurements on or over a skin site that allows undisturbed and direct thermal transfer to the surface. However, a solution is achieved by insulated contact sensors, which are based upon a thermal communication with the brain; this occurs via an internal high-heat-capacity/low-*k* configuration (blood/fat) coupled with an external high-*k* skin, one which is uniquely found in the biological thermal waveguides of the BTT (**Abreu et al., 2020a**).

This natural thermal waveguide facilitates the detection and quantification of brain/core discordance, and exposes a heretofore-unattainable distinction between the brain and body core values in multiple scenarios, including sedation, anesthesia, and sleep, as well as exercise. Clinical experiments and observations have shown that—as a component of the peri-hypothalamic thermoregulatory triune—signals traversing the BTT are in continuum with thermal changes associated with the hypothalamic response. Hence, the apparent aberrancies of vein, fat, bone, and skin (**Abreu et al., 2020a**) provide a tunnel which facilitates the unhindered capture of brain thermal patterns; this, in the context of COVID-19 screening, offers signals that reveal thermoregulatory dynamics responses to the onset of RNA viral infection.

Vaccines prevent the disease *of the host*, whilst temperature-based infection detection can reduce transmission *from the host* through the timely and effective isolation of the infected (and quarantine of contacts); they can also reduce replication *within the host* through timely and more effective COVID-19 treatments (addressed in the next manuscript of the series). Because human transmission is key for SARS-CoV-2 lineage survival and the emergence of viral mutations, the BTT-based methodology aims to continuously interrupt human-to-human transmission, by identifying viral infection at the earliest stages before peak viral replication, via continuous monitoring of brain-temperature kinetics using wearable devices.

Unless a solution *proactively* and continuously addresses mutations and human-to-human transmission using early infection detection, it will likely be *reactive* (e.g., attempting to develop new vaccines to address the vaccine-resistant mutants), thereby continuously exposing global populations—both vaccinated and non-vaccinated—to disease and death from new emerging viral variants.

Our findings suggests that detection of thermoregulatory activity—based on effective and optimal heat transfer—can proactively address mutations through continuous brain-temperature kinetics monitoring, to detect infection during pre-febrile and early febrile stages. This is supported by our study of the hypothalamic activity of 100 pediatric patients, multiple brain-temperature kinetics investigations showing the specificity of BTT° for brain temperature, and benchmark research showing the unique thermal emissions of the radiant high-*k* eyelid skin at the BTT terminus. This temperature-based brain-enabled approach effectively captures hypothalamic

thermal signals; thus, viral transmission can be interrupted before the period of highest infectivity (**He et al., 2020**), which is currently beyond the reach of authorities worldwide, as corroborated by a pandemic that continues to ravage the world.

As shown in **Table 3**, public health officials, professionals, military organizations, businesses, communities, and populations around the world currently assess the presence of fever (for protection against COVID-19) by measuring temperature on or over the lowest-thermal-conductivity tissue (fat) and in an highly reactive vascular region that produces considerable spontaneous temperature variations, as detailed in this report. Thermometric practices that embrace measurements on low-*k* surfaces and highly reactive vascular regions produce false-negative and -positive readings, reinforce the virus's ability to spread, and expose the world to mutations. This emphasizes the urgent need for rapid intervention that can be immediately implemented by all countries and communities free-of-cost (i.e., the BTT-Abreu Brain-Eyelid Technique, described below).

Is there a deadly COVID-19 resurgence looming on the horizon, and can collaborative global efforts based on temperature measurements in concert with physical and biological principles facilitate infection detection to reduce or prevent this resurgence?

Several factors indicate that a resurgence of COVID-19 may loom on the horizon and may occur within 8 months, though likely still during 2021. This is because of the 6–8 month period beyond which immunological memory to SARS-CoV-2 is lost (**Dan et al., 2021**); the 119-day duration of protection against SARS-CoV-2 achieved by the recently developed RNA vaccine (**Widge et al., 2020**), as confirmed by the 4-month protection provided, on average, by previous coronavirus vaccines (**Kapadia et al., 2005**) [which ranged from only weeks of protection (**Bisht et al., 2004; Zhou, 2005**) to up to ~12 months (**Deming et al., 2006**)]; and the 6–8 month interval before the devastating reinfection that occurred in Brazil's Amazon (**Taylor, 2021**). Taken together, these indicators suggest that immunity—both natural and post-vaccination—may be short-lived, placing the world at risk of a COVID-19 resurgence. This is confirmed by vaccine manufacturers, who indicate that vaccine immunity may be lost within approximately 8 months **(Lovelace Jr., 2021)**. This shows that populations vaccinated in the first trimester of 2021 may become infected and spread COVID-19 by the end of the year.

A major surge may occur because the loss of vaccine protection is likely to coincide with the dominance of the "double mutant" B.1.617, which has been shown to be more transmissible, to cause more severe disease, and to reduce vaccine protection (**Sheikh et al, 2021**). Hence, both vaccinated and non-vaccinated populations may be exposed to disease and death from deadly new variants that may emerge in 2021. Furthermore, the increased transmissibility (due to the aforementioned variants associated with "virgin" populations, who are vulnerable despite being vaccinated or previously infected) may produce a large number of fatal outcomes during re-infection or post-vaccination.

This is further supported by the loss of vaccine efficacy and the increased resistance to neutralizing antibody responses (**Andreano et al., 2021; Diamond et al., 2021; Hoffman et al., 2021; Wang P. et al., 2021; Wibmer et al., 2021**); the apparent impossibility of herd immunity for the U.S. **(Mandavilli, 2021**) and for the world at large (**Taylor, 2021)**; and, most critically, the potential for children—who by nature do not mount effective immune responses and are more infective (**Li et al., 2021**)—to act as large mutation reservoirs (**Day, 2021; LoTempio et al., 2021**).

Even strict border controls cannot offer protection against variants, because country-specific mutations that are resistant to vaccines and more lethal are already emerging; hence, the world urgently needs every tool available to fight this formidable and mutating deadly adversary,

to prevent a potentially more harmful and catastrophic COVID-19 resurgence in 2021 and 2022 as well as unexpected devastating surges, such as has already occurred in India because of the "double mutant" variant B.1.617 (**Ranjan et al., 2021**). Temperature measurements taken from the brain, in line with physical and biological principles for optimal heat transfer, facilitate early detection via hypothalamic activity; these, combined with associated public health measures to reduce viral replication and interrupt human-to-human transmission, may provide a tool to minimize or eliminate these potentially more powerful and more fatal viral attacks, which may impact the entire world.

Is a "rebirth of thermometry" for combating pandemics possible? If yes, is there an effective fever-detection technique for COVID-19 screening that can be immediately implemented by any country without undue burden and cost?

COVID-19 surges reiterate that the world needs every measure and intervention available to control COVID-19. No technique should be discarded, even the standard non-contact handheld infrared thermometers, which do not currently provide clinically useful data because their measurements do not accord with physical, anatomical, or physiological principles for effective and consistent heat transfer.

Noninvasive continuous brain-temperature kinetics monitoring, obtained from the eyelid at the $SMOS_{BTT}$ using a high-resolution wearable sensor—without the need for a correction factor to overcome the impact of compromised low-*k* transmission—constitutes the most effective method of detecting COVID-19. However, immediate worldwide implementation of high-resolution sensors via wearable-based BTT°-measurement devices [e.g., eyeglasses and headgear (**Figures 8A–D**)] for the continuous detection of hypothalamic activity is not readily achievable. Thus, in addition to introducing continuous brain-temperature kinetics monitoring for RNA virus infection detection, and considering our objective of providing actionable information, we freely share here our BTT-enabled, brain-based high-*k* thermometric method, which can be readily and immediately implemented by any country, community, or individual worldwide. This prevents the discarding of handheld infrared thermometers, which are currently being manufactured and employed around the world in attempts to screen for COVID-19.

The thermometric technique offered here free-of-cost to the world for brain-enabled high-*k* eyelid thermometry is based on the FDA-approved "Abreu-BTT 700 System" (noted earlier), referred to here as the "Abreu-BTT Brain-Eyelid Technique." Our previous research on coronavirus detection via wearable devices (e.g., eyeglasses) during the first coronavirus pandemic in 2003 (noted earlier); our work conducted during the H1N1 pandemic in 2009 (**Abreu, 2009**); our findings given here; and our current research on COVID-19 (the second manuscript of the series, in preparation), provide the basis for the parameters summarized and shared in this report.

To exploit the hypothalamic connection and barrier-free measurements—obtained via the eyelid skin overlying the BTT [shown here and in previous reports (**Abreu et al., 2020a; Abreu et al., 2020b**)]—as an initial and immediate application of the findings herein, we suggest the "Abreu-BTT Brain-Eyelid Technique" be implemented, by moving the measurement site from above to below the gracile brow ridge and from a low-*k* dark forehead (overlying a fat-laden barrier with thick dermis) to the high-*k* radiant thin medial upper-eyelid skin (overlying a brain ↔ surface tunnel). Secondly, we suggest the infrared sensor be aimed at the eyelid skin below the brow ridge and adjacent to the bridge of the nose, noting that the eyelid skin (and not the inner canthi of the eye or tear duct) is the measurement site. Thus, the detector should be aimed ~5 mm above the inner canthi, with detector notably coming from an inferior position and pointing up toward the eyelid, as depicted in **Supp. Figs. 43, 44**. The "Abreu-BTT Brain-Eyelid Technique" thereby

facilitates standard non-contact infrared thermometry—aligned with physical and biological principles for effective and undisturbed heat transfer from the brain—that can be immediately implemented for protection across all scenarios (including children), from small villages to major metropolises (as reported in **Table 3**), leading to the potential "rebirth of thermometry" as a pandemic-combating approach and preventing the rebirth of COVID-19 and infection spreading via the immature immune systems of children (**LoTempio et al., 2021; Huang et al., 2014; Rajapakse & Dixit, 2021**; **Worby et al., 2016**) and immunocompromised populations (**Choi et al., 2020; Hensley et al., 2021; Khatamzas et al., 2021; Truong et al., 2021)**. Considering that children are unprotected (due to their immunogenicity) and can be readily infected, infection detection efforts are warranted for teachers, parents, and people closely interacting with children, to provide daily assurance (by BTT-based spot-check as well as continuous monitoring) that children are protected from becoming infected by infected adults, and thereby perpetuate an infectious cycle.

Implications, Limitations, and Conclusions

Implications. Transmissibility is a key problem that must be addressed to eliminate pandemics, because higher infectivity leads to higher numbers of cases, mutations, hospitalizations, and fatalities. Infection detection is essential in addressing transmissibility, and temperature-measurement practices that facilitate accurate and timely infection detection are a fundamental component in tackling COVID-19. Targeting harmless infection-detection efforts upon unsuspecting sources for accelerated viral evolution and mutations [e.g., babies, children, and adolescents, who are characterized by higher infectivity (**Li et al., 2021**)] allows a cost-effective and focused strategy to be implemented to mitigate mutations. The proposed solution can address mutations via continuous brain thermal kinetics monitoring, to realize early infection detection prior to peak viral replication; this facilitates effective treatment and isolation, thereby reducing intra-host viral replication and mitigating mutations. This, combined with early isolation (achieved by early detection), can prevent COVID-19 from spreading, reducing the number of cases and—subsequently—the number of mutations. Whereas vaccines are designed to protect the individual, detection is aimed at protecting the community, because vaccines are designed to prevent infection but not transmission.

Hence, a complete solution to end the COVID-19 pandemic requires vaccines (addressing the host) as well as detection methods such as the brain-eyelid-enabled temperature measurements, to address "between hosts", and such transmission among hosts is what characterizes a pandemic. Notably, the first coronavirus (SARS-CoV) in 2003 (which caused the SARS pandemic) was eradicated by infection detection and public health interventions only (though remarkably without any vaccines); this approach was based on symptom detection. However, COVID-19 is primarily asymptomatic, requiring hypothalamic-based temperature measurements to detect early infection. Furthermore, the eradication of SARS-CoV in 2003 supports the efficacy of infection detection conducted via continuous noninvasive brain-temperature kinetics monitoring. This can be accomplished during sleep (obtained via the BTT) resulting in a harmless methodology that can be implemented worldwide and thus suitable for defeating COVID-19, and while the world sleeps the human brain detect the virus to prevent spread and harm. This approach, operating in cooperation with vaccines as a "vaccination–detection" pair solution, may lead to even more effective and expedient strategies toward ending the COVID-19 pandemic and eliminating the fear and risk regarding the emergence of a new, more dangerous SARS-CoV-2 mutants, and thereby bringing normalcy to the world.

Continual vaccinations (possibly every 6–12 months) may provide the necessary immunity, and new vaccines can be developed for new mutations; however, populations remain exposed to illness and death from new variants before the relevant vaccines are administered. Unless COVID-19 is eradicated, normal life around the world will be severely disrupted by (1) the need for continual vaccinations and the sudden COVID-19 surges causing disease and death; (2) the impacts on land, air, and sea (in particular, the imminent dangers on cruise and military ships); and (3) the "hanging sword" question of when and where a deadly new mutant will appear, as has occurred recently in many countries around the world. Here, we propose an early infection detection procedure to interrupt asymptomatic and symptomatic human-to-human transmission (including children-to-adult and adult-to-children transmission), opening a viable path toward eradicating SARS-CoV-2, as achieved in 2003 during the first coronavirus pandemic.

Eradicating pandemics caused by viruses such as SARS-CoV-2 poses a great challenge, since they are characterized by asymptomatic infection and thereby asymptomatic virus shedding (**Arons et al., 2020; Furukawa et al., 2020; Ing et al., 2020; Kasper et al., 2020; Letizia et al., 2020**). Asymptomatic afebrile COVID-19 transmission has been reported as the *Achilles' heel* of COVID-19 pandemic control (**Gandhi et al., 2020**). This has been confirmed by a 56% asymptomatic infection rate amongst residents of a nursing facility (**Arons et al., 2020**) and a report showing that, remarkably, 81% of passengers on a cruise ship who tested positive for COVID-19 were asymptomatic (**Ing et al., 2020**). This fatal vulnerability impacts even closely controlled U.S. military settings, as revealed by the report that 77% of the crew members of a nuclear-powered aircraft carrier were afebrile and asymptomatic at the time of COVID-19 diagnosis (**Kasper et al., 2020**). A separate military setting showed an even higher percentage of asymptomatic population: remarkably, 93% of the recruits who tested positive for SARS-CoV-2 infection were afebrile upon arrival at a quarantined campus for the U.S. Marine Corps (**Letizia et al., 2020**). This was recently confirmed by an analytical model from the CDC (**Johansson et al., 2021**) showing that asymptomatic individuals with COVID-19 account for 59% of all transmissions, further stressing the need for continuous, noninvasive, and automated detection of COVID-19 via brain temperature kinetics, to control the pandemic. Moreover, as an RNA virus, SARS-CoV-2 is also characterized by mutations, which may lead to catastrophic situations ranging from increasing transmissibility and disease severity (**Sheikh et al, 2021**) to vaccine evasion (**Roche, 2021; Wang P. et al., 2021**). The other portion of the solution to COVID-19 is automated detection, preferably prior to the febrile state and increased heart rate caused by sympathetic release (**Lazarus et al., 2007; Nakamura et al., 2009; Ott, 1884**); thus, the entire solution can be characterized as a "detection–vaccination" pair. Brain thermoregulatory signals naturally make the virus visible and therefore vulnerable to detection and prompt, effective, and low-cost treatment via readily available therapeutic modalities, to immediately save lives and prevent sequelae caused by COVID-19 around the world.

Although targeted lockdowns and shelter-in-place mandates are arguably valid interventions (**Flaxman et al., 2020; Hsiang et al., 2020**), such overarching actions should not form the foundation of pandemic control in the 21st century. These century-old approaches are not sufficient to contain COVID-19. Despite buying time, it is unlikely that these approaches will stop a widespread, highly transmissible virus such as SARS-CoV-2 (**Ferguson et al., 2020; Moore et al., 2020**). Additionally, public health interventions based on lockdowns allow SARS-CoV-2 to continue to ravage global economies (**Johns Hopkins University, 2020**). The key to controlling the COVID-19 pandemic is uninterrupted effective daily screening and early COVID-19 detection, ideally occurring in an automatic manner whilst populations are performing routine activities or

even sleeping. This is a reality that can be readily implemented by the miniaturized high-resolution wearable BTT sensors demonstrated here as eyeglasses, patches, frames, and headgear (**Figures 8A-D**); these offer the necessary continual, harmless daily infection detection in real time without any interruption of life and work. This temperature-based brain-enabled natural solution can be implemented without societal and work disruptions and without the need for arbitrary lockdowns, thereby averting the economic collapse and unemployment crisis characterizing the COVID-19 pandemic (**Johns Hopkins University, 2020**). By combating the COVID-19 pandemic and protecting public health without disrupting the economy, the brain-eyelid based detection methodologies introduced herein uniquely resolve the critical dilemma of "life vs. livelihood," by preserving life and livelihood simultaneously.

We offer readily implementable, and logistically simple, low-cost solution (because brain-eyelid-based wearables can be delivered by mail to any country, even remote villages); such solutions are even more pressing when considering the challenges of herd immunity, as observed in cases where the expected herd immunity proved nonexistent. For instance, populations in Brazil's Amazon survived infections from earlier versions of SARS-CoV-2; however, the Brazil mutant P.1 evaded their immune response and devastated the same Amazon populations with even greater damage and mortality. This raises an alarming question: Do these events in the Amazon reveal "*the final nail in the coffin for natural herd immunity?*" (**Taylor, 2021**); the impossibility of herd immunity was also reported for the U.S. **(Mandavilli, 2021**). Furthermore, by its nature as a harmless and natural solution (without the risks of short- or long-term adverse effects), the temperature-based brain-eyelid enabled methodology described here, which may be used during sleep, may achieve broad and global acceptance; thus, even populations who are not favorable to vaccines can now make a contribution to reduce human suffering, save lives, and end the COVID-19 pandemic, by an option that is completely natural, it does not invade the body and it is free of adverse effects.

Limitations. Although the proposed methodology aims to mitigate mutations, the actual impact of our findings upon mitigating mutations is unclear, because larger, sequential infection-detection studies and analyses of brain thermal kinetics monitoring procedures—that directly mitigate mutations in monitored groups (in comparison with control groups) in the context of infections from new variants—are required to determine the extent of the impacts of the temperature-based brain-enabled methodology proposed here. Despite observing thermal-pattern differences during asymptomatic afebrile infection (during sleeping and waking states) when comparing against our large database, the current study for detecting asymptomatic afebrile RNA viral infections is limited by the small sample size (n = 3), owing to the challenges of continuously monitoring pre-febrile asymptomatic subjects (who are unaware of infection or exposure to infected people). Nevertheless, the comparison to our large database shows that the thermal patterns identified during asymptomatic pre-febrile states are unique and distinct from all other non-infective thermal patterns, and our ongoing large-sample studies using the positive-sense RNA virus SARS-CoV-2 (manuscript in preparation) confirms the findings herein.

Conclusions. The BTT—along with its external terminus located in the eyelid skin between the eyes, below the eyebrow, and adjacent to the nose—was first described on April 22, 2002 (**Abreu, 2002**). That study revealed an optimal site for temperature measurement in a brain ↔ eyelid path, configured with a low-*k* and high-heat-capacity arrangement that can provide a metric consistent with Stefan–Boltzmann's law of black-body radiation. BTT measurement was later introduced by Yale University on July 3, 2003, as the first methodology to noninvasively measure brain temperature (**Yale University, 2003**). The discovery of the BTT and our numerous

subsequent investigations have rendered the hypothalamus—which had been "hidden" inside the cranium—accessible to science (**Abreu et al., 2020a**); this enables us to address the fundamental precept put forth by Lord Kelvin: "You cannot manage what you cannot measure" (**Scripture, 1892**). To effectively manage the COVID-19 pandemic, we may respond with our intention to measure continuously, automatically, noninvasively, harmlessly, and accurately on a daily basis [including the monitoring of children (and babies)], using thermal signals received from the brain via a natural thermal waveguide and the high-*k* radiant eyelid terminus, which are naturally structured for thermal transmission and emission. By protecting children using noninvasive continuous monitoring as well as spot-check thermometry (in concert with physical and biological principles), BTT offers a new dimension of thermometry for combating COVID-19, reducing spreading, and mitigating mutations. Early infection detection for children and adults is vitally and urgently needed to contain SARS-CoV-2, and our method can be implemented without delay, and spot-check detection can be accomplished free-of-cost and undue burden by any government in the world, using the "Abreu-BTT Brain-Eyelid Technique" shown here (**Suppl. Figs 43, 44**). Automated, continuous early infection detection (during sleep or whilst awake) can lead to early isolation and treatment and help to effectively interrupt human-to-human transmission, to reduce R_0 to < 1 and thereby open up a pathway toward ending the COVID-19 pandemic.

We also present here substantial evidence of the practical utility of the BTT for monitoring hypothalamic activity in children (with fever), to protect the lives of children via early detection of infection (or fever-generating Kawasaki disease). Whereas the risk to children for adverse effects (hospitalizations and/or death) from SARS-CoV-2 to date continues to be measurably less than that observed in older age ranges, emerging evidence underscores increasing reported cases in children and the highest number of hospitalizations in the U.S. since the beginning of the pandemic (**Toy & Wernau, 2021**). This exacerbation of the corresponding health risks and burdens in children is increased when SARS-CoV-2 affliction is combined with other viruses (e.g., respiratory syncytial virus). Although the majority of cases in children are due to the—reportedly more transmissible (**Sheikh et al, 2021)**—Delta variant, uncertainty remains regarding whether the Delta and other variants of concern may increase the transmissibility of SARS-CoV-2 by children. However, it is well documented that schoolchildren played a leading role in the transmissibility of another RNA virus, and children are a key target for outbreak control (**Huang et al., 2014; Rajapakse & Dixit, 2021; Worby et al., 2016)**. Despite the uncertainty regarding how this will be manifested in children during the current stage of the COVID-19 pandemic, the application of BTT is nonetheless well placed to offer a high practical global value in the early widespread noninvasive screening of this young population. It is also important to appreciate the potential vulnerability of young people, who may not be eligible or as effectively responsive to vaccines or treatments. The broad utility of a BTT monitoring and tracking application could be integral to averting transmissibility between children and from them to other susceptible groups. This would play a critical role in controlling outbreaks and mitigating further spread from children and babies, who may become a key reservoir for mutation and SARS-CoV-2 propagation by the fact that their immature immune systems make them unreachable by vaccines and continuously vulnerable to infection, and thereby a source for COVID-19 spreading.

There is light at the end of the tunnel: the radiant eyelids at the external terminus of the brain-eyelid tunnels, through overcoming—for the first time—the body's thermal barrier, provide an undisturbed and direct access to hypothalamic signals and facilitate early infection detection prior to symptom onset. The "detection–vaccination" pair solution succeeds by combining a "brain–muscle" approach, whereby the power of the brain signals is used for asymptomatic early infection

detection (thereby protecting the community) and the muscle is used to administer vaccines to induce immunity (thereby protecting the individual).

The birth of brain-enabled thermometry via a natural thermophysical and morphological blood/fat/skin configuration through brain-eyelid thermal tunnels will allow the global population to escape their current dependence on surface measurements across thermal barriers [k = 0.00004 Kcal/(s·N·C)] and highly reactive vascular regions (which can exhibit as much as a 6.8 °C thermal variability), by providing measurement practices—consistent with morphological, physiological, and thermophysical principles for effective and undisturbed heat transfer—to bring an end to the period of history in which human body temperatures are measured on or over low-k wood-like surfaces characterized by highly reactive vascular tones. The techniques used today have not been changed since the middle of the 18th century (**Moran & Mendel, 2000**); as such, they are fraught with errors and limitations that the world cannot afford if COVID-19—or any other deadly virus that may strike the human race in the near future (**Sun et al., 2020**)—is to be effectively combatted and defeated.

Acknowledgements. We would like to express our special gratitude to Dr. Roberta Hines of the Department of Anesthesiology at Yale School of Medicine, for allocating personnel and resources. We would also like to thank the Department of Ophthalmology and Visual Science of the Yale School of Medicine, and its former chairman Dr. M. Bruce Shields, for their support, guidance, and for reviewing the initial comprehensive manuscript; the Department of Morphology and Genetics at the Paulista School of Medicine of the Federal University of Sao Paulo, Brazil, for the anatomic and histologic preparations; and BTTCorp.com for providing us with the equipment and sensors free-of-charge. We are grateful to Dr. Marcos L. Brioschi and the University of Sao Paulo School of Medicine for providing us patients for the comparative intracranial temperature measurements as well as for their assistance with the thermographic images, Dr. William C. Amalu for his assistance with the thermal images and videos, Dr. Christian Renna for reviewing and editing our manuscript, J. Roger Titone for his assistance with equipment and sensors, Victor Spitz for the formatting of the citations and figures, Ricardo T. de Faria for his assistance with the images and graphs, Andrew M. Levy Abreu for his assistance with the photographic documentation of devices, Dr. Rebeca G. Guariento for assistance with the references, and Jacki Fitzpatrick for her administrative support.

Author contributions. M.M.A. discovered the BTT, engineered the BTT devices, and delineated the thermophysical configurations. M.M.A. and D.G.S. designed all the research protocols and collected the data for the various studies, analyzed the results, wrote the manuscript, and integrated the different components of our multidisciplinary investigation. R.L.S. and M.M.A dissected the cadavers; in addition, R.L.S. performed the histologic and correlational microscopic studies and associated data analysis. T.M.B. designed, performed, and analyzed the studies involving sedation and anesthesia. A.C.A. and R.F.G. designed, performed, and analyzed the pediatrics study. A.L.C. collected and analyzed the data for the thermometry correlation study. F.D. designed the statistical methodologies and analyzed the data. M.F.B. reviewed the entire manuscript and designed, performed, and analyzed the studies involving physical exercise. A.S.H. performed anatomic and thermographic analysis. T.J.S. collected data for clinical studies. A.F.S. acquired and prepared the radiological images and reviewed the manuscript.

Supplemental information *(including movies*) is included with this manuscript.

Data availability: Datasets generated during the studies are available upon request**.**

Funder Information. This work was supported by a grant from the Patient Protection and Affordable Care Act of the U.S. Federal Government under the Qualifying Therapeutic Discovery Project.

Declaration of Interests. The authors declare the following financial interests/personal relationships which may be considered as potential competing interests: M.M.A. holds patents on temperature measuring devices and stock in BTT Corp. All other authors declare that they have no known competing financial interests or personal relationships that could have appeared to influence the work reported in this paper.

References

Abreu, M. M. (2002). U.S. Patent No. *7187960* issued in 2007. Patent application filed on April 22nd, 2002. Washington, DC: U.S. Patent and Trademark Office.

Abreu, M. M. (2006). *U.S. Patent No. 8328420* issued in 2012. Patent application filed on October 24th, 2006. Washington, DC: U.S. Patent and Trademark Office.

Abreu, M. M. (2009, October 17). A Perfect Storm: Wrong Thermometry and Wrong Temperature Can Cause Social and Economic Turmoil During a Flu Pandemic. *Financial Content*. Retrieved February 22, 2021, from http://markets.financialcontent.com/stocks/news/read?GUID=10429586

Abreu, M. M., Smith, R. L., Ruskin, K., Silva, A. F., Haddadin, A. S., Bergeron, M. F., . . . Silverman, D. G. (2020). Previously unseen brain-eyelid thermal tunnel reveals biological waveguide and transorbital thermophysical pathway to the brain. *Authorea*. doi:10.22541/au.160225723.36016917/v1

Abreu, M. M., Banack, T. M., Haddadin, A. S., Silverman, T. J., Dai, F., Elefteriades, J. A., . . . Silverman, D. G. (2020). Brain/core Discordance due to Neuronal Activity Identified by Noninvasive Brain Temperature Measurement via Brain-eyelid Thermal Tunnels. *Authorea*. doi:10.22541/au.160315282.27681781/v1

Abu-Raddad, L. J., Chemaitelly, H., & Butt, A. A. (2021). Effectiveness of the BNT162b2 Covid-19 Vaccine against the B.1.1.7 and B.1.351 Variants. *New England Journal of Medicine*, *385*(2), 187–189. https://doi.org/10.1056/nejmc2104974

Andreano, E., Piccini, G., Licastro, D., Casalino, L., Johnson, N. V., Paciello, I., Monego, S. D., Pantano, E., Manganaro, N., Manenti, A., Manna, R., Casa, E., Hyseni, I., Benincasa, L., Montomoli, E., Amaro, R. E., McLellan, J. S., & Rappuoli, R. (2020). SARS-CoV-2 escape in vitro from a highly neutralizing COVID-19 convalescent plasma. *SARS-CoV-2 Escape in Vitro from a Highly Neutralizing COVID-19 Convalescent Plasma*. Published. https://doi.org/10.1101/2020.12.28.424451

Acosta, P. L., Caballero, M. T., & Polack, F. P. (2015). Brief History and Characterization of Enhanced Respiratory Syncytial Virus Disease. *Clinical and Vaccine Immunology: CVI*, *23*(3), 189–195. https://doi.org/10.1128/CVI.00609-15

Alamy. (2020, June 25). Stock Photo. Retrieved September 12, 2020, from https://www.alamy.com/vladivostok-russia-june-25-2020-a-police-officer-in-a-face-mask-has-her-temperature-screened-at-a-polling-station-during-the-2020-russian-constitutional-referendum-in-the-city-of-vladivostok-in-russias-far-east-most-regions-of-russia-will-vote-in-the-referendum-on-proposed-amendments-to-the-russian-constitution-from-25-june-to-1-july-2020-some-of-the-proposed-changes-raise-social-obligations-aimed-at-improving-living-standards-to-the-level-of-constitutional-norms-credit-itar-tass-news-agencyalamy-live-news-image364069013.html

Anglesey, A. (2021). Dangerously Mutated COVID Variant Detected in 47 U.S. States. Retrieved from: https://www.newsweek.com/dangerously-mutated-covid-r1-variant-detected-47-us-states-1631614

Arons, M. M., Hatfield, K. M., Reddy, S. C., Kimball, A., James, A., Jacobs, J. R., . . . Jernigan, J. A. (2020). Presymptomatic SARS-CoV-2 Infections and Transmission in a Skilled Nursing Facility. *New England Journal of* Medicine*, 382*(22), 2081-2090. doi:10.1056/nejmoa2008457

Associated Press. (2020a, August 22). World hits grim COVID-19 milestone with 800,000 confirmed deaths. Retrieved October 22, 2020, from https://www.cbc.ca/news/world/coronavirus-covid19-world-aug-22-1.5696347

Associated Press. (2020b, June 10). Brazil Begins Reopening After 2-Month Coronavirus Shutdown. Retrieved September 14, 2020, from https://www.voanews.com/covid-19-pandemic/brazil-begins-reopening-after-2-month-coronavirus-shutdown

Baldor, L. (2020, May 16). Sailors on sidelined USS Theodore Roosevelt infected with the coronavirus for second time. USA TODAY. Retrieved May 20, 2021, from https://www.usatoday.com/story/news/health/2020/05/16/coronavirus-sailors-test-positive-again-covid-uss-roosevelt/5206256002/

Baxter, A. (2020, March 20). Voluntary screenings begin at Juneau airport as local leaders advise would-be travelers to stay home. Retrieved September 11, 2020, from https://www.ktoo.org/2020/03/20/voluntary-screenings-begin-at-juneau-airport-as-local-leaders-advise-would-be-travelers-to-stay-home/

Bager, P., Wohlfahrt, J., Fonager, J., Rasmussen, M., Albertsen, M., Michaelsen, T. Y., Møller, C. H., Ethelberg, S., Legarth, R., Button, M., Gubbels, S., Voldstedlund, M., Mølbak, K., Skov, R. L., Fomsgaard, A., Krause, T. G., & Danish Covid-19 Genome Consortium (2021). Risk of hospitalisation associated with infection with SARS-CoV-2 lineage B.1.1.7 in Denmark: an observational cohort study. *The Lancet. Infectious Diseases*, S1473-3099(21)00290-5. Advance online publication. https://doi.org/10.1016/S1473-3099(21)00290-5

Benzinger T. H. (1969). Clinical temperature. New physiological basis. *JAMA*, *209*(8), 1200–1206. doi:10.1001/jama.1969.03160210032008

Bendix, A. (2020, June 17). US states are instituting temperature checks at offices and restaurants, but a quarter of coronavirus patients don't develop a fever. Retrieved September 13, 2020, from https://www.businessinsider.com/temperature-checks-flawed-coronavirus-cases-asymptomatic-no-fever-2020-5

Bergen, M. P. (1981). A literature review of the vascular system in the human orbit. *Acta Morphol. Neerl. Scand,* 19(4), 273-305.

Bisht, H., Roberts, A., Vogel, L., Bukreyev, A., Collins, P. L., Murphy, B. R., Subbarao, K., & Moss, B. (2004). Severe acute respiratory syndrome coronavirus spike protein expressed by attenuated vaccinia virus protectively immunizes mice. *Proceedings of the National Academy of Sciences of the United States of America*, *101*(17), 6641–6646. https://doi.org/10.1073/pnas.0401939101

Brandt, J. (2020, August 15). *Health Department Recommends Virtual Start for Chester County, Delco Schools*. NBC10 Philadelphia. https://www.nbcphiladelphia.com/news/coronavirus/schooling-in-a-pandemic/health-department-recommends-virtual-start-for-chester-county-delco-schools/2502896/

Brueck, H. (2021, July 24). *A fully vaccinated mom caught COVID-19 after her kids went to summer camp: "Our kids are Trojan-horsing us."* Insider. https://www.businessinsider.com/fully-vaccinated-mom-catches-covid-19-after-kids-summer-camp-2021-7

Carroll, L. (2020, June 12). *Who bought all the toilet paper? Study suggests who was most likely to stockpile during COVID-19*. NBC News. https://www.nbcnews.com/health/health-news/who-bought-all-toilet-paper-study-suggests-who-was-most-n1230586

CBS Austin. (2020, July 24). Nearly 100 babies have tested positive for COVID-19 in Travis County. Retrieved September 12, 2020, from https://cbsaustin.com/news/local/nearly-100-babies-have-tested-positive-for-covid-19-in-travis-county

CDC. (2021a) *COVID-19 in Japan - COVID-19 High - Level 3: COVID-19 High - Travel Health Notices | Travelers' Health | CDC*. (2021a). CDC.Gov. https://wwwnc.cdc.gov/travel/notices/covid-3/covid-19-japan

CDC. (2021b). *COVID-19 and your health.* Centers for Disease Control and Prevention. Retrieved May 20, 2021, from https://www.cdc.gov/coronavirus/2019-ncov/vaccines/fully-vaccinated.html

CDC. (2017). Definitions of Signs, Symptoms, and Conditions of Ill Travelers. Retrieved August 12, 2020, from https://www.cdc.gov/quarantine/maritime/definitions-signs-symptoms-conditions-ill-travelers.html

Choi, B., Choudhary, M. C., Regan, J., Sparks, J. A., Padera, R. F., Qiu, X., . . . Li, J. Z. (2020). Persistence and Evolution of SARS-CoV-2 in an Immunocompromised Host. *New England Journal of Medicine, 383*(23), 2291-2293. doi:10.1056/nejmc2031364

Chan, L. S., Cheung, G. T. Y., Lauder, I. J., & Kumana, C. R. (2006). Screening for Fever by Remote-sensing Infrared Thermographic Camera. *Journal of Travel Medicine*, *11*(5), 273–279. https://doi.org/10.2310/7060.2004.19102

Challen, R., Brooks-Pollock, E., Read, J. M., Dyson, L., Tsaneva-Atanasova, K., & Danon, L. (2021). Risk of mortality in patients infected with SARS-CoV-2 variant of concern 202012/1: matched cohort study. *BMJ*, n579. https://doi.org/10.1136/bmj.n579

Cheung, N., & Mcnab, A. A. (2003). Venous Anatomy of the Orbit. *Investigative Opthalmology & Visual Science, 44*(3), 988. doi:10.1167/iovs.02-0865

Childstats.govPOP1 (2021) *Child population: Number of children (in millions) ages 0–17 in the United States by age, 1950–2019 and projected 2020–2050*. (2021). Child Stats.Gov. https://www.childstats.gov/americaschildren/tables/pop1.asp

China Daily. (2003). http://www.chinadaily.com.cn/en/doc/2003-08/31/content_259908.htm

China Internet Information Center. (2003). Xinhua News Agency. http://english.china.org.cn/english/scitech/73828.htm

Collell, G., & Fauquet, J. (2015). Brain activity and cognition: A connection from thermodynamics and information theory. *Frontiers in Psychology, 6*, 818. doi:10.3389/fpsyg.2015.00818

Colchester, M. (2021, May 29). *Covid-19 Cases and Hospitalizations Rise in U.K. as Variant From India Takes Hold*. WSJ. https://www.wsj.com/articles/covid-19-cases-and-hospitalizations-rise-in-u-k-as-variant-from-india-takes-hold-11622289600

Dave, A. (2021). A healthcare worker checks the temperature of a rice mill worker during a coronavirus disease (COVID-19) vaccination drive at Bavla village on the outskirts of Ahmedabad, India, April 13, 2021. In *Reuters*. https://www.reuters.com/world/india/india-reports-132788-new-covid-19-infections-3207-deaths-2021-06-02/

Davies, N. G., Abbott, S., Barnard, R. C., Jarvis, C. I., Kucharski, A. J., Munday, J. D., . . . Edmunds, W. J. (2021). Estimated transmissibility and impact OF SARS-CoV-2 Lineage B.1.1.7 in England. *Science (New York, N.Y.), 372*(6538). doi:10.1126/science.abg3055

Daanen, H., Bose-O'Reilly, S., Brearley, M., Flouris, D. A., Gerrett, N. M., Huynen, M., Jones, H. M., Lee, J. K. W., Morris, N., Norton, I., Nybo, L., Oppermann, E., Shumake-Guillemot, J., & van den Hazel, P. (2020). COVID-19 and thermoregulation-related problems: Practical recommendations. *Temperature*, *8*(1), 1–11. https://doi.org/10.1080/23328940.2020.1790971

Dahl, E. (2020). Coronavirus (Covid-19) outbreak on the cruise ship Diamond Princess. *International Maritime Health*, *71*(1), 5–8. https://doi.org/10.5603/mh.2020.0003

Dan, J. M., Mateus, J., Kato, Y., Hastie, K. M., Yu, E. D., Faliti, C. E., Grifoni, A., Ramirez, S. I., Haupt, S., Frazier, A., Nakao, C., Rayaprolu, V., Rawlings, S. A., Peters, B., Krammer, F., Simon, V., Saphire, E. O., Smith, D. M., Weiskopf, D., Sette, A., … Crotty, S. (2021). Immunological memory to SARS-CoV-2 assessed for up to 8 months after infection. *Science (New York, N.Y.)*, *371*(6529), eabf4063. https://doi.org/10.1126/science.abf4063

Day, M. (2021). Covid-19: More young children are being infected in Israel and Italy, emerging data suggest. *BMJ*, n383. https://doi.org/10.1136/bmj.n383

Da Silva Francisco, R., Benites, L. F., Lamarca, A. P., De Almeida, L. G., Hansen, A. W., Gularte, J. S., . . . Spilki, F. R. (2021). Pervasive transmission of E484K and emergence of vui-np13l with evidence of SARS-COV-2 co-infection events by two different lineages in Rio Grande do Sul, Brazil. *Virus Research, 296,* 198345. doi:10.1016/j.virusres.2021.198345

Davis, R. (2020, May 08). IDF vs COVID-19. Retrieved October 21, 2020, from https://ajn.timesofisrael.com/idf-vs-covid-19/

De Souza, W. M., Amorim, M. R., Sesti-Costa, R., Coimbra, L. D., Toledo-Teixeira, D. A. D., Parise, P. L., Barbosa, P. P., Bispo-dos-Santos, K., Mofatto, L. S., Simeoni, C. L., Brunetti, N. S., Claro, I. M., Duarte, A. S. S., Coletti, T. M., Zangirolami, A. B., Costa-Lima, C., Gomes, A. B. S. P., Buscaratti, L. I., Sales, F. C., . . . Proenca-Modena, J. L. (2021). Levels of SARS-CoV-2 Lineage P.1 Neutralization by Antibodies Elicited after Natural Infection and Vaccination. *SSRN Electronic Journal*. Published. https://doi.org/10.2139/ssrn.3793486

Deming, D., Sheahan, T., Heise, M., Yount, B., Davis, N., Sims, A., Suthar, M., Harkema, J., Whitmore, A., Pickles, R., West, A., Donaldson, E., Curtis, K., Johnston, R., & Baric, R. (2006). Vaccine efficacy in senescent mice challenged with recombinant SARS-CoV bearing epidemic and zoonotic spike variants. *PLOS medicine*, *3*(12), e525. https://doi.org/10.1371/journal.pmed.0030525

Dimopoulou et al, 2004. *Hypothalamic-pituitary-adrenal axis dysfunction in. . . : Critical Care Medicine*. (2004). LWW. https://journals.lww.com/ccmjournal/Abstract/2004/02000/Hypothalamic_pituitary_adrenal_axis_dysfunction_in.12.aspx

Diamond, M., Chen, R., Xie, X., Case, J., Zhang, X., VanBlargan, L., . . . Gilchuk, P. (2021). SARS-CoV-2 variants show resistance to neutralization by many monoclonal and serum-derived polyclonal antibodies. *Research Square,* rs.3.rs-228079. doi:10.21203/rs.3.rs-228079/v1

Ellis-Petersen, H. (2021, April 24). *'The system has collapsed': India's descent into Covid hell*. The Guardian.

Eversden, A. (2020, September 22). *What does military AI need to detect COVID? Data from wearables*. C4ISRNet. https://www.c4isrnet.com/artificial-intelligence/2020/09/22/what-does-military-ai-need-to-detect-covid-data-from-wearables/

Farnell, S., Maxwell, L., Tan, S., Rhodes, A., & Philips, B. (2005). Temperature measurement: Comparison of non-invasive methods used in adult critical care. *Journal of Clinical Nursing, 14*(5), 632-639. doi:10.1111/j.1365-2702.2004.00916.x

FDA. (2010). 510(k) Regulatory Approval. Abreu BTT 700 System. Retrieved August 12, 2020, from https://www.accessdata.fda.gov/scripts/cdrh/cfdocs/cfpmn/pmn.cfm?ID=K100843

Ferguson, N., Laydon, D., Nedjati Gilani, G., Imai, N., Ainslie, K., Baguelin, M., . . . Ghani, A. (2020). Report 9: Impact of non-pharmaceutical interventions (NPIs) to reduce COVID19 mortality and healthcare demand. *Imperial College COVID-19 Response Team,* 1–20. doi:10.25561/77482

Festal A. 1887. Recherches anatomiques sur les veines de l'orbite. These de Paris DOI: https://exhibits.lib.unc.edu/exhibits/show/nyam-theses/item/5708.

Flaxman, S., Mishra, S., Gandy, A., Unwin, H. J. T., Mellan, T. A., Coupland, H., Whittaker, C., Zhu, H., Berah, T., Eaton, J. W., Monod, M., Perez-Guzman, P. N., Schmit, N., Cilloni, L., Ainslie, K. E. C., Baguelin, M., Boonyasiri, A., Boyd, O., Cattarino, L., . . . Bhatt, S. (2020). Estimating the effects of non-pharmaceutical interventions on COVID-19 in Europe. *Nature*, *584*(7820), 257–261. https://doi.org/10.1038/s41586-020-2405-7

Foster, J., Lloyd, A. B., & Havenith, G. (2021). Non-contact infrared assessment of human body temperature: The journal *Temperature* toolbox. *Temperature*, 1–14. https://doi.org/10.1080/23328940.2021.1899546

Forrest, A. J., Juliano, M. L., Conley, S. P., Cronyn, P. D., Mcglynn, A., & Auten, J. D. (2017). Temporal artery and axillary thermometry comparison with rectal thermometry in children presenting to the ED. *The American Journal of Emergency Medicine, 35*(12), 1855–1858. doi:10.1016/j.ajem.2017.06.017

Foreman, B., Ngwenya, L. B., Stoddard, E., Hinzman, J. M., Andaluz, N., & Hartings, J. A. (2018). Safety and Reliability of Bedside, Single Burr Hole Technique for Intracranial Multimodality Monitoring in Severe Traumatic Brain Injury. *Neurocritical Care*, *29*(3), 469–480. https://doi.org/10.1007/s12028-018-0551-7

French Armed Forces. Service de santé des armées. Investigation de l'épidémie de COVID-19 au sein du Groupe Aéronaval. Service de santé des armées. (2020). *Ministere Des Armees*. Published. https://www.defense.gouv.fr/content/download/583466/9938746/file/20200405_929_ARM_SSA_CESPA_rapport_epidemie_covid19_Gan_VEXP.pdf

Furukawa, N. W., Brooks, J. T., & Sobel, J. (2020). Evidence Supporting Transmission of Severe Acute Respiratory Syndrome Coronavirus 2 While Presymptomatic or Asymptomatic. *Emerging Infectious Diseases, 26*(7). doi:10.3201/eid2607.201595

Gagge, A. P., & Nishi, Y. (1977). Chapter 5: Heat exchange between human skin surface and thermal environment. In Handbook of physiology: A critical, comprehensive presentation of physiological knowledge and concepts (pp. 69–92). Bethesda, MD: American Physiol. Soc.

Gandhi, M., Yokoe, D. S., & Havlir, D. V. (2020). Asymptomatic Transmission, the Achilles' Heel of Current Strategies to Control Covid-19. *New England Journal of Medicine, 382*(22), 2158–2160. doi:10.1056/nejme2009758

Gates, B. (2020). Responding to Covid-19 — A Once-in-a-Century Pandemic? *New England Journal of Medicine, 382*(18), 1677–1679. doi:10.1056/nejmp2003762

Geijer, H., Udumyan, R., Lohse, G., & Nilsagård, Y. (2016). Temperature measurements with a temporal scanner: Systematic review and meta-analysis. *BMJ Open, 6*(3). doi:10.1136/bmjopen-2015-009509

Gilbertson, D. (2020, June 13). 3 nights, 3 hotels: What it's really like to stay in a hotel during the coronavirus pandemic. Retrieved August 18, 2020, from https://www.usatoday.com/story/travel/hotels/2020/06/13/hotel-safety-covid-19-coronavirus-las-vegas-open-new-york-new-york-caesars-palace/5341691002/

Golovkin, P. (2020, September 11). Russian schools open with classroom, cafeteria precautions. Retrieved October 21, 2020, from https://apnews.com/article/virus-outbreak-archive-russia-a17cd7313045e576392e5ef0858aafce

Haselhorst, S. (2021, August 16). *"Save our babies": As another Mississippi child dies of COVID-19, communities beg for help*. The Clarion-Ledger. https://www.clarionledger.com/story/news/local/2021/08/16/fifth-child-mississippi-dies-covid-19/8150426002/

He, X., Lau, E. H. Y., Wu, P., Deng, X., Wang, J., Hao, X., Lau, Y. C., Wong, J. Y., Guan, Y., Tan, X., Mo, X., Chen, Y., Liao, B., Chen, W., Hu, F., Zhang, Q., Zhong, M., Wu, Y., Zhao, L., . . . Leung, G. M. (2020). Temporal dynamics in viral shedding and transmissibility of COVID-19. *Nature Medicine*, *26*(5), 672–675. https://doi.org/10.1038/s41591-020-0869-5

Hensley, M. K., Bain, W. G., Jacobs, J., Nambulli, S., Parikh, U., Cillo, A., . . . Haidar, G. (2021). Intractable Coronavirus Disease 2019 (COVID-19) and Prolonged Severe Acute Respiratory Syndrome Coronavirus 2 (SARS-CoV-2) Replication in a Chimeric Antigen Receptor-Modified T-Cell Therapy Recipient: A Case Study. *Clinical Infectious Diseases*. *73*(3): e815–e821. doi:10.1093/cid/ciab072

Hindustan Times Auto News. (2020, April 22). Hindustan Times Auto News. https://auto.hindustantimes.com/auto/news/slow-restart-for-toyota-yaris-factory-amid-france-s-coronavirus-lockdown-41587538355599.html

Hines, M. U. T. (2021, June 11). *Two passengers test positive for COVID on Celebrity Millennium "fully vaccinated" cruise*. USA TODAY. https://eu.usatoday.com/story/travel/cruises/2021/06/10/passengers-positive-covid-after-sailing-100-vaccinated-cruise/7645511002/

Hodcroft, E. B., Domman, D. B., Snyder, D. J., Oguntuyo, K. Y., van Diest, M., Densmore, K. H., Schwalm, K. C., Femling, J., Carroll, J. L., Scott, R. S., Whyte, M. M., Edwards, M. W., Hull, N. C., Kevil, C. G., Vanchiere, J. A., Lee, B., Dinwiddie, D. L., Cooper, V. S., & Kamil, J. P. (2021). Emergence in late 2020 of multiple lineages of SARS-CoV-2 Spike protein variants affecting amino acid position 677. *BMJ Yale*. Published. https://doi.org/10.1101/2021.02.12.21251658

Hoffmann, M., Arora, P., Groß, R., Seidel, A., Hörnich, B., Hahn, A., Krüger, N., Graichen, L., Hofmann-Winkler, H., Kempf, A., Winkler, M. S., Schulz, S., Jäck, H. M., Jahrsdörfer, B., Schrezenmeier, H., Müller, M., Kleger, A., Münch, J., & Pöhlmann, S. (2021). SARS-CoV-2 variants B.1.351 and B.1.1.248: Escape from therapeutic antibodies and antibodies induced by infection and vaccination. *BioRxiv*. Published. https://doi.org/10.1101/2021.02.11.430787

Hsiang, S., Allen, D., Annan-Phan, S., Bell, K., Bolliger, I., Chong, T., Druckenmiller, H., Huang, L. Y., Hultgren, A., Krasovich, E., Lau, P., Lee, J., Rolf, E., Tseng, J., & Wu, T. (2020). The effect of large-scale anti-contagion policies on the COVID-19 pandemic. *Nature*, *584*(7820), 262–267. https://doi.org/10.1038/s41586-020-2404-8

Huang, K. E. (2014, March). *The US 2009 A(H1N1) influenza epidemic: quantifying the impact of school openings on the reproductive number*. PubMed. 25(2): 203–6. https://pubmed.ncbi.nlm.nih.gov/24434751/

Hyndman, B. W., Kitney, R. I., & Sayers, B. M. (1971). Spontaneous rhythms in physiological control systems. *Nature*, *233*(5318), 339–341. https://doi.org/10.1038/233339a0

Ing, A. J., Cocks, C., & Green, J. P. (2020). COVID-19: In the footsteps of Ernest Shackleton. *Thorax*, *75*(8), 693–694. doi:10.1136/thoraxjnl-2020-215091

Jalal, A. (2020, March 04). Coronavirus temperature check. Retrieved September 14, 2020, from https://www.abc.net.au/news/2020-03-04/coronavirus-temperature-check-1/12026250?nw=0

Jensen, B. N., Jensen, F. S., Madsen, S. N., & Løssl, K. (2000). Accuracy of Digital Tympanic, Oral, Axillary, and Rectal Thermometers Compared with Standard Rectal Mercury Thermometers. *The European Journal of Surgery, 166*(11), 848–851. doi:10.1080/110241500447218

Jeong, H., Lee, J. Y., Lee, K., Kang, Y. J., Kim, J.-T., Avila, R., Tzavelis, A., Kim, J., Ryu, H., Kwak, S. S., Kim, J. U., Banks, A., Jang, H., Chang, J.-K., Li, S., Mummidisetty, C. K., Park, Y., Nappi, S., Chun, K. S., & Lee, Y. J. (2021). Differential cardiopulmonary monitoring system for artifact-canceled physiological tracking of athletes, workers, and COVID-19 patients. *Science Advances*, *7*(20). https://doi.org/10.1126/sciadv.abg3092

Jessen, C., & Kuhnen, G. (1992). No evidence for brain stem cooling during face fanning in humans. *Journal of Applied Physiology, 72*(2), 664–669. doi:10.1152/jappl.1992.72.2.664

Johns Hopkins University (2020, April 16). *COVID-19's historic economic impact, in the U.S. and abroad*. The Hub. https://hub.jhu.edu/2020/04/16/coronavirus-impact-on-european-american-economies/

Johns Hopkins University (2021). COVID-19 Map - Johns Hopkins Coronavirus Resource Center (jhu.edu). Retrieved February 22, 2021 from https://coronavirus.jhu.edu/map.html

Johnson, N. P., & Mueller, J. (2002). Updating the Accounts: Global Mortality of the 1918-1920 "Spanish" Influenza Pandemic. *Bulletin of the History of Medicine, 76*(1), 105–115. doi:10.1353/bhm.2002.0022

Johansson, M. A., Quandelacy, T. M., Kada, S., Prasad, P. V., Steele, M., Brooks, J. T., Slayton, R. B., Biggerstaff, M., & Butler, J. C. (2021). SARS-CoV-2 Transmission From People Without COVID-19 Symptoms. *JAMA Network Open*, *4*(1), e2035057. https://doi.org/10.1001/jamanetworkopen.2020.35057

Kawamura, H. (1965, November 12). *Elevation in Brain Temperature during Paradoxical Sleep*. Science. https://science.sciencemag.org/content/150/3698/912

Kapadia, S. U., Rose, J. K., Lamirande, E., Vogel, L., Subbarao, K., & Roberts, A. (2005). Long-term protection from SARS coronavirus infection conferred by a single immunization with an attenuated VSV-based vaccine. *Virology*, *340*(2), 174–182. https://doi.org/10.1016/j.virol.2005.06.016

Kasper, M. R., Geibe, J. R., Sears, C. L., Riegodedios, A. J., Luse, T., Von Thun, A. M., McGinnis, M. B., Olson, N., Houskamp, D., Fenequito, R., Burgess, T. H., Armstrong, A. W., DeLong, G., Hawkins, R. J., & Gillingham, B. L. (2020). An Outbreak of Covid-19 on an Aircraft Carrier. *The New England Journal of Medicine*, 10.1056/NEJMoa2019375. Advance online publication. https://doi.org/10.1056/NEJMoa2019375

Kemp, S. A., Collier, D. A., Datir, R. P., Ferreira, I. A. T. M., Gayed, S., Jahun, A., Hosmillo, M., Rees-Spear, C., Mlcochova, P., Lumb, I. U., Roberts, D. J., Chandra, A., Temperton, N., Sharrocks, K., Blane, E., Modis, Y., Leigh, K. E., Briggs, J. A. G., van Gils, M. J., . . . Gupta, R. K. (2021). SARS-CoV-2 evolution during treatment of chronic infection. *Nature*, *592*(7853), 277–282. https://doi.org/10.1038/s41586-021-03291-y

Khatamzas, E. (2021, January 1). *Emergence of multiple SARS-CoV-2 mutations in an immunocompromised host*. MedRxiv. https://www.medrxiv.org/content/10.1101/2021.01.10.20248871v1

Kidd, M., Richter, A., Best, A., Mirza, J., Percival, B., Mayhew, M., . . . McNally, A. (2020). S-variant sars-cov-2 is associated with significantly higher viral loads in samples tested by Thermofisher taqpath rt-qpcr. *MedRxiv*. doi:10.1101/2020.12.24.20248834

Kiekkas, P., Aretha, D., Almpani, E., & Stefanopoulos, N. (2019). Temporal Artery Thermometry in Pediatric Patients: Systematic Review and Meta-Analysis. *Journal of Pediatric Nursing, 46*, 89–99. doi:10.1016/j.pedn.2019.03.004

Kiekkas, P., Stefanopoulos, N., Bakalis, N., Kefaliakos, A., & Karanikolas, M. (2016). Agreement of infrared temporal artery thermometry with other thermometry methods in adults: Systematic review. *Journal of Clinical Nursing, 25*(7–8), 894-905. doi:10.1111/jocn.13117

Kimberger, O., Cohen, D., Illievich, U., & Lenhardt, R. (2007). Temporal Artery Versus Bladder Thermometry During Perioperative and Intensive Care Unit Monitoring. *Anesthesia & Analgesia, 105*(4), 1042–1047. doi:10.1213/01.ane.0000281927.88935.e0

Kiyatkin, E. A. (2019). Brain temperature and its role in physiology and pathophysiology: Lessons from 20 years of thermorecording. *Temperature, 6*(4), 271–333. https://dx.doi.org/10.1080%2F23328940.2019.1691896

Kiyatkin, E.A. Brain hyperthermia as physiological and pathological phenomena. [Review] *Brain Res.* 50(1): 27–56 (2005). https://doi.org/10.1016/j.brainresrev.2005.04.001

Knowles, H (2021). Hospitals overwhelmed by covid are turning to 'crisis standards of care.' What does that mean? Retrieved from: What are crisis standards of care? - The Washington Post

Korber, B., Fischer, W. M., Gnanakaran, S., Yoon, H., Theiler, J., Abfalterer, W., . . . Wyles, M. D. (2020). Tracking Changes in SARS-CoV-2 Spike: Evidence that D614G Increases Infectivity of the COVID-19 Virus. *Cell*. doi:10.1016/j.cell.2020.06.043

Kustin, T., Harel, N., Finkel, U., Perchik, S., Harari, S., Tahor, M., Caspi, I., Levy, R., Leschinsky, M., Dror, S. K., Bergerzon, G., Gadban, H., Gadban, F., Eliassian, E., Shimron, O., Saleh, L., Ben-Zvi, H., Amichay, D., Ben-Dor, A., . . . Stern, A. (2021). Evidence for increased breakthrough rates of SARS-CoV-2 variants of concern in BNT162b2 mRNA vaccinated individuals. *BMJ Yale*. Published. https://doi.org/10.1101/2021.04.06.21254882

Kun, Z., & Wenting, Z. (2020, March 12). Young adults most stressed by virus. Retrieved September 14, 2020, from https://www.chinadaily.com.cn/a/202003/12/WS5e69730fa31012821727e50f.html

Lasek-Nesselquist, E. (2021, January 1). *The localized rise of a B.1.526 SARS-CoV-2 variant containing an E484K mutation in New York State*. MedRxiv. https://www.medrxiv.org/content/10.1101/2021.02.26.21251868v1

LaGrone, S. (2020, April 16*). Navy identifies carrier Roosevelt sailor who died from COVID-19. USNI* News. Retrieved May 19, 2021, from https://news.usni.org/2020/04/16/navy-identifies-carrier-roosevelt-sailor-who-died-from-covid-19

Lagakos, N., & Bucaro, J. A. (2010). *U.S. Patent No. 8195013* issued in 2012. Patent application filed on January25th, 2010. Washington, DC: U.S. Patent and Trademark Office.

Latman, N. S., Hans, P., Nicholson, L., DeLee Zint, S., Lewis, K., Shirey, A. (2001). Evaluation of clinical thermometers for accuracy and reliability. *Biomed. Instrum. Technol.,* 35(4), 259–265.

Lazarus, M., Yoshida, K., Coppari, R., Bass, C. E., Mochizuki, T., Lowell, B. B., & Saper, C. B. (2007). EP3 prostaglandin receptors in the median preoptic nucleus are critical for fever responses. *Nature Neuroscience, 10*(9), 1131–1133. https://doi.org/10.1038/nn1949

Letizia, A. G., Ramos, I., Obla, A., Goforth, C., Weir, D. L., Ge, Y., Bamman, M. M., Dutta, J., Ellis, E., Estrella, L., George, M. C., Gonzalez-Reiche, A. S., Graham, W. D., van de Guchte, A., Gutierrez, R., Jones, F., Kalomoiri, A., Lizewski, R., Lizewski, S., Marayag, J., … Sealfon, S. C. (2020). SARS-CoV-2 Transmission among Marine Recruits during Quarantine. *The New England Journal of Medicine*, 383: 24017–2416. Advance online publication. https://doi.org/10.1056/NEJMoa2029717

Lewis, W. C. (1968). *Thermal insulation from wood for buildings: Effects of moisture and its control* (USA, U.S.D.A.). Ft. Belvoir, VA: Defense Technical Information Center.

Li, F., Li, Y. Y., Liu, M. J., Fang, L. Q., Dean, N. E., Wong, G. W. K., Yang, X. B., Longini, I., Halloran, M. E., Wang, H. J., Liu, P. L., Pang, Y. H., Yan, Y. Q., Liu, S., Xia, W., Lu, X. X., Liu, Q., Yang, Y., & Xu, S. Q. (2021). Household transmission of SARS-CoV-2 and risk factors for susceptibility and infectivity in Wuhan: a retrospective observational study. *The Lancet Infectious Diseases*, *21*(5), 617–628. https://doi.org/10.1016/s1473-3099(20)30981-6

Lopez, M., Sessler, D. I., Walter, K., Emerick, T., & Ozaki, M. (1994). Rate and gender dependence of the sweating, vasoconstriction, and shivering thresholds in humans. Anesthesiology, 80(4), 780–788. https://doi.org/10.1097/00000542-199404000-00009

Lovelace, B., Jr. (2021, April 15). *Pfizer CEO says third Covid vaccine dose likely needed within 12 months*. CNBC. https://www.cnbc.com/2021/04/15/pfizer-ceo-says-third-covid-vaccine-dose-likely-needed-within-12-months.html

LoTempio, J., Billings, E., Draper, K., Ralph, C., Moshgriz, M., Duong, N., Bard, J. D., Gai, X., Wessel, D., DeBiasi, R. L., Campos, J. M., Vilain, E., Delaney, M., & Michael, D. G. (2021). Novel SARS-CoV-2 spike variant identified through viral genome sequencing of the pediatric Washington D.C. COVID-19 outbreak. *MedRxiv*. Published. https://doi.org/10.1101/2021.02.08.21251344

Lum, C. L., Jeyanthi, S., Prepageran, N., Vadivelu, J., & Raman, R. (2009). Antibacterial and antifungal properties of human cerumen. *The Journal of Laryngology & Otology, 123*(4), 375–378. doi:10.1017/s0022215108003307

Mandavilli, A. (2021). *Reaching 'Herd Immunity' Is Unlikely in the U.S., Experts Now Believe*. The New York Times. https://www.nytimes.com/2021/05/03/health/covid-herd-immunity-vaccine.html

Ma, Y., & Fang, M. (2013). Immunosenescence and age-related viral diseases. *Science China Life Sciences*, *56*(5), 399–405. https://doi.org/10.1007/s11427-013-4478-0

Maloney, S. K., Fuller, A., Mitchell, G., & Mitchell, D. (2001). Rectal temperature measurement results in artifactual evidence of selective brain cooling. *American Journal of Physiology-Regulatory, Integrative and Comparative Physiology*, *281*(1), R108–R114. https://doi.org/10.1152/ajpregu.2001.281.1.r108

Mackowiak, P. A., Wasserman, S. S., & Levine, M. M. (1992). A critical appraisal of 98.6 degrees F, the upper limit of the normal body temperature, and other legacies of Carl Reinhold August Wunderlich. *JAMA*, *268*(12), 1578–1580.

MacLean, J.D., 1941. Thermal conductivity of wood. *Heating, Piping & Air Conditioning.* 13:380–391. DOI: https://www.fpl.fs.fed.us/documnts/pdf1941/macle41a.pdf

Mallapaty S. (2020). What the cruise-ship outbreaks reveal about COVID-19. Retrieved March 7, 2021 from https://www.nature.com/articles/d41586-020-00885-w

Mallapaty, S., & Callaway, E. (2021, March 24). *What scientists do and don't know about the Oxford–AstraZeneca COVID vaccine*. Nature. Retrieved May 19, 2021, from https://www.nature.com/articles/d41586-021-00785-7

Mariak Z, Lebkowski W, Lysoń T, Lewko J, Piekarski P. (1999). Temperatura mózgu podczas kraniotomii w znieczuleniu ogólnym [Brain temperature during craniotomy in general anesthesia]. *Neurol. Neurochir. Pol*., 33(6), 1325–1337.

Martin, S. A., & Kline, A. M. (2004). Can There Be a Standard for Temperature Measurement in the Pediatric Intensive Care Unit? *AACN Clinical Issues: Advanced Practice in Acute and Critical Care, 15*(2), 254-266. doi:10.1097/00044067-200404000-00011

McCann, S. M., Kimura, M., Karanth, S., Yu, W. H., Mastronardi, C. A., & Rettori, V. (2006). The Mechanism of Action of Cytokines to Control the Release of Hypothalamic and Pituitary Hormones in Infection. *Annals of the New York Academy of Sciences*, *917*(1), 4–18. https://doi.org/10.1111/j.1749-6632.2000.tb05368.x

McDonnell, P. J., Linthicum, K., & Wilkinson, T. (2020, March 14). Mexico, Latin America gear up for next phase of coronavirus threat. Retrieved September 11, 2020, from https://www.latimes.com/world-nation/story/2020-03-14/mexico-latin-america-gear-up-for-next-phase-of-coronavirus-threat

Microsoft. (2017, June 9). How do you fast-track a biofeedback device to market in less than a year? Retrieved September 22, 2021, from https://advocacypublic.clouddamppe.microsoft.com/en-us/story/btt

Modell, J. G., Katholi, C. R., Kumaramangalam, S. M., Hudson, E. C., & Graham, D. (1998). Unreliability of the Infrared Tympanic Thermometer in Clinical Practice. *Southern Medical Journal, 91*(7), 649–654. doi:10.1097/00007611-199807000-00008

Mogensen, C. B., Wittenhoff, L., Fruerhøj, G., & Hansen, S. (2018). Forehead or ear temperature measurement cannot replace rectal measurements, except for screening purposes. *BMC Pediatrics, 18*(1). doi:10.1186/s12887-018-0994-1

Mosso, A. (1892, May 5). *The Temperature of the Brain*. Nature. https://www.nature.com/articles/046017a0?error=cookies_not_supported&code=f26d0a49-7964-4467-9447-c77221775bac

Moore, K. A., Lipsitch, M., Barry, J. M., & Osterholm, M. T. (2020, April 30). The CIDRAP Viewpoint. Part 1: "The future of the COVID-19 pandemic: Lessons learned from pandemic influenza". Retrieved August 25, 2020, from https://www.cidrap.umn.edu/covid-19/covid-19-cidrap-viewpoint

Moran, D. S., & Mendal, L. (2002). Core Temperature Measurement. *Sports Medicine, 32*(14), 879–885. doi:10.2165/00007256-200232140-00001

Mori, K. (2020, June 23). "Battle of Okinawa" 75th Anniversary Commemoration. Retrieved October 21, 2020, from https://www.upi.com/News_Photos/lp/9dcdaf90b290a644c2d40ae42bf56c94/

Moritsugu, K. (2020, March 2). China's crisis wanes as epidemic takes hold in US, elsewhere. Retrieved October 22, 2020, from https://apnews.com/article/45393d272612f46899d269b1966c869a

Murphy JV, Banwell PE, Roberts AH & McGrouther DA. (2000). Frostbite: pathogenesis and treatment. *J. Trauma*, 48(1): 171–8. doi: 10.1097/00005373-200001000-00036.

Myers, M. (2020, July 30). The military is seeing a higher COVID-19 infection rate in young people. Here's why. Retrieved October 21, 2020, from https://www.militarytimes.com/news/your-military/2020/07/30/the-military-is-seeing-a-higher-covid-19-infection-rate-in-young-people-officials-explain-why/

Nakamura, Y., Nakamura, K., & Morrison, S. (2009). Different populations of prostaglandin EP3 receptor-expressing preoptic neurons project to two fever-mediating sympathoexcitatory brain regions. *Neuroscience, 161*(2), 614–620. doi:10.1016/j.neuroscience.2009.03.041

Nielsen, B., & Nybo, L. (2003). Cerebral Changes During Exercise in the Heat. *Sports Medicine*, *33*(1), 1–11. https://doi.org/10.2165/00007256-200333010-00001

Niven, D. J., Gaudet, J. E., Laupland, K. B., Mrklas, K. J., Roberts, D. J., & Stelfox, H. T. (2015). Accuracy of Peripheral Thermometers for Estimating Temperature. *Annals of Internal Medicine, 163*(10): 768–777. doi:10.7326/m15-1150

Nordling, L. (2020, March 15). 'A ticking time bomb': Scientists worry about coronavirus spread in Africa. Retrieved August 12, 2020, from https://www.sciencemag.org/news/2020/03/ticking-time-bomb-scientists-worry-about-coronavirus-spread-africa

O'Grady, N. P., Barie, P. S., Bartlett, J. G., Bleck, T., Carroll, K., Kalil, A. C., . . . Masur, H. (2008). Guidelines for evaluation of new fever in critically ill adult patients: 2008 update from the American College of Critical Care Medicine and the Infectious Diseases Society of America. *Critical Care Medicine, 36*(4): 1330–1349. doi:10.1097/ccm.0b013e318169eda9

O'Brien, D. L., Rogers, I. R., Holden, W., Jacobs, I., Mellett, S., Wall, E. J., & Davies, D. (2000). The Accuracy of Oral Predictive and Infrared Emission Detection Tympanic Thermometers in an Emergency Department Setting. *Academic Emergency Medicine, 7*(9): 1061–1064. doi:10.1111/j.1553-2712.2000.tb02101.x

Ott, I. (1884) The Relation Of The Nervous System To The Temperature Of The Body. *The Journal of Nervous and Mental Disease.* LWW. https://journals.lww.com/jonmd/citation/1884/04000/the_relation_of_the_nervous_system_to_the.1.aspx

Oxford, J., Lambkin, R., Sefton, A., Daniels, R., Elliot, A., Brown, R., & Gill, D. (2005). A hypothesis: The conjunction of soldiers, gas, pigs, ducks, geese and horses in Northern France during the Great War provided the conditions for the emergence of the "Spanish" influenza pandemic of 1918–1919. Vaccine, 23(7): 940–945. doi:10.1016/j.vaccine.2004.06.035

Oxford, J., Sefton, A., Jackson, R., Innes, W., Daniels, R., & Johnson, N. (2002). World War I may have allowed the emergence of "Spanish" influenza. *The Lancet Infectious Diseases*, 2(2): 111–114. doi:10.1016/s1473-3099(02)00185-8

Patel, N., Smith, C. E., Pinchak, A. C., & Hagen, J. F. (1996). Comparison of esophageal, tympanic, and forehead skin temperatures in adult patients. *Journal of Clinical Anesthesia, 8*(6): 462–468. doi:10.1016/0952-8180(96)00103-1

Petersdorf, R. G., & Beeson, P. B. (1961). Fever Of Unexplained Origin: Report On 100 Cases. *Medicine, 40*(1): 1–30. doi:10.1097/00005792-196102000-00001

Planel, E. et al. (2009) Acceleration and persistence of neurofibrillary pathology in a mouse model of tauopathy following anesthesia. *FASEB Journal* 23, 2595–2604. https://doi.org/10.1096/fj.08-122424

Planel, E. et al. (2007) Anesthesia leads to tau hyperphosphorylation through inhibition of phosphatase activity by hypothermia. *J. Neurosci.* 27: 3090–3079. https://doi.org/10.1523/jneurosci.4854-06.2007

Priest, P. C., Duncan, A. R., Jennings, L. C., & Baker, M. G. (2011). Thermal Image Scanning for Influenza Border Screening: Results of an Airport Screening Study. *PLOS ONE, 6*(1). doi:10.1371/journal.pone.0014490

Protsiv, M., Ley, C., Lankester, J., Hastie, T., & Parsonnet, J. (2020). Decreasing human body temperature in the United States since the Industrial Revolution. *ELife*, *9*. https://doi.org/10.7554/elife.49555

Quatrara, B., Coffman, J., Jenkins, T., Mann, K., McGough, K., Conaway, M., & Burns, S. (2007). The effect of respiratory rate and ingestion of hot and cold beverages on the accuracy of oral temperatures measured by electronic thermometers. *Medsurg Nurs.: Official Journal of the Academy of Medical-Surgical Nurses*. 16(2): 105–100.

Rajapakse, N., Dixit, D. (2020, June 25). Human and novel coronavirus infections in children: a review. *Paediatrics and International Child Health*, *41*(1): 36–55. https://doi.org/10.1080/20469047.2020.1781356

Rampone, A. J., & Shirasu, M. E. (1964). Temperature Changes in the Rat in Response to Feeding. *Science*, *144*(3616), 317–319. https://doi.org/10.1126/science.144.3616.317

Rauhala, E. (2020, March 14). *Some countries use temperature checks for coronavirus. Others don't bother. Here's why.* Washington Post. https://www.washingtonpost.com/world/coronavirus-temperature-screening/2020/03/14/24185be0-6563-11ea-912d-d98032ec8e25_story.html

Ranjan, R. (2021, January 1). *Characterization of the Second Wave of COVID-19 in India*. MedRxiv. https://www.medrxiv.org/content/10.1101/2021.04.17.21255665v2

Repko, M. (2020, April 04). As coronavirus cases grow, some of the largest US employers including Walmart and Amazon turn to thermometers as detection tool. Retrieved September 12, 2020, from https://www.cnbc.com/2020/04/04/coronavirus-walmart-amazon-turn-to-thermometers-as-detection-tool.html

Reuters. (2020, March 08). Coronavirus death toll in Netherlands rises to 3. Retrieved November 11, 2020, from https://www.dailysabah.com/world/europe/coronavirus-death-toll-in-netherlands-rises-to-three

Reuters. (2020, May 22). Russia reports record daily rise in new coronavirus deaths. Retrieved September 14, 2020, from https://www.reuters.com/article/health-coronavirus-russia-cases/russia-reports-record-daily-rise-in-new-coronavirus-deaths-idINKBN22Y0WB

Robinson, J. L. (2004). Body temperature measurement in paediatrics: Which gadget should we believe? *Paedeatrics & Child Health, 9*(7): 457–459. doi:10.1093/pch/9.7.457

Roche, D. (2021). Mu COVID Variant, Which Could Be Resistant to Vaccines, Now in Almost Every State. https://www.newsweek.com/mu-covid-variant-could-resistant-vaccines-almost-every-state-1626119

Roxby, P. (2020, June 09). Can thermal cameras help spot coronavirus? Retrieved November 11, 2020, from https://www.bbc.com/news/health-52940951

Sailor, A. (2020). Brigade Completes Deployment Supporting COVID-19 Response. In *U.S. Department of Defense*. https://www.defense.gov/Explore/Features/Story/Article/2200697/2nd-meb-completes-deployment-supporting-national-covid-19-response/

Sang-Hun, C. (2020, May 16). *As South Korea Eases Limits, Virus Cluster Prompts Seoul to Close Bars*. The New York Times. https://www.nytimes.com/2020/05/09/world/asia/coronavirus-south-korea-second-wave.html

Sauret, M. (2020). A soldier scans her wrist and face at a newly installed terminal that screens for high temperatures of people entering Marshall Hall, the U.S. Army Reserve Command and U.S. Forces Command headquarters building at Fort Bragg, N.C., Sept. 29, 2020. In *U.S. Department of Defense*. https://www.defense.gov/Explore/Features/Story/Article/2382019/new-terminal-scanner-screens-temperatures-to-improve-safety/

Sessler D. I. (2000). Perioperative heat balance. *Anesthesiology*, *92*(2): 578–596. https://doi.org/10.1097/00000542-200002000-00042

Shea, A. (2020). Temperature Check. In *U.S. Department of Defense*. https://www.defense.gov/observe/photo-gallery/igphoto/2002273951/

Scheepers, C., Everatt, J., Amoako, D. G., Mnguni, A., Ismail, A., Mahlangu, B., Wibmer, C. K., Wilkinson, E., Tegally, H., San, J. E., Giandhari, J., Ntuli, N., Pillay, S., Mohale, T., Naidoo, Y., Khumalo, Z. T., Makatini, Z., Sigal, A., Williamson, C., & Treurnicht, F. (2021). The continuous evolution of SARS-CoV-2 in South Africa: a new lineage with rapid accumulation of mutations of concern and global detection. *MedRxiv*. https://doi.org/10.1101/2021.08.20.21262342

Schieber, A. M. P., & Ayres, J. S. (2016). Thermoregulation as a disease tolerance defense strategy. *Pathogens and Disease*, *74*(9), ftw106. https://doi.org/10.1093/femspd/ftw106

Scripture, E. (1892). The Need of Psychological Training. *Science, 19*(474), 127–128. Retrieved September 14, 2020, from http://www.jstor.org/stable/1766918

Sheikh, A., McMenamin, J., Taylor, B., & Robertson, C. (2021). SARS-CoV-2 Delta VOC in Scotland: demographics, risk of hospital admission, and vaccine effectiveness. *The Lancet*. Published. https://doi.org/10.1016/s0140-6736(21)01358-1

Shams, S. (2020, March 18). Coronavirus: Is Pakistan taking COVID-19 too lightly?: DW: 18.03.2020. Retrieved September 14, 2020, from https://www.dw.com/en/coronavirus-is-pakistan-taking-covid-19-too-lightly/a-52824403

Simkins, J. (2020, April 20). *French carrier surpasses Theodore Roosevelt with over 1,000 confirmed cases of COVID-19.* Navy Times. Retrieved May 20, 2021, from https://www.navytimes.com/news/your-navy/2020/04/20/french-carrier-surpasses-theodore-roosevelt-with-over-1000-confirmed-cases-of-covid-19/

Silverman, D. G., Brousseau, D. A., & Engelman, K. (1987). Fluorometric documentation of increased cutaneous blood flow after topical application of a PGE2 analog in man. *Prostaglandins*, *33*(5): 627–638. https://doi.org/10.1016/0090-6980(87)90030-x

Smarr, B.L., Aschbacher, K., Fisher, S.M. et al. (2020). Feasibility of continuous fever monitoring using wearable devices. *Sci. Rep.* 10: 21640. https://doi.org/10.1038/s41598-020-78355-6

Soto-Tinoco, E., Guerrero-Vargas, N. N., & Buijs, R. M. (2016). Interaction between the hypothalamus and the immune system. *Experimental Physiology, 101*(12): 1463–1471. https://doi.org/10.1113/EP085560

South China Morning Post (2020, March 9). *Thermometer guns are scammers' new weapon during coronavirus shortages*. South China Morning Post. https://www.scmp.com/abacus/culture/article/3074365/thermometer-guns-are-scammers-new-weapon-during-coronavirus

Suleman, M., Doufas, A. G., Akça, O., Ducharme, M., & Sessler, D. I. (2002). Insufficiency in a New Temporal-Artery Thermometer for Adult and Pediatric Patients. *Anesthesia & Analgesia, 95*(1): 67–71. doi:10.1097/00000539-200207000-00012

Sun, H., Xiao, Y., Liu, J., Wang, D., Li, F., Wang, C., . . . Liu, J. (2020). Prevalent Eurasian avian-like H1N1 swine influenza virus with 2009 pandemic viral genes facilitating human infection. *Proceedings of the National Academy of Sciences, 117*(29), 17204–17210. doi:10.1073/pnas.1921186117

Superville, D. (2020, March 15). White House implements coronavirus screening to protect Trump. Retrieved September 12, 2020, from https://www.washingtontimes.com/news/2020/mar/15/white-house-starts-coronavirus-screenings-protect-/

Tandberg, D., & Sklar, D. (1983). Effect of Tachypnea on the Estimation of Body Temperature by an Oral Thermometer. *New England Journal of Medicine, 308*(16), 945–946. doi:10.1056/nejm198304213081607

Taylor, L. (2021). Covid-19: Is Manaus the final nail in the coffin for natural herd immunity? *BMJ*, 372: n394. https://doi.org/10.1136/bmj.n394

Tchesnokova, V., Kulakesara, H., Larson, L., Bowers, V., Rechkina, E., Kisiela, D., . . . Sokurenko, E. (2021). Acquisition of The L452r mutation in the ACE2-binding interface of spike protein triggers recent massive expansion of SARS-Cov-2 variants. *BioRxiv*. doi:10.1101/2021.02.22.432189

Teunissen, L. P., de Haan, A., de Koning, J. J., & Daanen, H. A. (2012). Telemetry pill versus rectal and esophageal temperature during extreme rates of exercise-induced core temperature change. *Physiological Measurement*, *33*(6): 915–924. https://doi.org/10.1088/0967-3334/33/6/915

Tegally, H., Wilkinson, E., Giovanetti, M., Iranzadeh, A., Fonseca, V., Giandhari, J., . . . De Oliveira, T. (2020). Emergence and rapid spread of a new severe acute respiratory syndrome-related CORONAVIRUS 2 (SARS-CoV-2) lineage with multiple spike mutations in South Africa. *MedRxiv*. doi:10.1101/2020.12.21.20248640

Teller, J., Ragazzi, M., Simonetti, G., & Lava, S. (2013). Accuracy of tympanic and forehead thermometers in private paediatric practice. *Acta Paediatrica, 103*(2): e80–e83. doi:10.1111/apa.12464

TenWolde, A., Mcnatt, J. D., & Krahn, L. (1988). Thermal properties of wood and wood panel products for use in buildings. doi:10.2172/6059532

Thomas, N. (2021, August 17). *Child Covid-19 cases have "steadily increased" since the beginning of July, AAP says, with 121,000 new cases last week*. CNN. https://www.cnn.com/2021/08/17/health/child-covid-19-cases-increase/index.html

Thompson, M. G. (2021, April 1). *Interim Estimates of Vaccine Effectiveness of BNT162b2 and mRNA*. Centers for Disease Control and Prevention. https://www.cdc.gov/mmwr/volumes/70/wr/mm7013e3.htm

Thomson, E. C., Rosen, L. E., Shepherd, J. G., Spreafico, R., da Silva Filipe, A., Wojcechowskyj, J. A., Davis, C., Piccoli, L., Pascall, D. J., Dillen, J., Lytras, S., Czudnochowski, N., Shah, R., Meury, M., Jesudason, N., de Marco, A., Li, K., Bassi, J., O'Toole, A., . . . Snell, G. (2021). Circulating SARS-CoV-2 spike N439K variants maintain fitness wnoahile evading antibody-mediated immunity. *Cell*, *184*(5), 1171–1187.e20. https://doi.org/10.1016/j.cell.2021.01.037

Today Online. (2020, February 16). 'Thermometer guns' on Covid-19 front lines are 'notoriously not accurate'. Retrieved September 13, 2020, from https://www.todayonline.com/world/thermometer-guns-covid-19-front-lines-are-notoriously-not-accurate

TOI Staff. (2020, April 22). After decline in rate of new infections, Israel records biggest rise in a week. Retrieved September 14, 2020, from https://www.timesofisrael.com/after-decline-in-rate-of-new-infections-israel-records-biggest-rise-in-a-week/

Toy, S., & Wernau, J. (2021, August 22). *More Children Are Hospitalized With Covid-19, and Doctors Fear It Will Get Worse*. WSJ. https://www.wsj.com/articles/more-kids-are-hospitalized-with-covid-19-and-doctors-fear-it-will-get-worse-11629624602

Tomes, N. (2010). "Destroyer and Teacher": Managing the Masses during the 1918–1919 Influenza Pandemic. *Public Health Reports, 125*: 48–62. doi:10.1177/00333549101250s308

Truong, T. T. (2021, January 1). *Persistent SARS-CoV-2 infection and increasing viral variants in children and young adults with impaired humoral immunity*. MedRxiv. https://www.medrxiv.org/content/10.1101/2021.02.27.21252099v1

Varney, S. M., Manthey, D. E., Culpepper, V. E., & Creedon, J. F. (2002). A comparison of oral, tympanic, and rectal temperature measurement in the elderly. *The Journal of Emergency Medicine, 22*(2), 153–157. doi:10.1016/s0736-4679(01)00457-7

VOA News. (2020, July 11). Pandemic Worsens in US. Retrieved September 12, 2020, from https://www.voanews.com/covid-19-pandemic/pandemic-worsens-us

Walsh, B. (2020, July 12). *Disney World Opens and Florida Hits New Daily Infection Rate*. Barron's. https://www.barrons.com/articles/disney-world-opens-and-florida-hits-new-daily-infection-rate-51594569718

Wang, P., Nair, M. S., Liu, L., Iketani, S., Luo, Y., Guo, Y., Wang, M., Yu, J., Zhang, B., Kwong, P. D., Graham, B. S., Mascola, J. R., Chang, J. Y., Yin, M. T., Sobieszczyk, M., Kyratsous, C. A., Shapiro, L., Sheng, Z., Huang, Y., & Ho, D. D. (2021b). Antibody Resistance of SARS-CoV-2 Variants B.1.351 and B.1.1.7. *BioRxiv*. Published. https://doi.org/10.1101/2021.01.25.428137

Wang, Z., Schmidt, F., Weisblum, Y., Muecksch, F., Barnes, C. O., Finkin, S., Schaefer-Babajew, D., Cipolla, M., Gaebler, C., Lieberman, J. A., Oliveira, T. Y., Yang, Z., Abernathy, M. E., Huey-Tubman, K. E., Hurley, A., Turroja, M., West, K. A., Gordon, K., Millard, K. G., . . . Nussenzweig, M. C. (2021b). mRNA vaccine-elicited antibodies to SARS-CoV-2 and circulating variants. *Nature*, *592*(7855), 616–622. https://doi.org/10.1038/s41586-021-03324-6

Wardman, M. (2021, February 23). California coronavirus strain may be more infectious—and lethal. Retrieved February 24, 2020 from https://www.sciencemag.org/news/2021/02/coronavirus-strain-first-identified-california-may-be-more-infectious-and-cause-more

Wenger, C. B. (2002). Chapter 2: Human Adaptation to Hot Environments. In Textbooks of Military Medicine, *Medical Aspects of Harsh Environments* (Vol. 1, pp. 53-55). Dist. of Columbia, DC: Borden Institute, United States Army Medical Department, AMEDD Center & School. https://www.militarynewbie.com/wp-content/uploads/2018/12/2001-US-Army-MEDICAL-ASPECTS-OF-HARSH-ENVIRONMENTS-VOL1-623p.pdf

WHO. *A global pandemic requires a world effort to end it – none of us will be safe until everyone is safe*. (2020, October 1). WHO. https://www.who.int/news-room/commentaries/detail/a-global-pandemic-requires-a-world-effort-to-end-it-none-of-us-will-be-safe-until-everyone-is-safe

WHO (2021) *Statement on the eighth meeting of the International Health Regulations (2005) Emergency Committee regarding the coronavirus disease (COVID-19) pandemic*. (2021a, July 15). WHO. https://www.who.int/news/item/15-07-2021-statement-on-the-eighth-meeting-of-the-international-health-regulations-(2005)-emergency-committee-regarding-the-coronavirus-disease-(covid-19)-pandemic

William, James. (1892). American Science Series, Briefer Course: Psychology. *Henry Holt & Co.*

Wise, Jacqui. (2021) Covid-19: The E484K mutation and the risks it poses. *BMJ.* 372: n359. doi https://doi.org/10.1136/bmj.n359

Wibmer, C. K. (2021, March 2). *SARS-CoV-2 501Y.V2 escapes neutralization by. . .* Nature Medicine. https://www.nature.com/articles/s41591-021-01285-x?error=cookies_not_supported&code=6cc35b9d-d90d-4537-b223-a753be6582c2

Widge, A. T., Rouphael, N. G., Jackson, L. A., Anderson, E. J., Roberts, P. C., Makhene, M., . . . Beigel, J. H. (2020). Durability of Responses after SARS-CoV-2 mRNA-1273 Vaccination. *New England Journal of Medicine*. *384*: 80–82. doi:10.1056/nejmc2032195

Worby, C. J., Chaves, S. S., Wallinga, J., Lipsitch, M., Finelli, L., & Goldstein, E. (2015). On the relative role of different age groups in influenza epidemics. *Epidemics*, *13*: 10–16. https://doi.org/10.1016/j.epidem.2015.04.003

West, A. P., Barnes, C. O., Yang, Z., & Bjorkman, P. J. (2021). SARS-CoV-2 lineage B.1.526 emerging in the New York region detected by software utility created to query the spike Mutational landscape. *BioRxiv*. doi:10.1101/2021.02.14.431043

Yang, X. F., Chang, J. H. & Rothman, S. M. (2002) Intracerebral temperature alterations associated with focal seizures. *Epilepsy Research.* 52: 97–105. https://doi.org/10.1101/2021.02.14.431043

Yale University. (2003, July 2). Yale Researcher Discovers "Brain Temperature Tunnel" That For The First Time Allows External Continuous Measurement of Brain Temperature. Retrieved August 18, 2020, from https://news.yale.edu/2003/07/02/yale-researcher-discovers-brain-temperature-tunnel-first-time-allows-external-continuou-0

Zhang, W., Davis B. D., Chen S. S., Sincuir Martinez J. M., Plummer J. T., & Vail E. (2021). Emergence of a novel SARS-CoV-2 strain in Southern California, USA. *MedRxiv*. https://doi.org/10.1101/2021.01.18.21249786

Zhou, J., Wang, W., Zhong, Q., Hou, W., Yang, Z., Xiao, S. Y., Zhu, R., Tang, Z., Wang, Y., Xian, Q., Tang, H., & Wen, L. (2005). Immunogenicity, safety, and protective efficacy of an inactivated SARS-associated coronavirus vaccine in rhesus monkeys. *Vaccine*, *23*(24), 3202–3209. https://doi.org/10.1016/j.vaccine.2004.11.075

Supplemental Information

Brain thermal kinetics at brain-eyelid thermal tunnels overcoming COVID-19 thermometry limitations for asymptomatic infection detection and mutation mitigation in concert with thermophysical and biological principles

M Marc Abreu[1,2], Ricardo L. Smith[3], Trevor M. Banack[1], Alexander C. Arroyo[4], Robert F. Gochman[4], Anna L. Clebone[1], Feng Dai[5], Michael F. Bergeron[6], Ala S. Haddadin[1], Tyler J. Silverman[1], Adriano F. da Silva[7], David G. Silverman[1,8]†

1. Department of Anesthesiology, Yale University School of Medicine, 20 York Street, TMP3, New Haven, CT 06520-8051, USA

2. Department of Ophthalmology and Visual Science, Yale University School of Medicine, 333 Cedar Street, New Haven, CT 06520-8051, USA

3. Department of Morphology and Genetics, Paulista School of Medicine, Federal University of São Paulo, Rua Botucatu 740, São Paulo, SP 04023-900, Brazil

4. Department of Pediatric Emergency Medicine, North Shore - Long Island Jewish Medical Center, 430 Lakeville Road, New Hyde Park, NY 11040, USA

5. Yale Center for Analytical Sciences, Yale School of Public Health, Yale University, 60 College Street, New Haven, CT 06520-8034, USA

6. Department of Physical Therapy, Augusta University Medical Center, Medical College of Georgia, Augusta University, 987 St. Sebastian Way, Augusta, GA 30912, USA

7. Department of Radiology, Heart Institute, University of São Paulo Medical School, Av. Prof. Lineu Prestes, 2565, São Paulo, SP 05508, Brazil

8. John B. Pierce Foundation Laboratory, Yale University, 290 Congress Ave, New Haven, CT 06520, USA

† Correspondence and requests should be addressed to D.G.S. (david.silverman@yale.edu)

Table of Contents

1. **Supplementary Figures 1–38:** Global reliance on low-*k* temperature measurements

1.1. Military Bases and Checkpoints

Figure 1:

CHINA | *MILITARY CHECKPOINT:* A member of China's militia arm of the armed forces uses a digital thermometer to take a driver's temperature at a highway tollgate in Wuhan on January 23. *Chiu K. (South China Morning Post, 2020)*

Figure 2:

ISRAEL | *MILITARY BASE:* An Israeli soldier checks the temperature of a comrade as he enters a military base. *Davis, R. (AJN, Times of Israel, 2020)*

Figure 3:

RUSSIA | *MILITARY BASE:* A Russian conscript having his temperature measured in Kaliningrad. *Reuters Staff (Reuters, 2020)*

Figure 4:

U.S.A, Hawaii | *AIR FORCE BASE:* AFHSB's (Armed Forces Health Surveillance Branch) GEIS (Global Emerging Infectious Surveillance) collect data to support force protection. *Military Health System (health.mil, 2020)*

Figure 5:

U.S.A, North Carolina | *MARINE BASE:* Major General Stephen M. Neary having temperature taken at Marine Corps Air Station, New River, NC. *US Dept of Defense (Finerty M, 2020)*

Figure 6:

U.S.A, South Carolina | *ARMY BASE:* Military Times, US Army Base: Army staff sergeant taking temperature of an Ohio National Guardsman before he boards a bus at Fort Jackson, SC. *Shea, A. (U.S. Dept of Defense, 2020)*

Figure 7:

U.S.A, Virginia | *NAVY CHECKPOINT:* "Navy Releases New COVID-19 Guidance to Fleet." *Werner B (USNI, 2020)*

1.2. Large Indoor Entertainment Venues

Figure 8:

GERMANY | *INDOOR CONCERT:* A participant has his temperature checked upon arrival at an indoor concert in Leipzig, Germany. *Associated Press (CBC, 2020)*

1.3. Hotels

Figure 9:

U.S.A, Nevada | *HOTEL CASINO:* USA Today reporter getting her temperature checked at the New York, New York hotel in Las Vegas. *Gilbertson, D. (USA Today, 2020)*

1.4. Workplaces

Figure 10:

CHINA | *CONSTRUCTION SITE:* A worker has his temperature checked at a construction site in Chongqing. *Kun, Z., & Wenting, Z. (China Daily, 2020)*

Figure 11:

FRANCE | *FACTORY:* A worker's temperature is tested at the Toyota Motor Corp. plant in Onnaing, France, in April. *Hindustan Times (Agence France-Presse, 2020)*

1.5. Large Outdoor Entertainment Venues

Figure 12:

U.S.A, Florida | *AMUSEMENT PARK:* A child has her temperature taken at an amusement park in Orlando, FL. *Walsh, B. (Barrons, 2020)*

1.6. Outdoor Settings

Figure 13:

AUSTRALIA | *OUTDOOR SETTING:* A child has their temperature checked in Australia. *Jalal, A. (ABC, 2020)*

Figure 14:

JAPAN | *OUTDOOR SETTING:* A participant has her temperature checked before a memorial service at the Peace Memorial Park in Itoman, Okinawa, Japan. *Mori, K. (UPI, 2020)*

Figure 15:

NETHERLANDS | *STADIUM:* A patron has her temperature checked prior to the World Cup Speedskating Final at the Thialf Ice Arena in Heerenveen, Netherlands. *Reuters (Daily Sabah, 2020)*

1.7. Healthcare Settings

Figure 16:

U.S.A, Arizona | *HOSPITAL*: An employee of Oro Valley Hospital has her temperature checked in Tucson, AZ. *Voa News (VOA News, 2020)*

Figure 17:

U.S.A, Nevada | *MEDICAL SCHOOL:* Touro University Nevada medical student Taylor Vikery helps apply a contactless forehead thermometer. *Brandt, J. (NBC Philadelphia, 2020)*

1.8. Schools

Figure 18:

INDONESIA | *SCHOOL:* A school official checks the temperatures of students before they enter the International Islamic School Yogyakarta in Yogyakarta, Indonesia, on March 4. *Ruahala, E. (The Washington Post, 2020)*

Figure 19:

RUSSIA | *SCHOOL:* Students have their temperatures measured by a teacher in Moscow, Russia. *Golovkin, P. (AP News, 2020)*

Figure 20:

UNITED KINGDOM | *SCHOOL:* A child has her temperature checked with a digital thermometer at a school in the U.K. *Roxby, P. (BBC, 2020)*

Figure 21:

U.S.A, California | *HIGH SCHOOL:* Aracelia Gasper Andres performs a contactless temperature check at Hollywood High School in Los Angeles. *Caroll, L. (NBC News. 2020)*

Figure 22:

U.S.A, Texas | *HIGH SCHOOL:* Summer camp students have their temperatures checked by teachers at Wylie High School in Wylie, TX. *CBS Austin, & Associated Press (CBS Austin, 2020)*

1.9. Ports of Entry

Figure 23:

AUSTRIA | *TRAVEL CHECKPOINT*: A doctor in protective garments checks the temperature of a driver at the Brenner border crossing between Austria and Italy on March 10. *Ruahala, E., (The Washington Post, 2020)*

Figure 24:

CHINA | *AIRPORT:* A security staff member checks a passenger's temperature at the Sanya Phoenix International Airport in Sanya, south China's Hainan Province. *Xinhua (Xinhua Net, 2020)*

Figure 25:

HONG KONG | *TRAVEL CHECKPOINT:* A passenger has his temperature checked upon arrival in Hong Kong, China. *Today Online (Today Online, 2020)*

Figure 26:

ITALY | *TRAIN STATION:* A passenger has his temperature measured at a train station in Naples, Italy. *Bendix, A. (Business Insider, 2020)*

Figure 27:

MEXICO | *AIRPORT:* A passenger has her temperature checked at Benito Juarez International Airport in Mexico City, Mexico. *McDonnell, P. J. et al. (Los Angeles Times, 2020)*

Figure 28:

NIGERIA | *AIRPORT:* A passenger has his temperature checked upon arrival at Murtala Muhammed International Airport in Lagos, Nigeria. *Nordling, L. (Science Mag, 2020)*

Figure 29:

PAKISTAN | *TRAIN STATION:* A passenger has his temperature checked at a train station in Pakistan. *Shams, S. (DW, 2020)*

Figure 30:

U.S.A, Alaska | *AIRPORT:* A passenger has her temperature checked at the Juneau International Airport in Juneau, AK. *Baxter, A. (KTOO, 2020)*

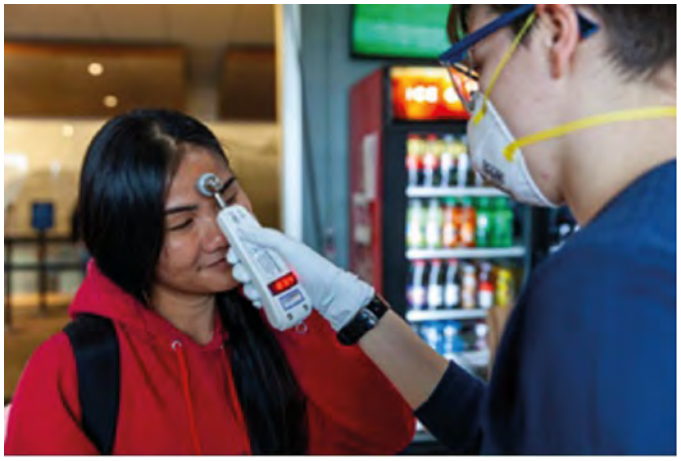

1.10. Cruise Ships

Figure 31:

SRI LANKA | *CRUISE SHIP:* Passengers undergo temperature checks as a part of precautionary measures to prevent the spread of coronavirus before they board a cruise at the Colombo Port in Colombo, Sri Lanka. *Dalton, M. & Barton, K. (W NYC Studios, 2020)*

1.11. Restaurants

Figure 32:

SOUTH KOREA | *CAFE:* A customer having her temperature checked at a cafe in Seoul. The government is trying to sustain a fragile balance between controlling the virus and safeguarding the economy. *Sang-Hun, C. (The New York Times, 2020)*

Figure 33:

U.S.A, California | *RESTAURANT:* CNBC, Alhambra, CA, Copyright: Getty Images. Customer has her temperature taken at the Sichuan Impression Restaurant in Alhambra, CA. *Repko, M. (CNBC, 2020)*

1.12. Stores

Figure 34:

BRAZIL | *RETAIL STORE:* Temperatures are measured at a retail store in Sao Paulo, Brazil. *Associated Press (VOA News, 2020)*

Figure 35:

ISRAEL | *STORE:* A worker's temperature is taken. Times of Israel, Jerusalem, Israel. Copyright: AFP. *TOI Staff (The Times of Israel, 2020)*

1.13. Government Buildings

Figure 36:

RUSSIA | *ELECTION POLLING STATION:* A police officer has her temperature checked at a polling station during the 2020 Russian Constitutional Referendum in Vladivostok, Russia. *Tass (Alamy, 2020)*

Figure 37:

THAILAND | *GOVERNMENT BUILDING:* Thailand's Prime Minister Prayut Chan-o-cha has his temperature checked before a meeting in Bangkok, Thailand. *Moritsugu, K. (AP News, 2020)*

Figure 38:

UKRAINE | *PRESIDENTIAL OFFICE:* Temperature checks at an entrance to the Presidential Office Building in Kyiv on March 13. *Ruahala., E. (The Washington Post, 2020)*

Figure 39:

U.S.A, Washington, D.C. | *WHITE HOUSE:* A member of the media has their temperature checked by a member of the White House Physician's Office on March 15, 2020. *Superville, D. (The Washington Times, 2020)*

1.14. Ear-temperature measurements: Airports

Figure 40:

GERMANY | *AIRPORT:* Temperature check of an airport worker in Germany. *Agencies (The New Indian Express, 2020)*

2. **Supplementary Figure 41:** Biological and thermophysical variables influencing wrist-skin temperature measurements

Figure 41:

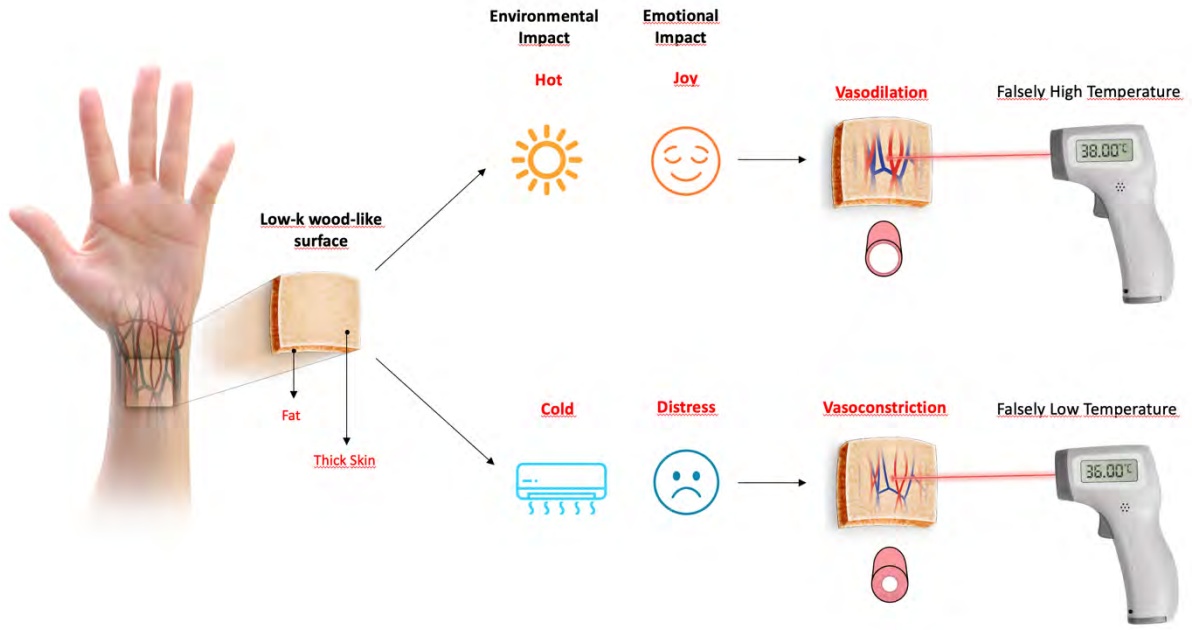

(41) Schematic example demonstrating the combination of low-*k* surface and environmental (e.g., ambient temperature and air velocity) and emotional interference on the surface temperature readings taken at wrists. Hot weather and positive emotions cause vasodilation and thereby lead to higher wrist temperatures and false positive readings; meanwhile, cold weather and distress leads to vasoconstriction and thereby false negative readings. This illustrates the multiple factors present in the wrist (and body surface, except the eyelid at $SMOS_{BTT}$) such as variable amounts of fat and dermis thickness (see Table 2 of main manuscript for details) leading to variable thermo-conductivity as well as variable environments and emotions that affect vascular reactivity and lead to variable heat capacitance, causing inaccurate temperature readings.

3. **Supplementary Figure 42:** Multiple and unpredictable combinations of thermophysical and biological variables upon FH and wrist.

Figure 42:

How biological variables influence the thermophysical readings, producing false results

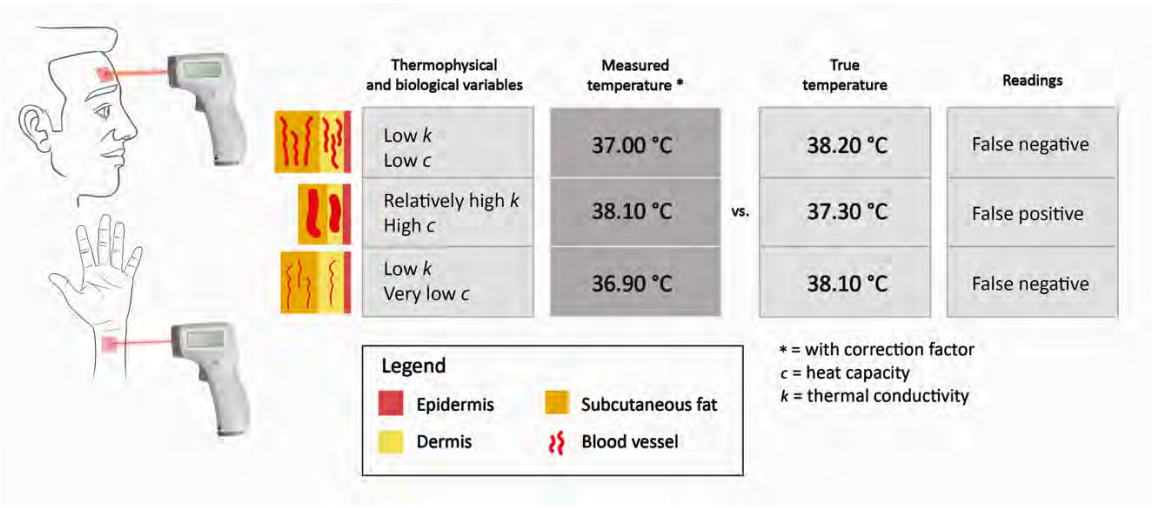

(42) Schematic example showing how the unpredictable morphological (i.e., skin thickness and fat quantity), physiological (i.e., variable vascular reactivity) and thermophysical (i.e., variable low-*k* and variable volumetric heat capacity) of the FH (including the temporal region) and wrist affect the accuracy of the temperature reading (See Section 3 of the manuscript for details). The subsequent impossibility of measuring the exact morphological structure, thermophysical features, and physiological responses may lead to false negative and false positive readings, and thereby to clinically erroneous results during COVID-19 screening. These false readings apply to the body surface (except the eyelid at $SMOS_{BTT}$) including finger, chest, and arm temperature measurements. Different vascular responses are shown as vasodilated and vasoconstricted blood vessels dispersed along multiple skin surfaces (with different thickness of fat and dermis). The epidermis has a uniform thickness. See Table 2 of the manuscript for histomorphometry.

4. **Supplementary Figure 43:** Description of Abreu-BTT Brain-Eyelid technique for accurate temperature measurement at the BTT site.

Figure 43:

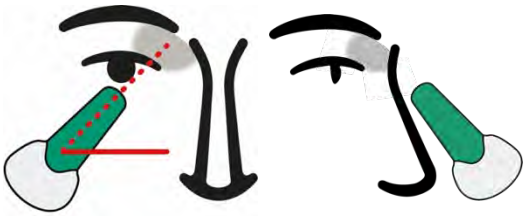

45° angle
Frontal View

45° angle
Side View

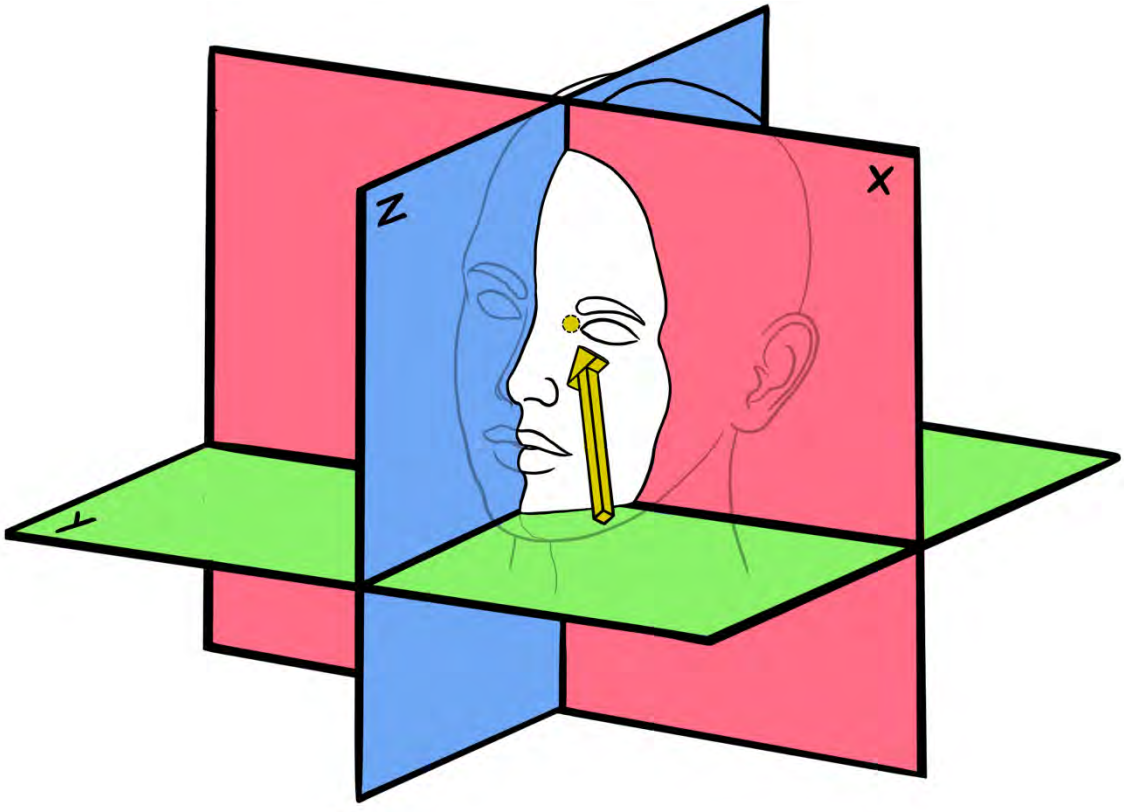

(43) Abreu-BTT Brain-Eyelid Technique. (1) *Upper panel*. a) Left: Correct angle for applying the Abreu-BTT Brain-Eyelid Thermometer, here being held by the examiner; the detector points (at the right eyelid in the $SMOS_{BTT}$ of the patient) from an inferior position (relative to the eyes) and diagonally at ~45°. b) Right: Upper image: Reading at $SMOS_{BTT}$ without any correction factor (or algorithm), representing brain tunneling temperature (36.2 °C). A temperature reading above 37.9 °C indicates infection and the need for proper isolation and medical care alongside confirmation by nucleic acid testing (PCR); other causes of fever in the context of the COVID-19 pandemic should be considered including vaccine reactions and other infectious agents. Lower image: Schematic of 45° detector angle from frontal and side views. (2) *Lower panel*. Cartesian XYZ coordinates showing the proper angle for the detector (yellow arrow) relative to the $SMOS_{BTT}$ in dimensional space.

5. **Supplementary Figure 44:** Use of Abreu-BTT Brain-Eyelid Technique for BTT-based temperature measurement with standard infrared thermometry (without correction factors)

Figure 44:

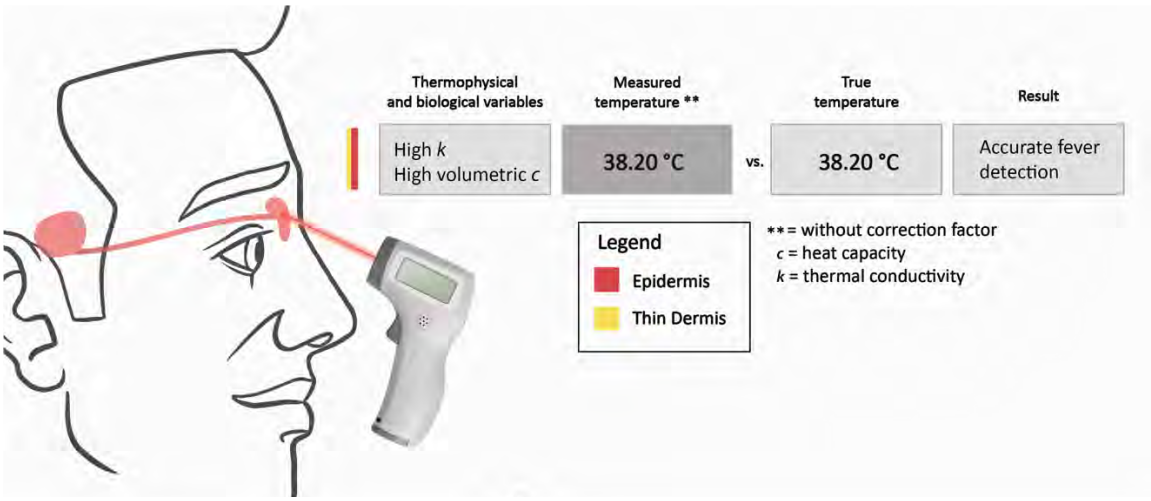

(44) Schematic showing the angled position of standard infrared thermometer (as per Supp. Fig. 43), without correction factors; this facilitates fever detection in accordance with physical and biological principles, which can be accomplished by employing thermometers available wordwide, through harnessing the optimal location for temperature measurement at the eyelid, which can be immediately used around the globe free-of-charge, from villages in economically-challenged nations to the metropolises of the industrialized world, for fever detection and protection against COVID-19 for adults and children alike

6. **Supplementary Figure 45:** Intelligent automatic topographic locator

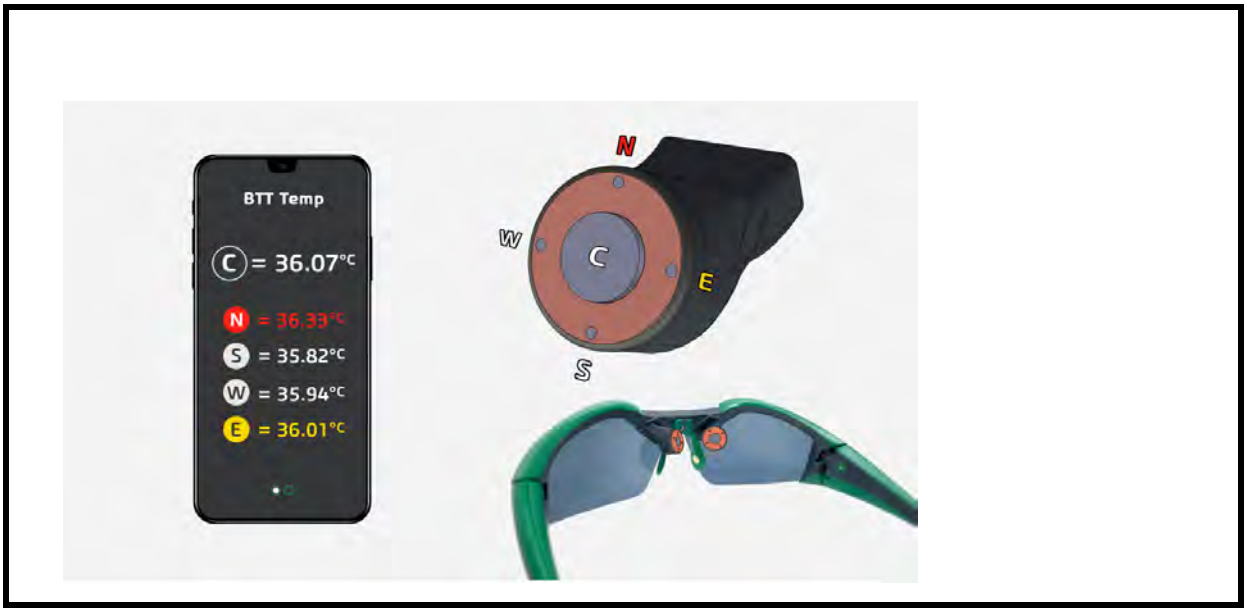

(46) Schematic of the intelligent automatic topographic locator (IATLo) for detecting peak thermal intensity, containing a ring with four high-resolution thermal sensors (positioned in the cardinal points of the ring); these measure temperature simultaneously with the central high-resolution sensor, to determine the region of the highest temperature at the SMOS. IATLo is shown here in BTT eyeglasses, which are remotely connected to a mobile device (see text) that displays temperatures according to the precise SMOS region.

7. **Supplementary Figure 46:** Comparison of 2020 vs. 2021 (September 3rd) for new COVID-19 cases in the US, showing the need for additional measures, besides vaccines, to control COVID-19, as the automated detection of brain thermal kinetics as part of the «detection-vaccination » pair solution presented here

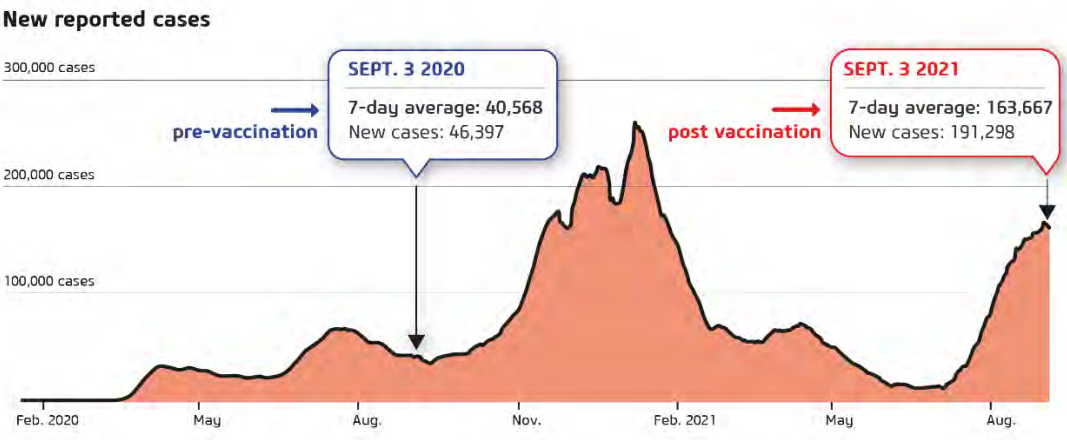

People Vaccinated (US)	At least one dose	Fully vaccinated
Total	206,908,710	175,968,266
% of total population	62.3%	53%

CDC | Data as of: September 4, 2021 6:00am ET. Posted Saturday, September 4, 2021 1:53 PM ET

8. Supplementary Figure 47: BTT° noninvasive brain-temperature monitoring during sleep with BTT headgear (here used by an adult).

(47) BTT wireless headgear with high-resolution thermal sensor, primarily for monitoring during sleep in traumatic brain injury and stroke patients in ICU. This system facilitates continuous brain temperature monitoring and multiple data capture, storage, and analysis; furthermore, it transmits signals to a computer or cell phone, which facilitates the automated detection of brain thermal disturbances when subjects are awake or asleep (see text and material/methods for details).

9. Supplementary Table 1

Supp. Table 1. Mandatory criteria for infrared thermal imaging of BTT site

Detector	• Detector should have a narrow field to capture thermal image of the central BTT site zone.
	  ◦ preferably <15 cm (depending on camera resolution) to focus on BTT,
	  ◦ ideally at < 5 cm, as suggested for handheld infrared thermometers due to narrow light beam, as shown here.
	• Measurements should be taken at a uniform detector distance, preferably in a room that facilitates control of ambient temperature and under minimal air movement conditions (e.g., 4 m x 3 m).
	• Detector should be adjusted to subject's height and aligned with angled emergence of the infrared beam via the SMOS BTT.
	  ◦ i.e., it should be angled medially and slightly upward (~30° with respect to ground), depending on face size.

Environment	• Avoid uncertain outdoor environments.
	• Acquisition of the image should occur in a confined environment comprising a draft-free room with stable temperature, low humidity, and controlled air movement (see below).
	  ◦ the room's ambient temperature should be carefully controlled to the range 22–23°C, to avoid vasomotor inconsistencies and sweating.
	  ◦ the room's air current velocity should not exceed 0.2 m/sec; speeds exceeding this limit can lead to reduced temperature readings, potentially producing false negative readings and further preventing detection of COVID-19.
	  ◦ the room should not feature incident light; thus, appropriate window coverage (and blinds) should be used.

Subject	• **Acclimatization:** Subject should be acclimatized to the environment for ~ 15 min. • **Subject must remain motionless** (thus, subject cannot simply walk by a thermal imaging camera). • **Head Immobility:** Subject should remain still and avoid any turning of the head [any minor motion can remove central BTT site from field of view **(Movies #1–3)]**. • **Mouth should remain closed** (to prevent interference from oral heat). • **Acne and Facial Infections:** Account for any facial infections (including herpes and acne) that can interfere with infrared thermography measurements. Camera may read temperature of an infected pimple on the forehead or periocular region, resulting in false positive reading (which may spread COVID-19 by placing normal healthy subjects with infected ones). • **Eye and Periocular Infections, Inflammation, and Allergies:** Account for eye and periocular mucosal changes (caruncle, inner canthi, tear duct, and conjunctiva), including inflammatory, allergic, and infectious conditions (which may cause false positive readings), as well as dry eye or desiccated mucosa, which may lead to spurious thermal measurements. • **Make-up Removal:** All make up and creams around the eyes must be removed. • **Contact Lenses:** Identify whether the test subject wears contact lenses, as this can produce eye inflammation and changes in the caruncle (inner canthi), conjunctiva and periocular region.

10. Supplemental Movies – Legends

Supplemental Movies 1–3. Real-time Facial Thermal Emission: Movies show the infrared (IR) light emission via the BTT of resting volunteer (bright red pulsating pixels) sitting in a neutral environment. The BTT area (represented by the red isotherm) exhibits the highest light-emission intensity across the face. All other areas lack radiation emissions comparable to the BTT site. Instead, the remainder of the face is characterized by low and variable IR light emission, represented by a gray scale (white to black, representing decreasing emission intensity); however, no bright red bright light (as seen at the eyelid of the BTT site) is observed elsewhere on the face. The ear canal and forehead exhibit low thermal emissions (indicating low temperature) compared to the higher temperature at the eyelid of the BTT site. A bright white corona can be observed around BTT, representing the second highest temperature.

Supplemental Movie 1: Subject moves from right to left, to expose left BTT and left forehead and ears. At all times, the eyelid at the BTT site is the only area that consistently exhibits highest emissions (bright red pixels); the corona, representing the second highest thermal emission, is visible around the BTT site.

Supplemental Movie 2: Infrared light emission from the right side of the face, with focus on the ear and medial forehead over the superficial temporal artery. Lighter area (in linear shape) in right forehead indicates the location of the right superficial temporal artery; however, despite its large caliber (Fig. 2Ci), the superficial temporal artery (which is used by temporal scanner) shows a low emission relative to the emission at the $SMOS_{BTT}$ over the BTT, leading to inaccurate results, shown in detail in the main manuscript. No other area (including the ears) exhibits such high infrared light emissions. The second-brightest (white) area is the corona. The superior palpebral region, outside $SMOS_{BTT}$, is visible as a small linear whitish streak on the eyelid

Supplemental Movie 3: As the subject turns from left to right, emission is detected initially from the left BTT and then from the right BTT (when the BTT region is aligned with the IR thermal detector). The eyelid at the BTT site is visible as a set of pulsing bright red pixels, and no other comparable emission is observed from other facial regions.